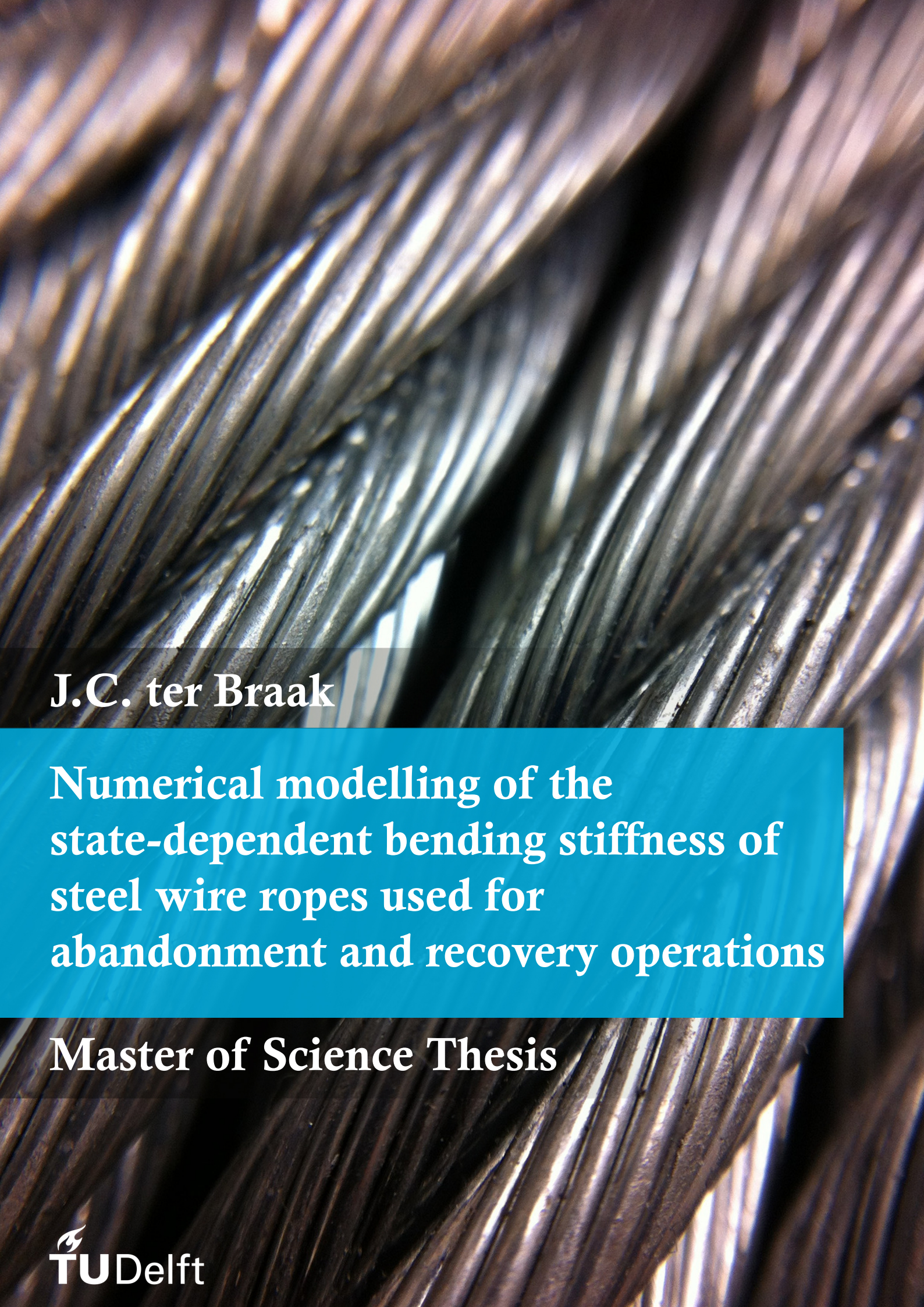

J.C. ter Braak

Numerical modelling of the state-dependent bending stiffness of steel wire ropes used for abandonment and recovery operations

Master of Science Thesis

TU Delft

Numerical modelling of the state-dependent bending stiffness of steel wire ropes used for abandonment and recovery operations

by

J.C. ter Braak

to obtain the degree of Master of Science
at the Delft University of Technology,
to be defended publicly on Tuesday February 21, 2017 at 11:00 AM.

Student number:	4103262	
Project duration:	April 25, 2016 – February 21, 2017	
Thesis committee:	Prof. Dr. A. V. Metrikine,	TU Delft, Chairman
	Ir. P. C. Meijers,	TU Delft
	Dr. F. Pisanò,	TU Delft
	Ir. J. E. van Leeuwen,	Allseas B.V.

TU Delft

Preface

This thesis has been written to conclude my studies at the Delft University of Technology and to achieve a Masters degree in Offshore and Dredging Engineering. The committee overseeing my progress consist of the following members:

Prof. Dr. A.V. Metrikine	Delft University of Technology	(Chairman)
Ir. P.C. Meijers	Delft University of Technology	(University supervisor)
Dr. F. Pisanò	Delft University of Technology	
Ir. J.P.H. van Leeuwen	Allseas Engineering B.V.	(Company supervisor)

For eight months I have joined the innovations department located at Allseas's headquarters in Delft. Many thanks to Allseas for the opportunity to research steel wire rope behaviour and to contribute to their continued success. By making use of the free and friendly atmosphere at the department, I gained a lot of knowledge on ongoing projects and innovative ideas. My stay at Allseas provided me with engineering experience in my own and other disciplines.

My thanks go out to all the authors from papers I have used for completing my research. Dansong Zhang and Francesco Foti, thanks for your input and answers to my questions concerning your papers.

I would specifically like to thank my colleagues at Allseas for their help and guidance throughout the graduation process. These thanks go out to Sven Hendricks and Andrys Posthuma, for aiding me in understanding the finite element program Marc which I used during the graduation. For providing useful feedback and criticism on my thesis and findings, I would like to thank Jeroen Breukels. Throughout the process of writing my thesis, Jeroen van Leeuwen continuously pushed me in the right direction and helped me achieve my goals, my thanks go out to him.

Thanks to Andrei Metrikine, for his ever useful feedback and clever insights during progress meetings. Especially, I would like to thank my University supervisor for his time and enthusiasm for the graduation topic and my efforts. Meetings with Peter Meijers were always interesting and mostly resulted in new realizations which gave me a lot more work to do. Without you, The whole process would have progressed quite a lot slower.

J.C ter Braak
Delft, February 2017

Abstract

During Abandonment and Recovery (A&R) operations, steel wire ropes can experience torsional deformation. This deformation is a result of the helical configuration and the tension gradient in the rope due to its self-weight. The latter is very high when the ropes are used in deep water operations. Since the static component of the torque is constant over the length of the rope, it unlays in the direction of the greater tension while winding up in the direction of the lesser tension. The torsional energy in a steel wire rope can lead to instability of the straight shape of the rope. Tension and bending stiffness of the rope will play the most important role in the process. Instability of a wire rope can lead to hockling and loop formation which, in turn, may translate into irreversible damage to the rope, delaying the A&R operation. Currently, a very low value for the bending stiffness is used to predict these failure mechanisms, leading to conservative values for the allowable tension and torsional deformation. This reduces the time window in which operations involving steel wire ropes will be allowed. To improve the understanding of wire rope instability, research into the state-dependent bending stiffness of steel wire ropes has to be performed. Therefore, the objective of this thesis is to numerically model the state-dependent bending stiffness of steel wire ropes used for A&R operations.

A literature study revealed a large variety of modelling approaches of the bending behaviour of wire ropes. Most analytical models describe the bending stiffness to be dependent on tension and curvature of the wire rope. This bending behaviour of steel wire ropes is found to be dominated by friction between the wires. In theory, large differences are found between the theoretical minimum and maximum value for the bending stiffness. Assumptions made in these models could cause the outcome to be uncertain and could affect the large difference between these theoretical limits. Analytically generated results for simple strands and spiral ropes match those experimentally found quite well for a limited curvature range. Stranded steel wire ropes used in A&R operations are difficult to model analytically due to their complex configuration. Therefore, numerical modelling has to be used to describe the bending behaviour.

In this thesis, a numerical model which can be used to generate the state-dependent bending stiffness of arbitrary steel wire rope configurations has been developed. The bending stiffness due to friction has been numerically modelled using the finite element programme MSC Marc. A sensitivity study has been performed to test the boundary conditions and settings of the numerical model.

A practical implementation of the obtained results is carried out to develop insight into the variation of the bending stiffness along a wire rope length. A subroutine is written to implement the obtained bending stiffness into a model consisting of several beam elements which can be used to simulate steel wire ropes during, for example, A&R operations.

The results for simple strands from the new numerical model match the analytically generated ones quite well. The results of larger stranded rope configurations show less resemblance. Compared to the analytical results, the numerically generated results show a less extreme difference between minimum and maximum bending stiffness. This difference is influenced by the level of detail of the mesh. It seems likely – but cannot be confirmed with the available data – that the maximum and minimum bending stiffness for simple strands will match the theoretical ones if the element size will be considered infinitesimal. It is concluded that the developed modelling method generates valid results for arbitrary wire rope configurations as long as the level of detail of the mesh is sufficiently high and the correct model length is taken into account. However, increasing wire rope complexity while maintaining a high level of detail increases the computational time significantly.

A critical situation during an A&R operation, when high torsional deformation, low tension and a low bending stiffness occur simultaneously, is simulated. An indication is given for the likelihood of loop formation and hockling when performing an A&R operation in certain sea states.

Experiments should be performed to test the validity of the numerical model. The new insights into the state-dependent bending stiffness should be used to create an experimental set-up to find the critical parameters that result in loop formation and hockling. Further studies into friction modelling in FEM are needed to reduce the computational time when wire rope complexity is increased.

Nomenclature

List of Acronyms

$A\&R$	Abandonment and Recovery
$ACSR$	Aluminium Conductor Steel Reinforced
BC	Before Christ or Boundary conditions (depends on context)
CAD	Computer aided design
CoG	Centre of Gravity
DNA	Deoxyribonucleic acid
FEA	Finite Element Analysis
FEM	Finite Element Method
Hex	Hexagonal
hr	Hour
inc	Increment
$IWRC$	Independent Wire Rope Core
RAO	Response Amplitude Operator
SWR	Steel Wire Rope
$3D$	Three dimensional
$2D$	Two dimensional
WS	Warrington Seale

List of Symbols

s	[m]	Arc length
EI	[Nm^2]	Bending stiffness
M_b	[Nm]	Bending moment
δ_t	[Nm^2]	Bending stiffness correction value
M_{stick}	[Nm]	Bending moment in the sticking regime
M_{slip}	[Nm]	Bending moment in the slipping regime
EI_{stick}^{wire}	[Nm^2]	Bending stiffness in the sticking regime
EI_{slip}^{wire}	[Nm^2]	Bending stiffness in the slip regime
V	[N]	Cross sectional shear force
M	[Nm]	Cross sectional bending moment
N	[N]	Cross sectional axial force
κ	[m^{-1}]	Curvature
ρ	[m]	Curvature radius
A	[m^2]	Cross sectional surface area
κ_{slip}	[m^{-1}]	Critical curvature
κ_s	[m^{-1}]	Curvature of the strand
p_1	[Nm^{-1}]	Distributed force in transverse direction
p_3	[Nm^{-1}]	Distributed force in axial direction
ρ	[kgm^{-3}]	Density
h	[m]	Distance between neutral line and centreline wire cross section
w	[m]	Displacement of the mid-surface in lateral direction
dN	[N]	Distributed wire load
μ	[−]	Friction coefficient
F_x	[N]	Force contributing to the torque in wire ropes
θ	[°]	Helix orientation angle
h_r	[m]	Helical wire winding radius

dR	[N]	Incremental radial force
β	[rad]	Lay angle of the strand
α	[rad]	Lay angle of a wire in a strand
h_w	[mm]	Lay length
L	[m]	Length of a strand
Z	[N]	Local wire tensile force
L_{strand}	[m]	Length of the strand along its centreline
m	[kg]	Mass
m	[−]	Greenhill constant
σ_{min}	[Nm^{-2}]	Minimum possible stress in wires
EI_{min}^{wire}	[Nm^2]	Minimum bending stiffness
EI_{max}^{wire}	[Nm^2]	Maximum bending stiffness
d	[m]	Nominal rope diameter
σ_n	[Nm$^-$2]	Normal stress
f_n	[N]	Normal force
G	[Nm^{-2}]	Shear modulus
ϕ	[rad]	Swept angle or angle of rotation of the normal to the mid-surface of the beam
I	[m^4]	Second moment of inertia
$L_{straight}$	[m]	Shortest distance between two ends of a strand
h_s	[m]	Strand lay length
$TorS$	[N]	Tension
F_{crit}	[N]	Tension threshold
M_t	[Nm]	Torsional moment
Z_T	[N]	Tensile force on a wire before bending has taken place
f_t	[N]	Tangential (friction) force
Z_{slip}	[N]	Tensile or compressive force as a result of inter wire friction
u_1	[−]	Vector defining the transverse direction
u_3	[−]	Vector defining the axial direction
r	[mm]	Winding radius of a wire in a strand
R	[mm]	Winding radius of a strand
r_w	[mm]	Wire winding radius
r_s	[mm]	Strand winding radius
δ	[m]	Wire diameter
dl	[m]	Wire element length
p	[Nm^{-2}]	Wire normal pressure
σ_{stick}	[Nm^{-2}]	Wire stress in sticking regime
σ_{slip}	[Nm^{-2}]	Wire stress in slipping regime
E	[Nm^{-2}]	Young’s modulus

List of Figures

List of Tables

Contents

1 Introduction

1.1. Company

The Swiss-based Allseas Group founded in January 1985 in Châtel Saint-Denis, Switzerland, and The Hague, the Netherlands is headed by Edward Heerema. The company specializes in offshore pipeline installation while also performing heavy lifts and subsea construction. Allseas operates a versatile fleet of pipe lay, heavy lift and subsea installation vessels. All vessels are designed in-house, with the latest being the Pioneering Spirit, which is designed to install and remove offshore platforms with a single lift. The vessel can also be used for pipeline installations in up to three kilometres of water depth.

By possessing a large and productive Innovations Department, Allseas is a company that strives towards new and creative ideas to help improve the quality of delivered work. By establishing three Innovations Offices in the Netherlands, located close to Technical Universities, high end tools and systems are developed and tested to increase the efficiency of the operations performed by or on the vessels. One frequently used and researched piece of equipment is a steel wire rope (SWR).

1.2. Steel wire ropes

Allseas uses steel wire ropes frequently and in numerous different applications. Investigation of the behaviour of these ropes is therefore of major importance. Modelling wire ropes and researching their response to loads and moments is not new. Researching wire rope behaviour has been done for several years. The usage of wire ropes date back even further in history as will be explained in this chapter.

This chapter will provide an introduction to steel wire ropes and to their usage in abandonment and recovery (A&R) operations. This section will be divided into five parts where the first part will provide the reader with a short summary on the history of wire ropes. To properly understand the modelling strategies explained further in this thesis, the basics of wire rope geometry and configuration will be addressed in part two. Perhaps the best way to understand the geometry and composition of steel wire ropes is to know how they are made. Manufacturing and the impact of machining on wire rope behaviour will be presented afterwards. The load characteristics will be discussed in the last part as they have an influence on the non-linear behaviour of a steel wire rope at the onset of tensioning or bending. This short introduction to wire ropes will provide a basis to discuss the implications of implementing wire ropes in the offshore industry with a focus on A&R operations.

1.2.1. History

Ropes made from materials such as plants and hides are among the first technological achievements of mankind and date back to 12000 BC. These ropes where made for fishing nets and traps but also for lifting and dragging of loads. The iron wire rope was invented in the 19^{th} century when the German mining engineer Albert tried to improve the transportation in the mining pits by combining the advantages from hemp rope and those of iron chains. Hemp rope has the advantage of bearing elements in a parallel arrangement which increases redundancy while iron chains are constructed in a series arrangement with a high tensile strength. After his attempt to construct wire ropes for the mining industry a lot has changed. Numerous different wire rope configurations are invented and are applied in

a great variety of industries. The offshore industry is one that makes use of and contributes to these developments. Nowadays, engineers at such companies are still trying to improve and understand the way these wire ropes behave under loads and in different circumstances.

1.2.2. Configuration

The most basic components of a steel wire rope are, as the name already implies, the wires. Figure 1.1 clearly displays a single wire, which is an element of a bigger component, namely the strand. The strand consists of a core wire together with multiple wires helically wound around it. These wires can be located in single or in several layers as is shown in the figure. Wire ropes are made out of several strands and can consist of different kinds of helical configurations around a core strand.

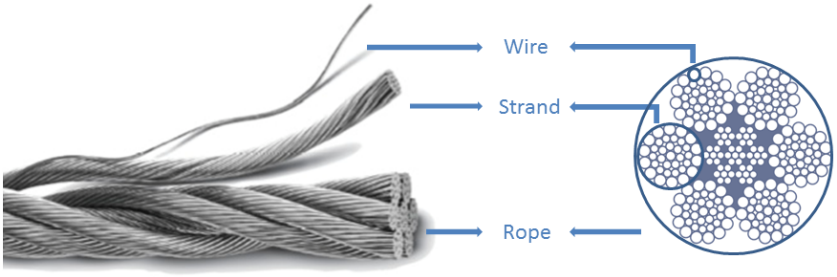

Figure 1.1: Steel wire rope components [24]

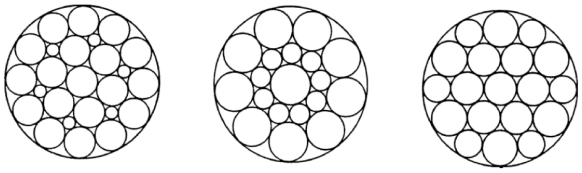

Figure 1.2: Strand configurations from left to right; Filler, Seale and Warrington strand [10]

The way different components in a wire rope are numbered and named in this thesis can be explained quickly by taking a look at figure 1.3. The figure displays a typical cross section configuration of a wire rope. The orange arrows indicate the way the strand layers are numbered while the green arrows indicate how the wire layers in a certain strand can be numbered. For example, the red coloured wire in figure 1.3 is in the first wire layer of a second layer strand. Different wire rope configurations can be described by using the same method of numbering wire and strand layers.

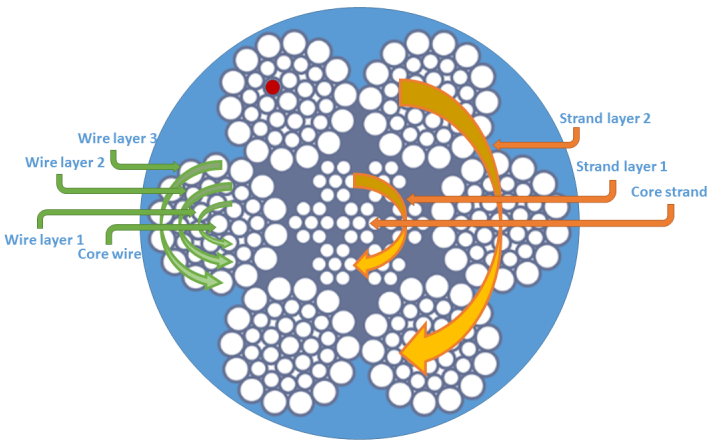

Figure 1.3: Typical wire rope configuration and numbering [5]

There are four different winding orientations in which the wires in the strand and the strand itself

can be wound. In figure 1.4 these lay configurations can be found. A type of lay is used to describe the way the strand and the wires are orientated. The thick black lines in figure 1.4 describe the coding method of recognizing the lay orientation, where the black line forms a Z when the wires or strands are wound in a clockwise direction, and forms a S when they are wound anticlockwise resulting in right or left handed lays. In ordinary lay, the lay direction of the wires in the strand and the lay direction of the strand are always opposite while in Lang's lay the lay directions of wire and strand are always the same.

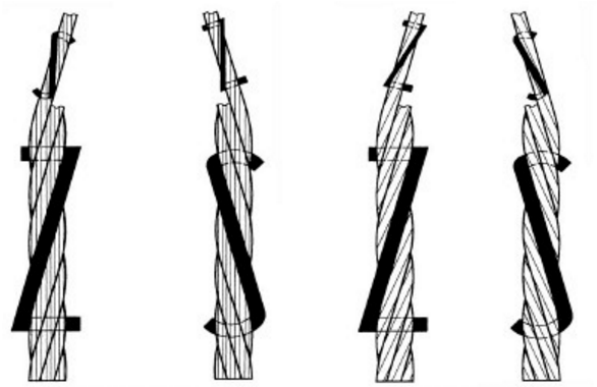

Figure 1.4: Typical wire lays (from left to right: right hand ordinary lay, left hand ordinary lay, right hand Lang's lay, left hand Lang's lay) [5]

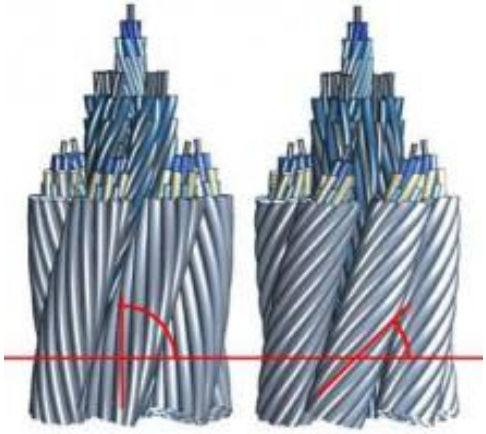

Figure 1.5: Direction of the wires as seen from the outside of the outer strands with respect to the wire rope cross section for ordinary lay (left) and Lang's lay (right) [42]

In ordinary lay ropes, wires are twisted in one particular direction while the strand is laid up in the opposite direction. This results in the fact that wires in strands are parallel to the centreline of the wire rope core when observing the outside of the rope as can bee seen in figure 1.5. The wires are orientated diagonally to the centreline of the rope when they touch the wire rope core. This situation is opposite when looking at Lang's lay wire ropes. Lang's lay is a lay orientation where the strands are laid up in the same direction as the wires they are made of. The wires are now diagonally orientated with respect to the centreline of the core when observing the outside of the rope as can be seen in figure 1.5. Wires make contact with the core of the wire rope when they are orientated parallel to the centreline of the rope.

Due to the helical geometry of wire ropes, torque is introduced when the rope is loaded in tension. There are ropes however that generate almost no torque when loaded in tension. These ropes are called rotation resistant. The characteristic that defines rotation resistant ropes is that the outer layer of strands is wound in the opposite direction of the layer underneath so that the generated torque can be cancelled out. This technique is illustrated in figure 1.6.

Each configuration has its advantages and disadvantages. Lang's lay has the advantage of a better

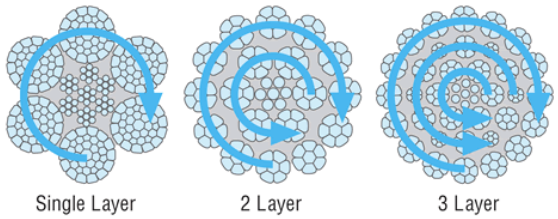

Figure 1.6: Rotation resistant wire rope [46]

connection and behaviour between cable and sheave. However, ordinary lay rope is more flexible than Lang's laid rope which can be spliced more easily, it is therefore considered more convenient to use.

The geometry of a wire rope component such as a strand or wire, can be described by a number of parameters which can be seen for a simple strand in figure 1.7 and are described in table 1.1. These parameters are given for a simple strand but can be implemented on components of larger diameter ropes and strands as well.

Table 1.1: Strand geometry

Parameter	Symbol	Description
Wire lay length	$[h_w]$	The length along the core describing one complete turn of a strand
Strand lay length	$[h_s]$	The length along the core describing one complete turn of a rope
Wire lay angle	$[\alpha]$	The angle between the wire and the centreline of the straight strand
Lay angle	$[\beta]$	The angle between the strand and the centreline of the wire rope
Wire winding radius	$[r_w]$	The radius of the circle passing through the centre of all wire in a straight strand
Strand winding radius	$[r_s]$	The radius of the circle passing through the centre of all strands in a wire rope

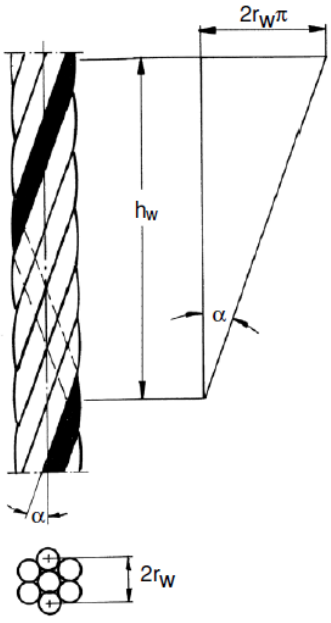

Figure 1.7: Strand properties [10]

In figure 1.7 a helically wounded wire (black wire) is shown in a simple strand along with its most important parameters. However, more complex wire rope configurations such as can be seen in figure 1.14 also have wires which describe a double helix. These wires are located in the first and second strand layer. The method of describing the properties of these wires is as if the wire is located in a straight strand. When combining the parameters from the wires and those of the helically wounded

strand, the geometry of double helical wounded wires in the first and second layer of strands can be derived.

1.2.3. Manufacturing

Steel wire ropes are mostly made out of carbon steel wires with 0.35 to 0.85 % carbon. The rope manufacturing process starts with rods made out of high carbon steel billets in a hot rolling process. Typical dimensions for these rods are between 5.5 to 8 mm. After these rods have been cleaned and inspected they are entered in the drawing process where their diameter will be reduced and tensile strength increased.

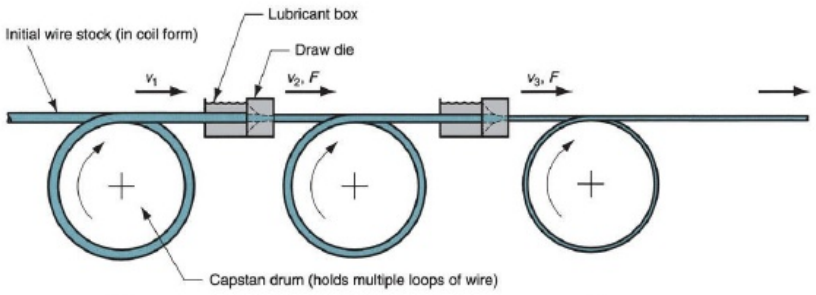

Figure 1.8: Wire rope manufacturing process [15]

The rods enter the drawing process which is schematically shown in figure 1.8. This is a continuous process where in each step, the wire in the making will experience a process called cold forming. Forming at high speed and pressures, cold working of the metal increases the hardness and yield and tensile strengths. In each step the wire is fed through a lubricant bath and a draw die to smoothly reduce its diameter. After going through a draw die the wire has a lower diameter thus increasing the speed of which the wire has to be wound around the next drum to ensure a continuous process. This process will go on until the required diameter and material specifications are reached.

After the wire manufacturing process, strands which make up a wire rope are formed. The individual wires are combined to form a strand. To keep stresses due to the manufacturing out of the wire rope, the wire and strands are pre-formed before they are added to the strand or wire rope. In figure 1.9 an old wire rope manufacturing machine can be seen. The method of manufacturing wire ropes today remains approximately the same. Nowadays, the companies that produce wire ropes keep their machines and manufacturing techniques a secret to the outside world.

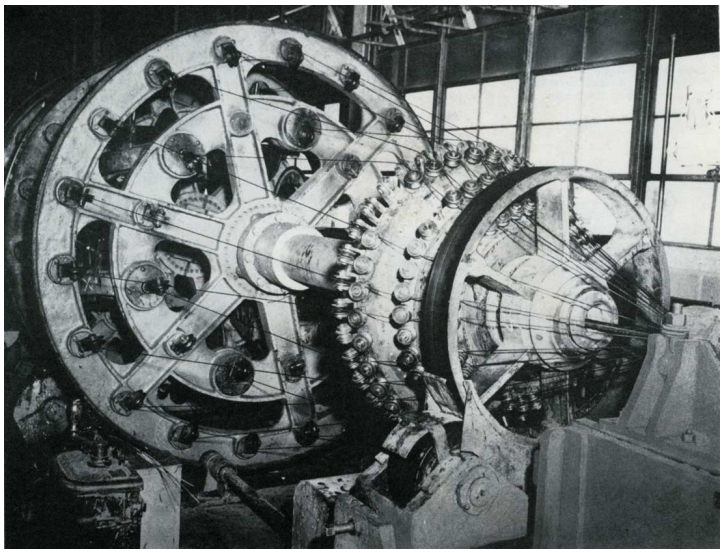

Figure 1.9: Wire rope manufacturing machine [9]

1.2.4. Redundancy

Due to the repetitive or continuous loading of wire ropes, breaks can occur in individual wires due to fatigue or overloading of the rope. Wire ropes have the unique feature that these wire breaks do not necessary have to result in a reduction of the performance of the rope due to the parallel arrangement of the load bearing elements. Clamping and friction forces from other wires in the rope are sufficient enough to keep the wires which can be broken many times along their length in place.

Figure 1.10 shows a schematic arrangement of multiple wires inside a wire rope. Each one of these wires is broken one time along the displayed length. Because of the parallel arrangement of the load bearing elements in wire ropes, the reduction in breaking strength is only reduced locally as can be seen in the schematic graph in figure 1.10.

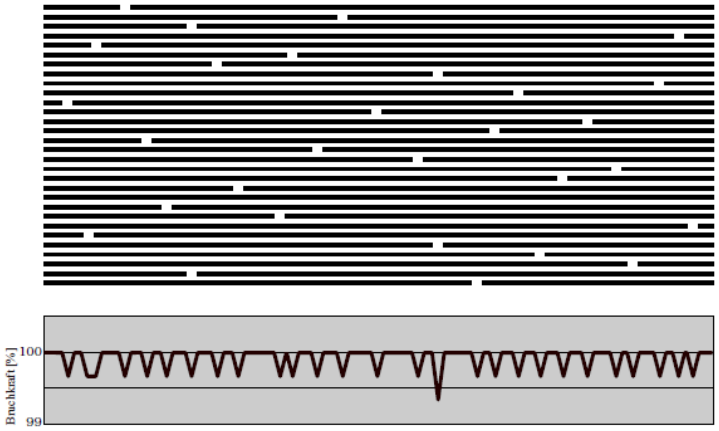

Figure 1.10: Wire breaks and their contribution towards the reduction in breaking strength [50]

However, wire breaks can be dangerous when they are concentrated in one location and the wire rope is loaded critically. For example, suppose the outer layer strand of a wire rope has a large concentration of wire breaks. When loaded in axial direction this rope could be fine as the more inner located wires will take more of the load. When loaded in bending, outer wires will experience more load than the inner wires as they are bended along a large curvature and the rope could fail because off the already weakened section will fail. Hereafter, other wires would have to take over the load and they eventually will also fail.

1.2.5. Loading characteristic

Wire ropes responds differently to loading than rods do. A straight rod or a centre wire will start to elongate linearly according to Hooke's Law as can be seen by the green part in figure 1.12a. After a certain elongation the rod will start to yield an the relationship between load and elongation will be non-linear until the rod breaks.

For a simple strand of six helical wires wound around a core wire, the relationship between load and elongation will be a bit different. The core wire will start to take axial loading immediately at the onset of loading while the helical wires will need some elongation and thus time to resist the loading with their full potential. This is because of their orientation compared to the straight wire. The helical wires will elongate less than the straight wire does when the whole rope elongates.

Pre-tensioning the wire rope is of importance to the loading characteristic as the wires inside the strands have to be in contact with each other so that they can resist the loading with their full potential. This closing of the gap due to pre-tensioning is illustrated in figure 1.11a. Gaps have to be present between outer wires or strands in a simple strand or wire rope respectively to ensure flexibility in bending. The wire rope is designed so that these gaps exist after pre-tensioning the rope.

When a certain elongation is reached, further loads will be spread evenly over all wires and the load-elongation relations will be linear again as can be seen in figure 1.12b. The non-linear behaviour at higher elongations will start with the yielding of the core wire. Hereafter, wires in the penultimate layer will start yielding because they cannot take over the load from the core wire and so on.

When looking at complete wire rope configurations experiencing axial loads, core (straight) wires will take the first loads, it will elongate as a result. When the elongation reaches a certain value, other

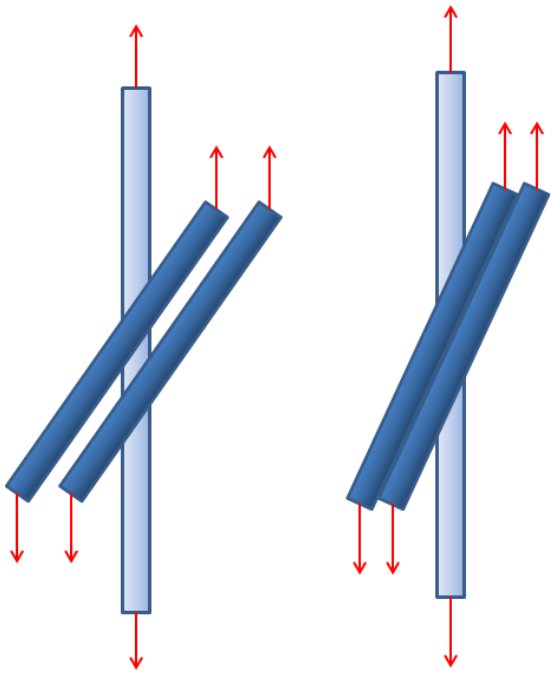

(a) Initial situation with a gap between the helical wires

(b) Deformed situation where the gap is closed and the helical wires will take up similar load

Figure 1.11: Illustration of the initial loading of the helical wires in a strand or wire rope

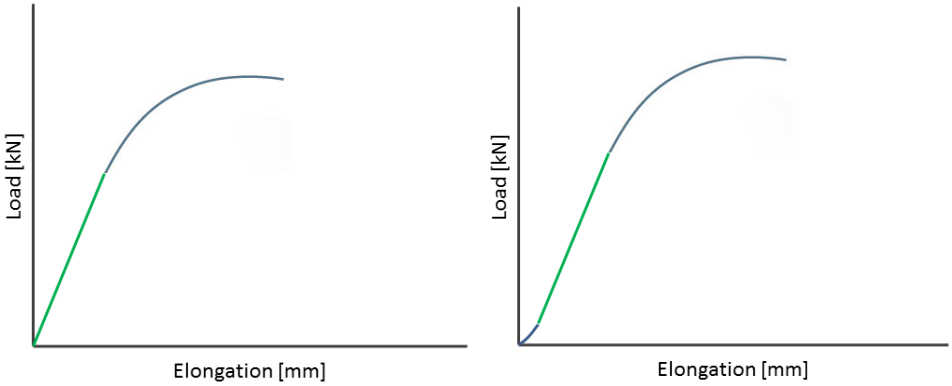

(a) Schematic load-elongation graph for a straight wire [48]

(b) Schematic load-elongation graph for a simple strand [48]

wires will start to take loads until all wires share the increasing load evenly, with the wires in the outer layer being the latest who do so. The behaviour between load and elongation becomes linear if all wires contribute evenly to further loading as can be seen in figure 1.13. The non-linear relation between load and elongation at the start will be longer than that of the strand in figure 1.12b due to the fact that there are more and differently orientated wires in a wire rope that have to be aligned to take axial loads.

1.3. Implementation

In the previous section a short introduction to steel wire ropes is presented. Geometry, configuration and the behaviour towards axial loading is made clear. With this knowledge more can be stated about the implementation of these ropes in offshore operations.

Offshore used wire ropes generally consist of multiple strands and wires that form a large diameter

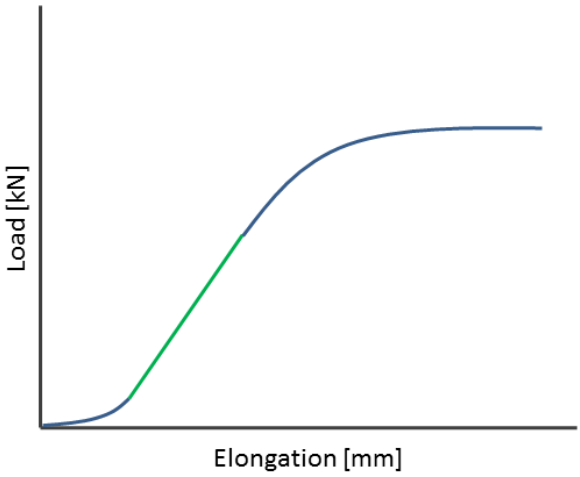

Figure 1.13: Schematic wire rope load-elongation graph [48]

rope. An example of a cross section of a rope that is used in the offshore industry can be found in figure 1.14. The name of the wire configuration is 6x36WS+IWRC, parameters of which can be found in appendix A. The six in the name stands for the number of strands in the outer or in this case the second layer. The 36 stands for the number of wires in one of the second layer strands. WS is an abbreviation for Warrington Seale, describing the way the wires are orientated in the second layer strands. An example of a strand with a Warrington Seale configuration can be found in figure 1.2. All the outer layer strands are wound around an Independent Wire Rope Core (IWRC) which forms the basis of the rope.

As the ”easy to drill” oil fields are depleting, offshore oil companies have to find and extract hydrocarbons in the deeper parts of the ocean. This causes for extra technical challenges, including the need for wire ropes with different properties and dimensions which are able to withstand ever increasing loads and stresses. Steel wire ropes used in the offshore industry are of a large size and complex configuration which contains multiple layers of wires. This results in a difficult determination of their behaviour.

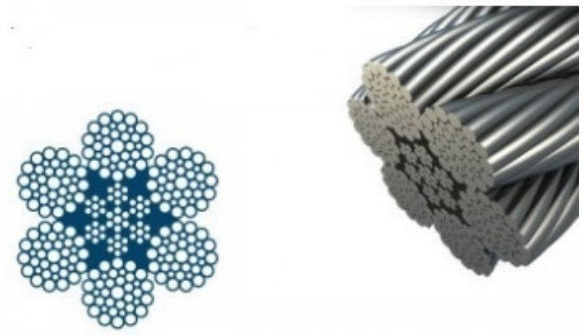

Figure 1.14: 6x36WS+IWRC [23]

1.3.1. Abandonment and Recovery

Allseas uses these steel wire ropes in for example: deep water offshore operations, installation of subsea structures, lifting of jacket legs or the installation of pipelines. An operation which is an essential component of pipe lay is an A&R operation. This operation uses large diameter wire ropes which are prone to failure mechanisms that can influence the outcome of a project. These A&R operations and the accompanying failure mechanisms will be explained in this section.

When installing a pipeline with an offshore vessel, it can be necessary to lay down (abandon) the

pipeline and possibly later pick up (recover) the pipe line. This operation has to be executed in case of bad weather forecasts, operational circumstances or at the end of a pipeline installation scope. The way this operation is executed is by mounting a head on the pipeline with a pad eye which can be attached to a hook via a shackle and a sling. By lowering the hook with the so called abandonment and recovery (A&R) wire to the seabed while maintaining a sufficient horizontal force in the system, the pipeline can be lowered while its structural integrity is warranted. The pipeline can be recovered by the reverse process. When performing this operation in deep water, the helical structure of the rope and the tension gradient along the length of the rope due to the self weight of the cable cause the wire rope to generate torque and torsionally deform.

When a rope stores torsional energy, it is more likely for it to become unstable. Instability of the rope can lead to damage and can bring a project into jeopardy as a new rope has to be installed which can cause delay or even failure of the project. There are a number of factors that contribute to the stability of a rope: tension, bending stiffness and the torsional deformation are considered the most important. The bending stiffness of wire ropes is not a constant value. Complex interactions between individual wires result in a state-dependent bending stiffness which is dependent on tension, friction coefficient, torsional deformation and the curvature of the rope.

Low tension at the bottom end of an A&R wire rope, combined with torsional deformation due to the tension gradient over its length and a low bending stiffness because of a high local curvature, will result in the fact that wire ropes used in A&R operations are prone to a phenomenon called hockling. Hockles or loops in a wire rope (figure 1.15) may cause damage and may lead to failure of an operation. Hockling occurs when a wire rope is slackened while a torque present, so that a section of it forms a loop.

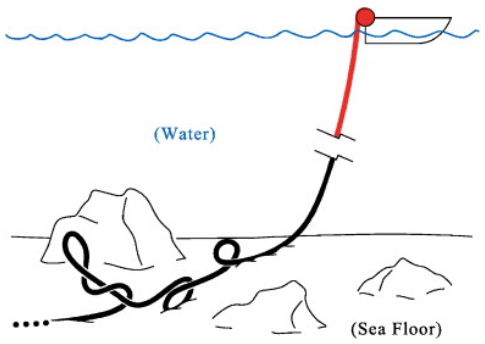

Figure 1.15: Low tension cable forming loops (hockles) at seafloor [13]

This feature is not only present in the offshore industry. Other applications include 'snarling', this is a term used in the textile industry to describe the onset of highly twisted helical plies [12]. The hockling of marine wire ropes is a mechanism that is also topologically equivalent to 'plectonemic supercoiling' of long DNA molecules.

1.3.2. Torsional stability

An introduction has been given about the A&R operation Allseas performs using large diameter steel wire ropes. Stability of a wire rope in these situations has been addressed, accompanied by the main factors that contribute to it: tension, bending stiffness and torsional deformation. This section will address the actual mechanisms that occur in and with a wire rope during for example an A&R operation. Why the main problems with using wire ropes over large vertical distances arise will also be discussed in this section.

A wire rope used horizontally with both ends restricted from twisting while enduring an axial load, will experience forces and moments corresponding to this external tensile force and the cross sectional properties of the wire.

In a horizontal wire rope section which can be seen in figure 1.16 there is an equilibrium of forces

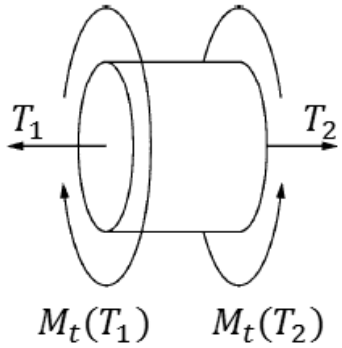

Figure 1.16: Forces and moments on a horizontal cable section [50]

and moments because gravity does not effect the tension or moment along the wire length.

$$T_1 - T_2 = 0 \tag{1.1a}$$
$$M_t(T_1) - M_t(T_2) = 0 \tag{1.1b}$$

The torsional moment generated due to the orientation of the helical wires can be considered equal to equation 1.2. The relationship between tension and torque for the simple strand with dimensions which can be found in appendix A can be seen in figure 1.17. For this figure the equations by Costello [7] are used. The equations from Costello [7] which are used can be found in the appendix in section D.2.

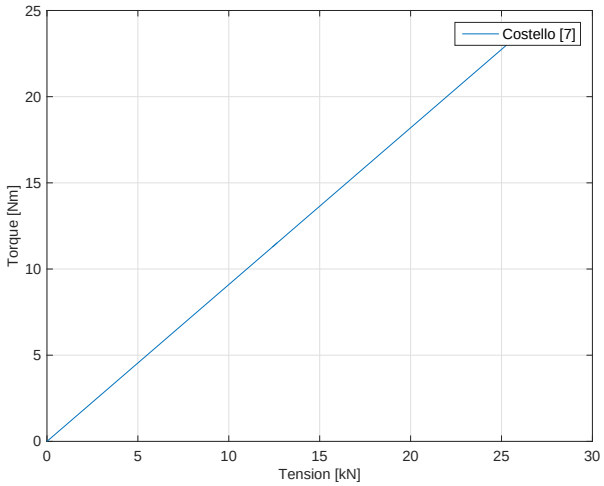

Figure 1.17: Axial-torsion relationship of a simple strand according Costello [7]

$$M_t = c_1 dT. \tag{1.2}$$

M_t is equal to the torsional moment, c_1 is a constant, d is the nominal rope diameter and T is the axial tension. The torsional moment changes if the rope is twisted before loading. According to Feyrer [10] the equation becomes:

$$M_t = c_1 dT + c_2 d^2 T\omega + c_3 G d^4 \omega. \tag{1.3}$$

c_2 and c_3 are constants, G is the shear modulus and ω is the angle of rope twist per unit length. In equation 1.3, two terms are dependent on the twist ω and two terms are equal to the external axial tension T. Values for c_1, c_2 and c_3 are determined in [10] and will not be discussed in this section.

Rope twisting during rope service and installation is almost inevitable. The angle of rope twist ω will assume a certain value and when the external axial tension is reduced to zero there will still be a torsional moment in the system. This is shown by equation 1.4.

$$M_t(T = 0) = c_r G d^4 \omega \tag{1.4}$$

When there is a torsional moment in the rope and it becomes slack, it has the tendency to form a loop. This mechanism is explained in figure 1.18 while using a rubber rod. The twisting of the cable due to axial loading is simulated by turning one end of the rod. When the ends are moved closer together, the rod will start to form a loop. When the tension is removed even further, the loop can transform in a hockle.

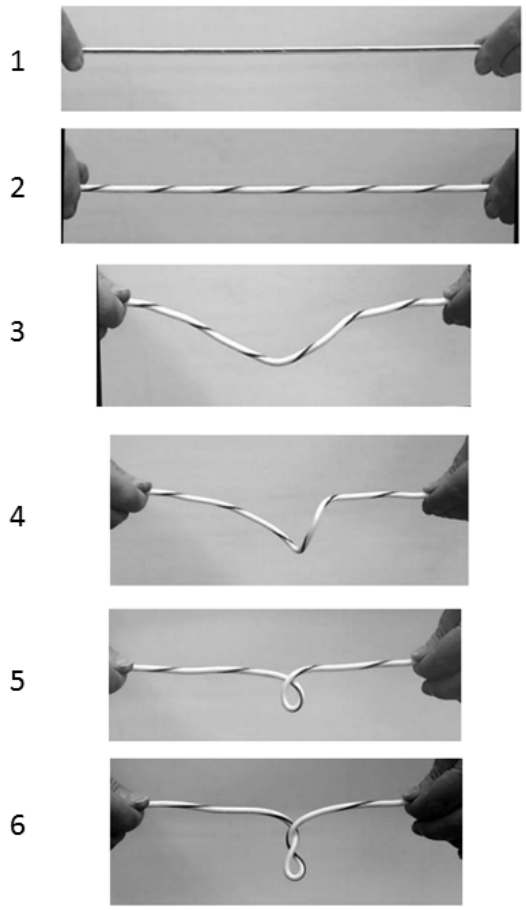

Figure 1.18: Loop forming mechanism from top to bottom: 1: tensioning of the rod, 2: twisting of the rod, (3,4): removing the tension on the rod and the beginning of loop forming, (5): Loop has formed in the rod, (6): The loop has transformed in a hockle [12]

Rope twist can be limited or avoided when using ropes in horizontal applications. If a rope is hanging down vertically, even if both ends are protected against twisting, rope twist is almost impossible to avoid. Because of the self weight of the rope, each rope segment will be effected by the external force plus the weight of the rope hanging underneath it. This will cause the wire rope to have a higher axial tension at the top than at the bottom. In this undeformed situation, per wire rope segment (figure 1.19) there will still be force equilibrium but no equilibrium of moments.

The wire rope will respond to this instability by starting to unlay in the direction of the greater moment so that the moment equilibrium is restored. If both rope ends are fixed, the number of rope lays cannot change. Therefore the rope lay lengths in the upper part of the rope will increase while in the lower parts, the lays will decrease as is visually illustrated in figure 1.20. The F_x in the figure represents the constant torque that has to present over the whole vertical cable length.

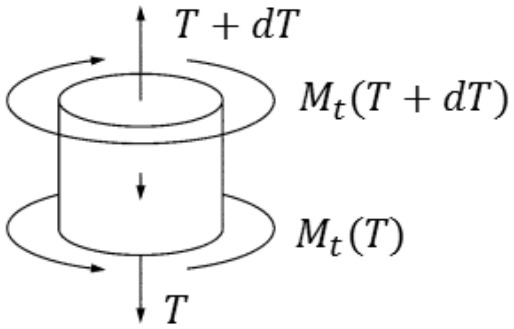

Figure 1.19: Forces and moments on a vertical cable section [50]

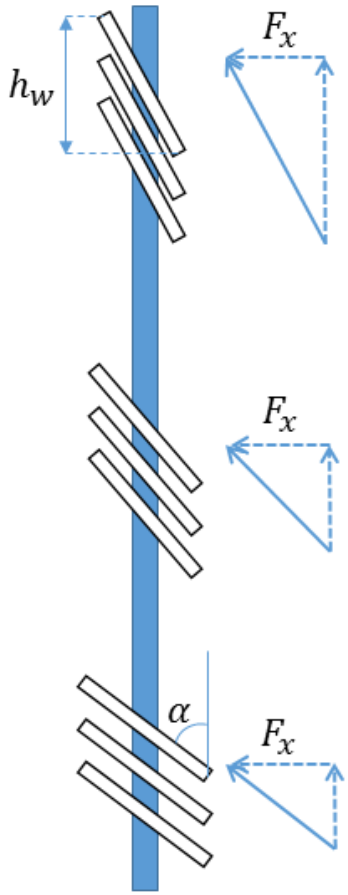

Figure 1.20: Lay angle change in long vertical rope

There will be three sections along the length of the vertical rope where the lay length is equal to the original lay length. This is at the top, bottom and approximately in the middle of the rope as can been seen in the schematic figure 1.21. For clarity a lay length increase corresponds with a decrease in lay angle as is also illustrated in figure 1.20.

Slack in a rope is most likely to occur at the lower end of the cable when for example a load is set down on the seabed. Slack in combination with a torque will cause a rope to be in danger of forming loops or hockles which are previously mentioned in section 1.3. This torque will be present due to the tension gradient and the helical orientation of the wires in a cable which has been explained in section 1.3.2. Because of the lay angle increase in the lower parts of the cable the bending stiffness will reduce [55], which will decrease the resistance to loop formation even further. This statement is numerically

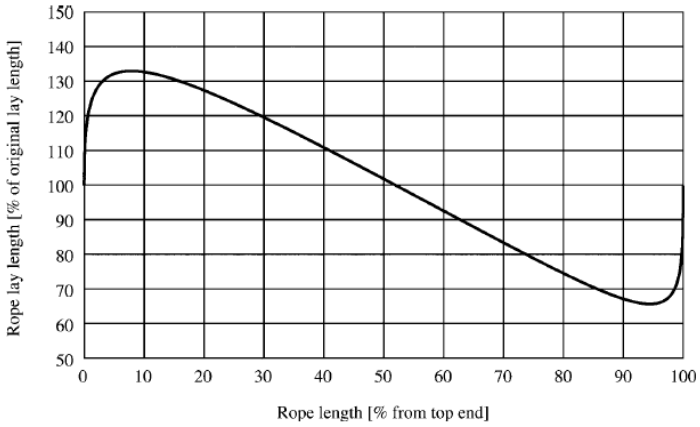

Figure 1.21: schematic graph of the change of lay length along the length of the rope [49]

analysed further on in chapter 4.

Hockling as a result from loop formation happens rather quick and so wire breaks have been reported as a consequence [49]. The damage due to hockling can be seen in the examples from figure 1.22. These wire breaks are generated on a single location along the length of the rope and can be very concentrated thus reducing the breaking strength of a wire rope significantly which was discussed in (section 1.2.4). The real problem occurs when tensioning a rope after it has formed a hockle somewhere along its length. This could result in a knot or when the hockle remains intact during tensioning, the rope could tare itself appart due to the generation of excessive shear forces.

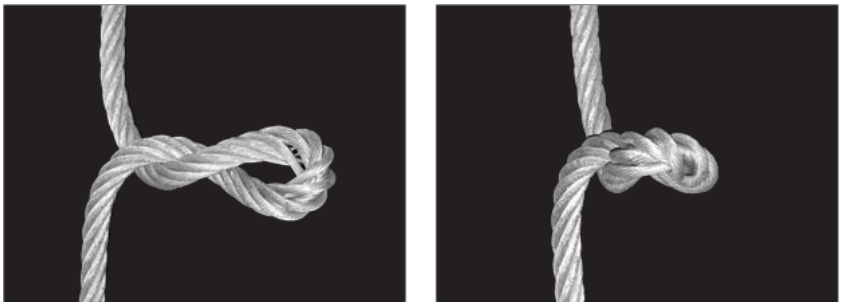

Figure 1.22: Damage to wire ropes because of hockling [51]

1.4. Problem definition & research questions

Previous sections of this chapter have provided information about steel wire ropes and their usage in offshore operations. Now that the basic knowledge about the subject is acquired, the problem definitions will be elaborated upon in this section.

The objective of the industry is to numerically model the state-dependent bending stiffness of steel wire ropes used for A&R operations. The influence of the tension and torsional deformation on the bending behaviour is also taken into account. As is shown before, these parameters influence the likelihood of hockling of wire ropes during A&R operations. More knowledge about the bending stiffness of wire ropes will provide Allseas with more understanding about the operational limits of an A&R procedure involving wire ropes, as more can be stated off the likelihood of loop formation and hockling.

To this day it is common practice at Allseas to assume that the bending stiffness of a wire rope is equal to the theoretically determined minimum possible value. This results in conservative values for the torsional instability of wire ropes and to the prediction of loop formation and hockling. Investigating the state-dependent bending stiffness of steel wire ropes into more detail can lead to a better understanding about the stability of wire ropes used during an A&R operation.

A better understanding of the bending stiffness of steel wire ropes is not only important to the offshore industry. Mining operations require steel wire ropes of immense length where torsional stability

has to be monitored closely to keep all mining operations safe. Lifting of objects with multiple wires in the construction sector is another example of an industry which would greatly benefit from more knowledge about the bending stiffness of steel wire ropes. Rope lengths are not that long in these lifting configurations compared to those used in offshore or mining applications, nevertheless a phenomenon called ”Cabling” which is triggered by the same parameters as are found during hockling. This can be explained in more detail if more information about the bending stiffness is acquired.

Numerical finite element modelling (FEM) is used to improve understanding about the main objective of this research, which is consequently the *description of the bending behaviour of steel wire ropes and the impact on A&R operation operability*. The objective is divided into four parts, each with a set of associated questions which serve as a guidance throughout the report.

Create an overview of all available research on wire rope modelling:
Which modelling techniques can be used to describe wire rope bending behaviour?
Which modelling technique corresponds best with experimentally found results?

Elaborate and study the chosen modelling technique:
What are the main advantages and disadvantages of this model?
Which assumptions are taken into account and how do they affect the model outcome?
Do the results from the model resemble those generated with experiments?

Evaluate and describe the generated numerical model:
What are the advantages of numerical modelling compared to the analytical model?
Can numerical modelling be applied to every wire rope geometry and configuration?
Which uncertainties do the results of numerical modelling have?

Implement the state-dependent bending stiffness in a wire rope model to simulate critical situations during A&R operations:
Are the results from the simulation using the state-dependent bending stiffness derived in this thesis different than the current method used by Allseas?
What does Allseas gain from the knowledge constructed in this report?

1.5. Report outline

The thesis is divided into seven chapters: (1.) *Introduction*, (2.) *Wire rope modelling*, (3.) *Bending stiffness: Analytical analysis*, (4.) *Bending stiffness: Numerical analysis*, (5.) *Results*, (6.) *Practical implementation: Beam model simulation*, (7.) *Conclusions and recommendations*.

The first chapter consists of an detailed introduction to steel wire ropes, including its history and use in the offshore industry. The problem definition as well as the main questions to be answered in this report are clarified in this chapter. The second chapter is about all previous wire rope models that have been derived to research the behaviour of wire ropes under tension, bending and/or torsion. All relevant research has been categorized and shortly addressed. Two types of analyses regarding the bending stiffness of wire ropes have been elaborated upon in this thesis and are divided into the two chapters Analytical and Numerical analysis. In the first chapter, an existing analytical model has been worked out and evaluated. A numerical analysis using a finite element program is performed in the next chapter and compared to the analytical results from the previous chapter. Both analyses will be used in the practical implementation to calculate the impact of the differences between both models in a realistic situation. The last chapter is used for conclusions and recommendations where answers to the research questions are given and recommendations are made for further research concerning the same or similar topics.

2

Wire rope modelling

The purpose of this chapter is to gain insight into the developments in modelling wire ropes with a focus on bending behaviour. The final goal is to select a consisting analytical model to compare the in this thesis generated numerical model to.

Modelling considerations which are used for these models will be discussed. These modelling considerations are divided into subcategories explained in section 2.1. The change of wire orientation during axial loading or bending is discussed in section 2.2 to understand the change in wire rope response when it is deformed in axial or rotational direction.

Previous wire rope research and wire rope models are described in section 2.3. After a discussion comparing all models, the model is chosen which resembles reality in the best way. The numerical model generated in this thesis will be compared to the analytical model chosen in this chapter.

2.1. Modelling considerations

The main goal of a wire rope model is to map the behaviour of a certain property of that rope. Because of the complex geometry of wire ropes, it is hard to take all mechanisms and parameters into account when modelling analytically. Modelling considerations have to be assumed, depending on the information being sought. The impact of the assumptions made has to be checked and monitored for its influence on the desired parameter. The modelling consideration topics treated in this section are considered the ones having the most impact on the results of the corresponding model. All assumptions can be subdivided into the following categories:

1. *Boundary conditions*
2. *Inter wire contact*
3. *Wire cross sectional geometry*
4. *Radial contraction*
5. *Additional wire forces and moments*
6. *Friction regimes*
7. *Lay angle*
8. *Material*

All cable models need a number of hypotheses and assumptions that have to be implemented to simplify the calculations. In the following subsections, these hypotheses and their repercussion on the outcome will be discussed.

1. *Boundary conditions*
Boundary conditions describe the allowed movement of helical and core wires at both ends of the rope. In general, the wire/strand length under investigation is assumed to be long enough so that the effect of the boundary conditions implied can be neglected. When comparison has to be made between a model where a limited strand length is considered and experimental results, the influence of the boundary conditions on the outcome of the model has to be checked.

A very short model could neglect mechanisms that only play a part in longer cables such as the axial torsional relationship and the lay angle change it accommodates as was explained in section 1.3.2. Models which focus on large scale mechanisms could miss the small interactions that take place on a much smaller scale. Neglecting these interactions could effect the results they generate.

2. *Inter wire contact*
Assuming a strand where all wires are ideally configured, three possible contact conditions can exist in the strand: interlayer, intralayer and mixed contact. The first two contact conditions are illustrated in figure 2.1.

- Interlayer: A condition where there is no contact between wires in the same layer. Commonly present in wire ropes or strands with small lay angles.
- Intralayer: Wires will only have contact with adjacent wires which are present in the same layer and no or negligible contact with wires from other layers. Commonly present in wire ropes or strands with large lay angles.
- Mixed: Both inter- and intralayer contact exist.

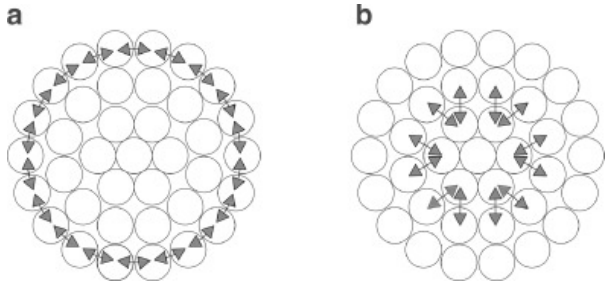

Figure 2.1: Spiral strand rope used for the visualisation of different contact modes (a) intralayer contact; (b) interlayer contact [11]

These contact conditions depend on the way the strands and wires are orientated in the cable or strand respectively. This is influenced by for example the manufacturing process, wire breaks, or gaps between individual wires.

Intralayer contact modes have been implemented by many authors in the past such as Feyrer [10] and Costello [7]. This type of contact takes place along a continuous line resulting in intralayer friction as a result from hoop actions. However, typical strand constructions allow for intra-layer gaps which deny the aforementioned circumferential contact to be realised. These intra-layer gaps can be generated by strand manufacturing or wear and tear of the wire rope during its lifetime [20]. When there are intralayer gaps between wires only interlayer contact can be present.

3. *Wire cross sectional geometry*
When small lay angles are assumed (typically, from $5°$ to $20°$ [4]) cross sections of the round shaped helical wires within a strand are approximately elliptical. For lay angles larger than $40°$ [4], this cross sectional shape cannot be considered elliptical any more.

The contour of a round strand wire in a cross section perpendicular to the strand axis is not circular but assumes a ”kidney” shape as can be seen in figure 2.2. In this particular example, the lay angle has been given the value $\alpha = 60°$ which is a much higher value than is used in practise. By selecting a high value, the effect of a changing cross sectional geometry can be made more clear.

The fact that the contour of a wire in a strand perpendicular to the strand axis is of a kidney shape will have an influence on the calculated clearance between wires. This again has an effect on the

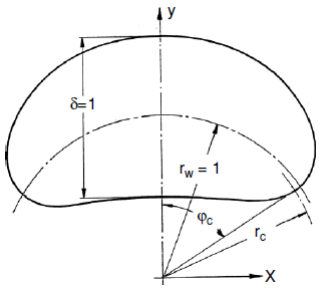

Figure 2.2: Contour of a round lay wire in the section perpendicular to the strand axis [10]

contact conditions considered and thus on the interaction between wires inside a rope or strand. It will also have an influence on the cross sectional area as it is larger than that corresponding to a wire in a strand with a lower lay angle.

4. *Radial contraction*
Poisson's ratio is the ratio of transverse contraction strain to longitudinal extension strain in the direction of axial force. The length related radial strain between the wires is very small in a strand. Therefore, the deformation of the wire circumference and the wire diameter is mainly caused by the elongation of the wire. The effect on strands is difficult to determine but it is known that the influence of the Poisson's ratio declines with an increasing number of wires [10].

Wire ropes are commonly under tensile loads which result in a clamping effect of outer on inner wires due to their helical geometry, thus introducing normal stresses which have an effect on the cross section of the wires. Transverse contraction of the wires due to the Poisson's effect and because of these local contact deformations, contact conditions of the model will be influenced. The main consequence is that the wire rope and individual wire diameters and circumferences will start to decrease as the tension on the rope increases which could lead to larger stresses.

5. *Additional wire forces and moments*
During the axial loading of a wire rope, tensile loads will be distributed over all individual wires. Due to these tensile loads, wires will experience friction loads, shear force, bending and torsion loads due to their kinematic properties within the strand. The to be researched parameter can depend on all or some of these loads and forces. Taking the correct mechanisms into account and neglecting others which do not influence the result can reduce model complexity significantly.

6. *Friction regimes*
The way friction plays a role in wire ropes is best described by Papailiou [33]. While bending a strand, three friction regimes can be defined, these regimes can be identified by figure 2.3 which displays a relation between bending stiffness and curvature of a simple strand [33].

- Stick regime: The friction between individual wires and core wire are considered to be large enough to prevent the wires from slipping relative to each other and the core wire.
- Transition regime: The curvature of the strand is increased so that some wires in the strand will start slipping over a limited amount of their length.
- Slip regime: When the curvature of the strand is increased even further, the fully slipped regime is reached where all wires are slipping until eventually they are slipping over their entire length and the minimum bending stiffness is reached.

By neglecting this state-dependent bending stiffness in bending related models, especially at low curvatures where this change has the most impact, not all information is taken into account and results have to be interpreted with caution.

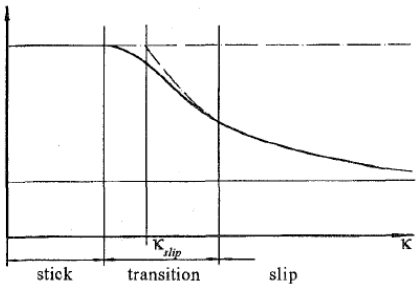

Figure 2.3: Bending stiffness as a function of cable curvature [34]

7. *Lay angle*
The lay angle of wires in a strand has an influence on the geometry of the cross-section perpendicular to the strand axis as has been explained before and can be seen in figure 2.2. The lay angle will influence the width of the gap between wires in a layer. As the lay angle increases, the gap between adjacent wires will diminish. This has a profound effect on the contact conditions. The lay angle of wires in a strand could change while the strand bends, elongates and/or rotates. This effect can change the contact conditions during loading.

Because of the tension gradient in vertically suspended wire ropes, lay angle variations influence the axial and bending response of wire ropes as the geometry of a wire rope changes with it. Lay angle change due to the tension gradient has been explained in section 1.3.2. As will be seen later in this thesis, a change in lay angle also has an effect on the state-dependent bending stiffness of a rope or strand.

8. *Material*
The material is commonly chosen to be linear elastic and isotropic to simplify the mathematical model. Other material choices are possible, although they could complicate the system.

2.2. Wire kinematics

Modelling considerations mentioned in section 2.1 will have to be addressed while working with wire rope models as they can influence their outcome. If it is chosen to neglect some of these considerations, it has to be checked if and how these assumptions will influence the results.

Kinematic parameters of a wire inside a rope are very much different for a wire in a straight or in a bent rope. Due to the change in kinematic properties, stresses and forces will be distributed over the wire length differently when rope curvature increases.

Due to the helical structure of wires around a rope, not only axial forces in each wire arise during tensioning. Bending stress and torque can be found in the individual wires. Due to bending and torsion of the wires, it's geometry will change under tension. To properly map the bending and torsion stresses in a wire and of the strand, curvature and torsion along the wire length have to be determined. For straight stranded ropes the value for the curvature and torsion of a helical wire will be constant.

During bending of a wire rope, the orientation of the wires that move helically along the strand will change as can be seen in figure 2.4.

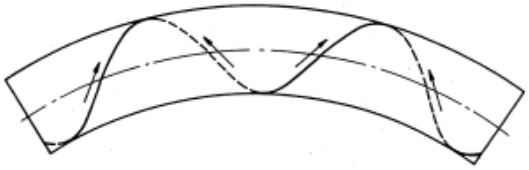

Figure 2.4: Bended wire rope [10]

Because of this change in orientation, curvature and torsion will no longer be constant over the length of the rope, which was still the case when considering straight wire ropes. Figure 2.5 shows the

first full rotation of a wire corresponding with six different strand curvatures, each situation corresponds with a strand curvature displayed in the legend.

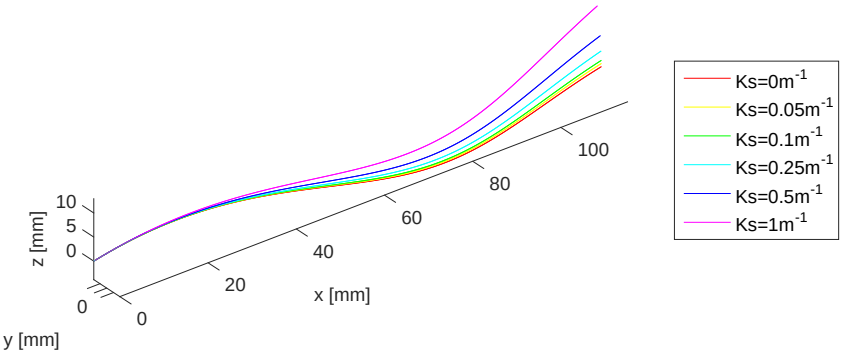

Figure 2.5: Helical wires for different strand curvatures (Ks)

Using Frenet-Serret equations which are worked out in appendix B, curvature and torsion of the wire along its length can be derived. With zero curvature of the strand, the wire curvature and torsion will remain constant. With increasing strand curvature, the wire curvature and torsion along the wire length will assume a sinusoidal shape with opposing phase. It can be seen in figure 2.6 that the absolute difference between the average curvature and torsion corresponding with $k_s = 0\text{m}^{-1}$ with their maximum value along the first half of the pitch length of the strand is larger than that of the second half. This is because of the effect displayed in figure 2.4, where it is shown that wires inside a bended rope will move towards the more stretched part of the strand.

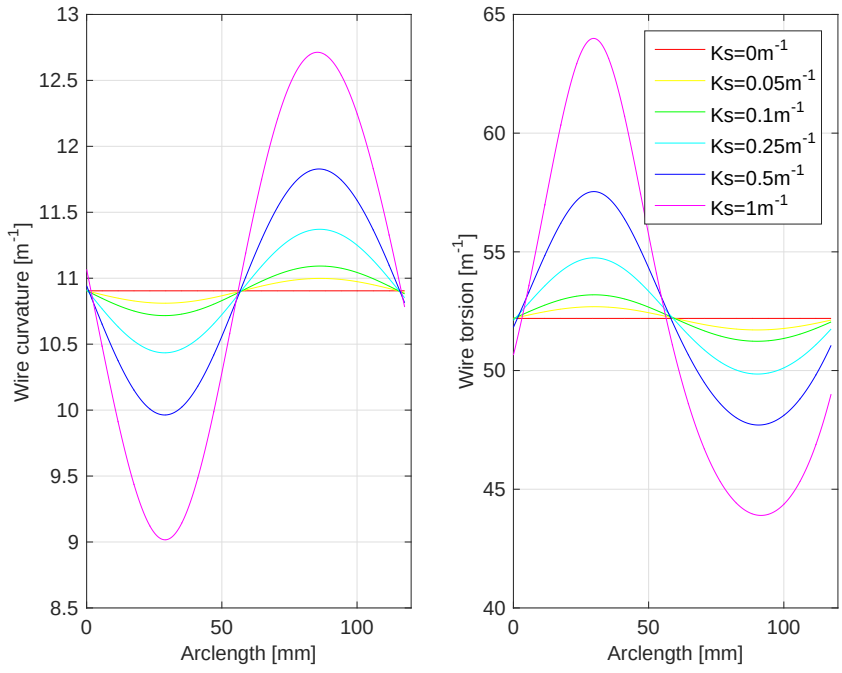

Figure 2.6: Curvature and torsion as a function of arclength for different strand curvatures Ks

More mechanisms that enhance the differences in wire stresses are the change in lay angle along the different layers of wire. As individual wires in the strand have a variable curvature and torsion along their length they will also experience a variable axial force.

The fact that there is spacing between individual wires before the moment of tensioning results in non-immediate loading of all the wires at the start, which makes behaviour of the cable at the start non-linear. These gaps between wires and strands also have a positive effect on the ropes. The fact that ropes can bend more easily than solid beams is because they consist of wires and/or strands which

can move independent of each other due to the gaps between the wires and the slipping condition that is reached with increasing curvature. This effect has been explained previously in section 2.1.

2.3. Previous research

Now that most modelling considerations have been discussed and the way wires in strands and ropes behave when deformed has been analysed, previous research can be presented. This section will start with a short history on cable modelling and a quick explanation of the model categories present.

The first cable models date back to the 1950s, with the researching of stresses and strains of wires in wire ropes. The first models described wires as springs which are loaded in tension to simulate the properties of a cable. This method neglected any bending or torsional stiffness. For small diameter cables these assumptions would not influence the results. However, for offshore applications, cable dimensions are such that the bending and torsional stiffness do play a significant role in the characteristics of a steel wire rope thus using these early models would not be preferable.

An early way to take these stiffness's into account is to model the cable as a beam or thin rod, which would lead to the so called thin rod models first described by Costello in his book *Theory of Wire Rope* [7].

Semi-continuous models were created later and are first described by Jolicoeur and Cardou [20] and Raoof and Hobbs [37]. The strategy used in these models is to create homogeneous layers out of the helically twisted wires in a wire rope. Each layer is then modelled as a cylinder or sheet with its own properties.

Using these methods described above, a large number of papers have arisen on the subject, which can be explained by the great variety of parameters and situations that can be investigated. The three aforementioned modelling techniques, spring, thin-rod and semi continuous modelling are used for computing both the behaviour of strands and ropes under axial loading and under bending. All these modelling methods provide answers taking different modelling conditions into account such as they are defined in section 2.1.

Papailiou [33] created a promising model which fits in the thin-rod category that combines the loads in tension and bending. The model incorporates friction and the stick-slip behaviour between the wires. This will result in a state-dependent bending stiffness depending on tension, friction coefficient, lay angle and the curvature of the wire rope. Because of this state-dependent bending stiffness, according to his model, the cable will have a non linear bending behaviour, as has been verified by experiments. Hence, it is realistic [52]. He described the three different regimes; stick, transition and slip, which are explained in section 2.1.

A relatively new method of modelling wire rope is the use of finite element method (FEM) to model wire ropes. This technique is used in this thesis to compute a model of a simple strand and of larger configurations to compute their response to bending.

All advantages and disadvantages of the four aforementioned modelling techniques will be discussed in the next sections. Hereafter, one of the analytical models is chosen as the most reliable and realistic after which it will serve as comparison to the numerical model generated in this thesis.

The four modelling categories are:

1. String/beam
2. Thin-rod
3. Semi-continuous
4. Finite element

2.3.1. String/beam models

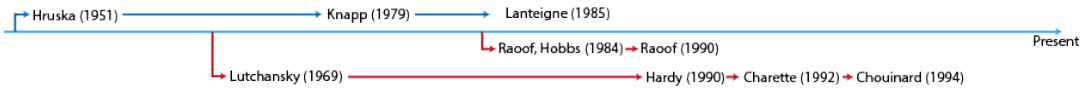

Figure 2.7: Time line string models

Table 2.1: Modelling consideration for string/beam models

Modelling consideration	
Boundary conditions	No boundary condition effect; zero end rotation is assumed
Inter wire contact	Purely interlayer contact is assumed
Wire cross sectional geometry	Cross sectional geometry is not considered as wires are infinitely thin
Radial contraction	Radial contraction is neglected
Additional wire forces and moments	Wires are assumed to be subjected to tensile forces only
Friction regimes	Friction is neglected
Lay angle	The lay angle is assumed constant over the length of the wire
Material	Material is considered linear elastic

The first string/beam model from Hruska [16] was based on the simplest of hypotheses [4]. These accompanying modelling assumptions can be found in table 2.1.

The equations from Hruska [16] have been extended and improved over the years by various other researchers to incorporate more level of detail. Representative governing equations for the string/beam models are

$$\text{String: } m\ddot{w} - Tw'' = 0$$
$$\text{Euler-Bernoulli: } \rho A\ddot{w} + EIw'''' - Tw'' = 0$$
$$\text{Timoshenko: } \rho A\ddot{w} - KGA(w'' - v') = 0, EIv'' + KGA(w' - v) = 0.$$

Meaning of the different variables can be found in the nomenclature. Starossek [44] discussed the history of string models from the 18th century to the present. His work includes the basic equations and explanation on how these models are derived and presented. As mentioned before, these models do not include any bending and torsional stiffness.

Modelling a steel wire rope as a collection of multiple ”beams”, increases the level of detail. Beams are outfitted with properties developed to correctly incorporate the bending and torsional stiffness of the rope. Lutchansky [26] proposed a model where this method will be used to compute the behaviour of the bending of strands. Hereby it is assumed that the wire diameter is very small compared to the helix radius.

In short, string/beam models are among the first methods for describing the characteristics of helical strands and cables. They include models which use simple but efficient methods for computing the desired parameter but lack detail in some regions as for example friction is mostly neglected and wires can only be in interlayer contact.

2.3.2. Thin-rod

Figure 2.8: Timeline Thin-rod models

Thin-rod models can incorporate more detail and more realistic modelling considerations such as can be seen in table 2.2.

Thin rod theory was a leap forward in cable modelling. This was introduced when Costello [6] presented a helical rod model based on Love’s equations for the equilibrium of a curved rod [25]. Velinsky [47] incorporated bending and torsion and modelled the wires of a steel wire rope as thin rods. When modelling the wires of a rope as thin rods, cable geometry (Figure 2.9) is of major importance. At first, the bending stiffness of the entire rope was modelled as the sum of the bending stiffness’s of al individual wires. Inter wire friction was supposed to be non existing which would result in conservative values regarding the bending and elongation of the rope under stress.

Continuing from the models at hand, Jiang [18] incorporated small lay angle variations of the length of the strand and presented a linearised solution.

Table 2.2: Modelling consideration for thin-rod models

Modelling consideration	
Boundary conditions	No boundary condition effect
Inter wire contact	Inter- or intralayer contact can be assumed
Wire cross sectional geometry	Cross sectional geometry is not considered as wires are assumed infinitely thin
Radial contraction	Radial contraction is neglected
Additional wire forces and moments	Wires are assumed to be subjected to tensile forces and moments
Friction regimes	Friction is mostly neglected but is incorporated into modern thin-rod models
Lay angle	Lay angle can be assumed to be constant or changing over the length of the wire
Material	Material is considered linear elastic

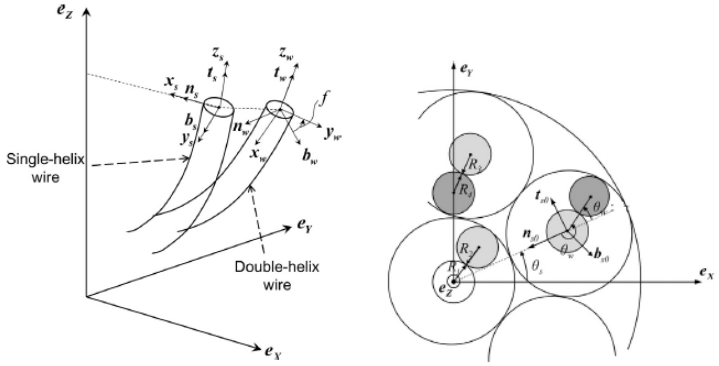

(a) Local coordinate system of a wire

(b) Geometric features o the cross-section of a rope

Figure 2.9: Geometric properties [33]

In a model described by Raoof and Davies [36], a simplified method to determine the bending stiffness of a single strand was presented. However, to come up with a solution they had to assume that the contributions from all other internal moments and forces that would exist in the entire cable are sufficiently small so that they could be neglected. Another assumption was that the lay length of the cable would not change in loaded and unloaded condition.

Wire bending and its influence on slip and stick regimes in the strand has been thoroughly addressed by Papailiou [34], where the slip criterion was based on the difference between tension along a wire in a strand.

Over all, Raoof and Hobbs [38] compared different kinds of models and found that thin-rod theory became more reliable when modelling small diameter cables with fewer strands because of the high level of geometric detail that the model requires.

2.3.3. Semi-continuous

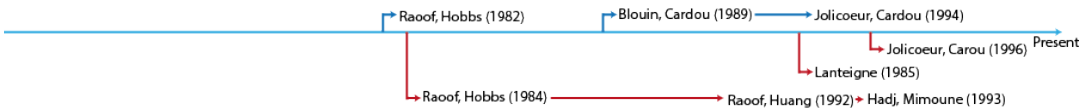

Figure 2.10: Timeline Semi-continuous models

A semi-continuous model is a collective name for orthotropic sheet or cylinder models. The modelling considerations present in these models can be found in table 2.3.

Semi-continuous models were created by Raoof and Hobbs [37]. This type of modelling is best described by using their own words. ”In essence, the individual layers of wires in a multi-layered strand are treated as a series of partly self-pre-stressed cylindrical orthotropic sheets whose non-linear elastic properties are averaged to form an equivalent continuum.” [38]. Semi-continuous modelling is particularly efficient for larger diameter cables consisting of spiral strand where these strands can be simplified by making use of orthotropic sheets. When considering axial loaded strands the method allows for the

Table 2.3: Modelling consideration for semi-continuous models

Modelling consideration	
Boundary conditions	No boundary condition effect
Inter wire contact	Inter-, intralayer or mixed contact can be assumed
Wire cross sectional geometry	Cross sectional geometry of the wires is replaced with that of a sheet or a cylinder
Radial contraction	Radial contraction is neglected
Additional wire forces and moments	Wires are assumed to be subjected to tensile forces and moments
Friction regimes	Friction is mostly neglected but is incorporated into some semi-continuous models
Lay angle	Lay angle is assumed to be constant over the length of the wire
Material	Material is considered linear elastic or hypo elastic

quick calculation of axial and torsional stiffness as has been done by Raoof and Hobbs [4]. The main advantage of these types of models is that they simplify the problem of inter-wire contact significantly over thin-rod methods. The model created by Raoof and Hobbs [37] used kinematic relations based on the discrete theory of strands while assuming thin cylinders, thus making a bi-dimensional problem (plane stress) with material elastic properties defined in the tangential plane of the layer [19]. Slip is chosen to occur between wires of the same layer which mainly has an influence on the torsional stiffness of the cable. The model has been improved and extended over the years by Raoof and Huang [39] and Mimoune et al. [31]

Jolicoeur and Cardou [20] also made use of the orthotropic sheet model. The main difference from the model by Raoof and Hobbs [37] is that the model is based on continuum mechanics and that the sheets are considered thick walled so that they can be modelled as cylinders. This orthotropic cylinder model (figure 2.11) describes the problem in three dimensions with material properties in three orthogonal directions. An important feature of the model by Jolicoeur and Cardou [20] is that: in bending, the model is extremely sensitive to the shear modulus while in the model by Raoof and Hobbs [37] this is not the case.

Another extended version of the orthotropic sheet model has been derived by Blouin and Cardou [2] where the model also consists of orthotropic cylinders, but with variable thickness. These models were used to determine the axial behaviour of ropes.

Jolicoeur and Cardou [20] discus the main differences and features of the orthotropic sheet and cylinder models described above. In their conclusion they depict that for bending predictions, the model by Jolicoeur and Cardou [20] should be preferred because it has the capability to produce stiffness results in the complete range between theoretical minimum and maximum. On the point of shear modulus evaluation, it appears that this model is preferable for torsion stiffness predictions while the model by Raoof and Hobbs [37] is preferable in bending [19].

These semi-continuous models are mostly used for spiral stranded ropes with wires in concentric layer configurations. Wire ropes used in the offshore industry consist of more complex configurations. No semi-continuous models can be found which describe these wire ropes.

2.3.4. Finite Element Models

Table 2.4: Modelling consideration for finite element models

Modelling consideration	
Boundary conditions	Boundary conditions do have an effect on results
Inter wire contact	Inter-, intralayer or mixed contact can be assumed
Wire cross sectional geometry	Cross sectional geometry (the kidney shape) is realistically defined such as in figure 2.2
Radial contraction	Radial contraction can be taken into account
Additional wire forces and moments	Wires are assumed to be subjected to all possible forces and moments
Friction regimes	Friction can be taken into account
Lay angle	Lay angle change over the length of the wire will depend on the selected boundary conditions
Material	Material is considered linear elastic or hypo elastic

Three-dimensional (3D) finite element methods (FEM) have been created to study the axial and bending behaviour of steel wire ropes. Pure bending behaviour without friction was one of the first researches that have been performed using finite element methods. Jiang [18] created such a finite element method where the bending moments from the numerical model matched that of the analytical

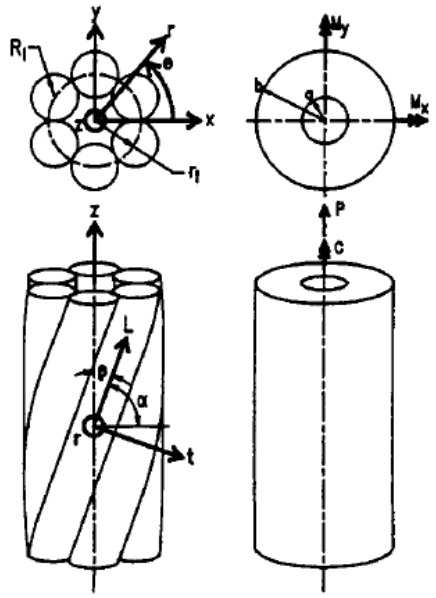

Figure 2.11: Geometry of one layer of wire with equivalent orthotropic cylinder [20]

model by Costello [7]. However, only Zhang and Ostoja-Starzewski [55] constructed a finite element model specifically focused on the bending stiffness variation of cables with friction. In the paper a simple strand was modelled with Coulomb friction present between the wires and core in all contact conditions. Stick, transition and slip regions have been analysed and compared to the analytical models derived by Papailiou [33].

Finite element modelling has offered a means of predicting the friction condition and behaviour of bent cables in recent years [54]. However, these models require numerous elements to be generated, thus computational time is considerable. This relativity new type of modelling has potency to find solutions which resemble the results from experiments in the best possible way currently available.

2.3.5. Evaluation

Now that all categories have been treated along with their advantages and disadvantages the best model for generating bending stiffness can be selected. This is done by reading the researches described in this chapter and comparing results and methods found and used.

The amount of interest in finding solutions to unknown behaviours and parameters of wire ropes is substantial. Over the years, techniques have improved so that users of steel wire ropes have a better understanding of their behaviour. A model in which the bending moment contribution comes mostly from the tension effect, calculated using the Euler-Bernoulli hypothesis and from independent wire bending is found to resemble experiments best. As curvature increases, outer layers will start slipping which will result in a state-dependent bending stiffness. The theory from Papailiou [33] uses this method to provide slip criteria for different wire elements inside strands and wire ropes. Static bending tests on transmission line conductors were performed where a transverse centre load was applied on the cable. The paper [34] shows the deformed shape of the specimen. Measured and calculated values for the bending stiffness is found to be in good agreement. However, the analytical model by Papailiou [33] is based on assumptions and uses the theoretical limits for the minimum and maximum bending stiffness which will be explained in the next chapter. Because of the good comparison with experimental results, the model by Papailiou [33] can be assumed realistic for simple strands and spiral strands such as transmission line conductors.

Numerical models can provide more insight in the validity of the assumptions and theoretical limits stated in the analytical model. Larger and different wire rope geometries can be modelled more easily using numerical modelling. Finite element models such as the ones generated by Zhang and Ostoja-Starzewski [55] and Yu et al. [54] already provide information about numerical modelling of simple or spiral strands comparing their results to the thin-rod model by Papailiou [33]. However, these models do not research the validity of all the assumptions made by Papailiou [33] and so a more extensive

research is needed.

Independent Wire Rope Cores (IWRC's) or other larger and more complex stranded rope configurations however have not been researched using numerical and analytical models. In this thesis, numerical modelling will be used to generate results for larger wire rope configurations. The drawbacks and difficulties will also be addressed.

A numerical model is created in this thesis to test the validity of the assumptions and limits of the model created by Papailiou [33]. Larger configurations such as IWRC's of larger and more complex cable configurations are investigated using the numerical model, extending the knowledge of numerical modelling steel wire ropes.

3

Bending stiffness: Analytical analysis

In chapter 2.3 the most important model considerations have been shown which could be categorized into the following categories: string/beam models, thin-rod models, semi-continuous models and finite element models. The influence of these assumptions on the found results has been addressed in the previous chapter and will be checked using the analytical and numerical model derived in this thesis. Changes of the wires inside a wire rope or strand while it is being bend have been discussed and shown. The chapter concluded with a summery of different cable models which could be used to describe the bending behaviour of wire ropes. After a discussion it has been chosen that the analytical model by Papailiou [33] will be used to predict the bending behaviour. A numerical model using FEM is generated in this thesis to compare the analytical model to. The impact of the assumptions made in the model by Papailiou [33] will be checked using the results of the numerical model as well.

Both the analytical and numerical model will be constructed for a simple strand after their expansion to work with larger wire rope configurations such as IWRC's or complete wire ropes will be investigated. This chapter focusses on the development of the analytical model described by Papailiou [33].

It is divided into four sections in which all aspects of the model will be analysed: geometry and forces, model description of a simple strand, model description of multiple layers and a discussion. The first section will focus on the kinematic relations involved in the 3D modelling of wire ropes. After these kinematic parameters are known the model itself can be developed and analysed for simple strands and multiple layered ropes. In the discussion, the model will be evaluated along with its strong and weak points.

3.1. Geometry and forces

One sound and practical analytical model of a state-dependent bending stiffness became available through the work of Papailiou [33]. In his model, Papailiou takes inter-wire friction and inter-layer slipping into account which results in a state-dependent bending stiffness which is dependent on wire rope curvature, lay angle, friction coefficient and tension. Assumptions used in the theory are as in table 3.1.

Table 3.1: Modelling considerations Papailiou [33]

Modelling consideration	
Boundary conditions	Clamping forces are neglected, long wire considered so that boundary conditions can be neglected.
Inter wire contact	Purely interlayer contact is assumed
Wire cross sectional geometry	Cross sectional geometry change is partly taken into account
Radial contraction	Radial contraction is neglected
Additional wire forces and moments	Wires are assumed to be subjected to additional wire forces and moments
Friction regimes	Interwire friction is taken into account
Lay angle	The lay angle is assumed constant over the length of the wire during bending
Material	Material is assumed to be linear elastic

The model constructed by Papailiou begins with the statement that in practically all bending applications, a tension T is present. The following assumption is that all wire cross sections in a layer

have the same diameter δ. The helix orientation angle ϕ is oriented as can be seen in figure 3.1. This aforementioned tension T causes a local tensile force Z on each wire. The tensile force will act on a small element along the wire length $dl = \rho d\alpha$, with ρ and α being the radius of curvature and the so called wrap angle of the wire respectively. Tension, in combination with the curvature and lay angle of the wire will exert a pressure on the wire(s) below.

$$p = \frac{Z}{\rho} \tag{3.1}$$

A distributed load can be derived combining equation 3.1 for the pressure and the aforementioned equation for the element length.

$$dN = p\rho d\alpha \tag{3.2}$$

From the geometrical configuration shown in figure 3.1b, a relationship for the lay angle β can be concluded.

$$\frac{r d\phi}{\rho d\alpha} = \sin\beta \tag{3.3}$$

Combining the equations 3.1, 3.2 and 3.3 with the equation for the curvature of a helix which is commonly known to be equal to $\rho = r/\sin\beta^2$, the equation 3.4 for the radially directed force can be derived,

$$dN = Z \sin\beta d\phi \tag{3.4}$$

which has a direct relationship with the friction that exists between the wires in a layer and the penultimate layer. This frictional force can either be higher, lower or equal to the local tensile force on that particular wire. The situations described in chapter 2.3 are defined as the friction regimes stick, slip and transition. The stick regimes corresponds with high frictional forces while the slip region is dominated by low friction forces. In the transition regions, parts of the wires start slipping due to the increase of tensile forces on the wires.

When bending a wire rope to a constant curvature, the bending stress in each wire will consist out of two components:

1. The bending stress, which will result from the bending of a wire around its own neutral axis. With E for the Young's modulus of the material, δ for the diameter and κ for the curvature of the wire this will be equal to equation 3.5. This minimum stress contribution from an individual wire is always present.
$$\sigma_{min} = E\frac{\delta}{2}\kappa \tag{3.5}$$
2. A second term which is depended on the curvature of the strand has to be added to that of equation 3.5. When low curvatures are considered, bending stress of the wire is in the sticking regime (σ_{stick}), which was previously described as a regime where the normal forces between wires are still to high to prevent slipping. After wires start slipping at higher curvature of the strand, internal friction will be not enough to prevent wires from sticking and the second term will be equal to the frictional slip stress (σ_{slip}).

The previously mentioned (σ_{stick}), is dependent on the distance h,

$$h = r \sin\phi \tag{3.6}$$

from the neutral axis of the strand to that of the wire. This is calculated in equation 3.6 where ϕ is the helix angle which is indicated in figure 3.1a as the angle from the neutral axis of the strand. The variable r is equal to the wire winding radius. Using Euler-Bernoulli beam theory the stress in the sticking regime

$$\sigma_{stick}(\phi) = E\kappa h \cos^2\beta = E\kappa r \sin\phi \cos^2\beta \tag{3.7}$$

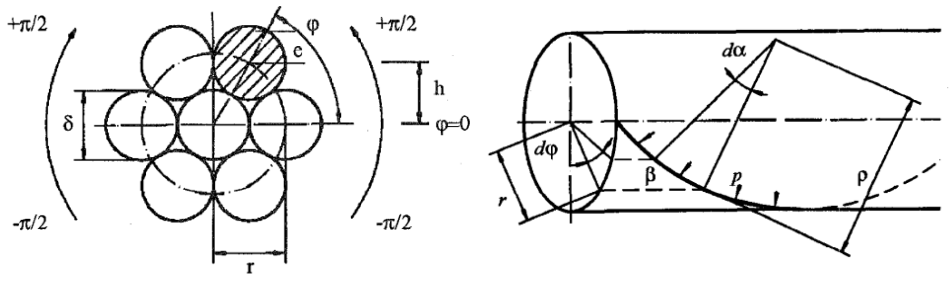

(a) Cross section (b) Helix geometry

Figure 3.1: Definitions of parameters cross-section and helix geometry as described in [33]

will depend on the curvature κ, the Youngs modulus E and the lay angle β of the wire. The factor $\cos\beta$ compensates for the fact that the wire has a helical shape which will decrease the stress slightly.

When bending curvature is increased, internal friction forces will not be enough to prevent the wires from slipping over other wires and the core. Leider [22] showed that relative wire slip will start in at the neutral plane of the strand. When curvature reaches even higher values, the part that has slipped of each wire will propagate along their length beginning from their starting positions on the neutral plane of the strand.

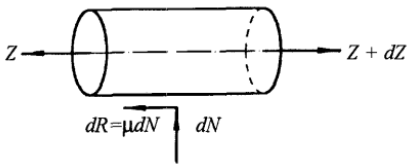

Figure 3.2: Free body diagram of a wire element [33]

Radial force as is expressed in equation 3.4 together with a friction coefficient μ will generate a frictional force,

$$dR = \mu dN = \mu Z \sin\beta d\phi \tag{3.8}$$

which will effect the axial force Z on each wire. Integrating this equation with boundary conditions $\phi = 0 : Z(\phi) = Z_T$ will result in equations 3.9 and 3.10,

$$dZ = dR = \mu Z \sin\beta d\phi \tag{3.9}$$

$$Z(\phi) = Z_T e^{\mu \sin\beta\phi} \tag{3.10}$$

where the value Z_T is the tensile force on a wire before bending has taken place. When only a tension T acts on the strand, the tensile force in each wire can be calculated by equation 3.11.

$$Z_T = \frac{EA\cos^2\beta}{\sum_{allwires} EA\cos^3\beta} T \tag{3.11}$$

$Z(\phi)$ in equation 3.11 is the maximum tensile force which acts on a wire during bending. The value varies with the helix angle ϕ which can be seen in figure 3.1a, and so the value changes along the wire length. During bending, in addition to the original tensile force Z_T there exists an tensile or compressive force Z_{Slip} which is the result of inter-wire friction.

$$Z(\phi) = Z_{Slip} + Z_T \tag{3.12}$$

When combining equation 3.10 with 3.12 an expression for Z_{Slip} can be found,

$$Z_{Slip} = Z(\phi) - Z_T = Z_T(e^{\mu \sin\beta\phi} - 1) \tag{3.13}$$

where this frictional slip force can be converted to a slip stress as is shown in equation 3.14,

$$\sigma_{slip}(\phi) = \frac{Z_{Slip}(\phi)}{A} \tag{3.14}$$

where the σ_{slip} is again dependent on ϕ and so variable along the length of the wire.

These equations describe the kinematic model where a strand is made of. Forces and stresses in wire elements have been calculated. In the next section more information about the bending stiffness of a particular strand is shown using the kinematic relations from this section.

3.2. Model description: Simple strand

In the previous section all parameters involved in generating a force and geometry profile of a simple strand are calculated. How these forces and displacements relate to a response in bending will be explained in this section.

Papailiou [33] takes into account that strands will follow with good approximation the bending equation,

$$M = EI\kappa \tag{3.15}$$

where EI stands for the bending stiffness of the strand. Bending moments during the stick and slip regimes arise from the geometry in figure 3.1a, by multiplying the bending stresses with their distance from the wire neutral axis e and from the neutral axis of the conductor h while integrating over the wire cross-section.

$$M_{stick} = \int \sigma_{min} \cos\beta e dA + h \int \sigma_{stick} \cos\beta dA \tag{3.16a}$$

$$M_{slip} = \int \sigma_{min} \cos\beta e dA + h \int \sigma_{slip} \cos\beta dA \tag{3.16b}$$

The $\cos\beta$ term is implemented in equations 3.16a and 3.16b because it compensates for the actual inclined area of the wire inside the strand. Combining these equations with the equations 3.5, 3.7 and 3.14 and taking into account the relationship described in equation 3.15, the following equations for the different regimes can be derived:

$$EI_{min}^{wire} = E\frac{\pi\delta^4}{64}\cos\beta \tag{3.17a}$$

$$EI_{stick}^{wire} = EA(r\sin\phi)^2\cos^3\beta \tag{3.17b}$$

$$EI_{slip}^{wire} = \sigma_T A e^{\mu\sin\beta\phi - 1} r\sin\phi\cos\beta/\kappa. \tag{3.17c}$$

When bending is first introduced in a straight cable, the wires will act as a solid body. When this mechanism occurs, the bending stiffness is a result from equation 3.17b plus the minimum bending stiffness from equation 3.17a. Where not only the bending resistance of the wires around their own neutral axis is taken into account but also the distance from the neutral axis of the cable to the axis of the wires is accounted for as it is assumed that all wires are sticking to each other. This can be seen in figure 3.3 and in equation 3.18 corresponding to the low curvatures.

When the wires start slipping due to the increase of curvature of the wire rope, the bending stiffness will start to change accordingly. Equation 3.17c takes into account the friction stress which acts on each individual wire as a result of the tension and the applied moment. The value of the stiffness will decrease gradually and will approach the minimum value determined by equation 3.17a. This value is determined as the sum of all individual wire stiffness's. Thus, the minimum bending stiffness will only consist of the bending resistance of all wires around their own neutral axis. This corresponds with the higher curvatures in figure 3.3 and is shown in equation 3.19.

The bending stiffness for the stick region in figure 3.3 is equal to the sum of equation 3.17a and 3.17b. In the slip region equation 3.17c has to be added to the minimum bending stiffness.

$$EI_{max} = EI_{min} + EI_{stick} \tag{3.18}$$

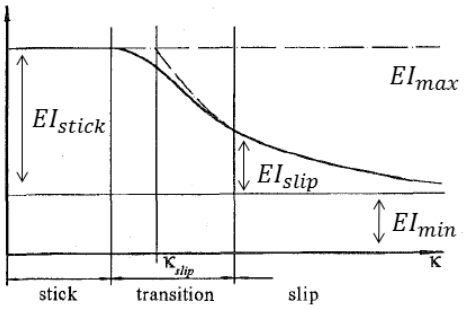

Figure 3.3: Bending stiffness as a function of cable curvature [33]

$$EI(\kappa, T) = EI_{min} + EI_{slip} \tag{3.19}$$

The transition from sticking to slipping should be smooth, as can be seen by observing the solid line in figure 3.3. This is due to the fact that the transition of each wire from stick to slip is accomplished at a different curvatures and at different positions along the length of the wire. In the work of Papailiou [33], the moment of transition is described by calculating the critical curvature where wires start to slip. De dashed lines in figure 3.3 have an intersection which corresponds to κ_{slip}. This point can be calculated by equating equations 3.18 and 3.19 and solving for κ. This κ_{slip} is used to divide the stick and slip part. In the more extensive thesis report by Papailiou [33], equations are stated to smoothen the transition from stick to slip. This correcting of the realtionship in the transition zone is neglected as it only slightly adjusts the values. When neglecting the smoothing the statement becomes,

$$\kappa < \kappa_{slip} \rightarrow EI = EI_{max} \tag{3.20a}$$
$$\kappa_{slip} < \kappa \rightarrow EI = EI(\kappa, T) \tag{3.20b}$$

were the value for EI is equal to the solid lines outside and to the dotted section in the transition regime in figure 3.3. When calculating the bending stiffness according to Papailiou [33] for a simple strand with a cross sectional geometry as in appendix A, friction coefficient of $\mu = 0.125$ and a tension of $T = 20000$N, the relationship between bending stiffness and curvature would be as in figure 3.4.

3.3. Model description: Multiple layers

Papailiou [33] also extended his theory to multilayer strands. In his theory he only considers transmission line conductor configurations for example as can be seen in figure 3.5.

These configurations differ from the ones used in steel wire ropes because the lay direction changes per layer. Another dissimilarity is that the transmission line conductors only have concentric layers of wires with helical wound wires. Steel wire ropes can contain helical wound strands resulting in wires which describe double helical paths.

However, minimum and maximum values for the bending stiffness of larger wire rope configurations can be easily derived from the model described by Papailiou [33]. In stick all wires are stuck together and Steiner's theorem can be used, in full slip only the individual contribution will be taken into account.

In the transition region where the wires are slipping but not over their entire length the model by Papailiou [33] has to be adapted. It is assumed that a strand of the IWRC will behave as a helical wound cylinder with a cross sectional area equal to that of the wires inside the corresponding strand corrected for the lay angle of the wires in the strand. This assumption reduces the problem to a simple strand with six wires in the outer layer. All calculations performed to come up with the relationship between bending and curvature for an IWRC can be found in C.

3.4. Evaluation

Papailiou [33] presented an analytical model which is described in this chapter based on the thin-rod theory, where frictional slip is taken into account for the full range of curvatures. In his model, the thin rod approximation is used where the axial pretension in the cable leads to a pressure difference

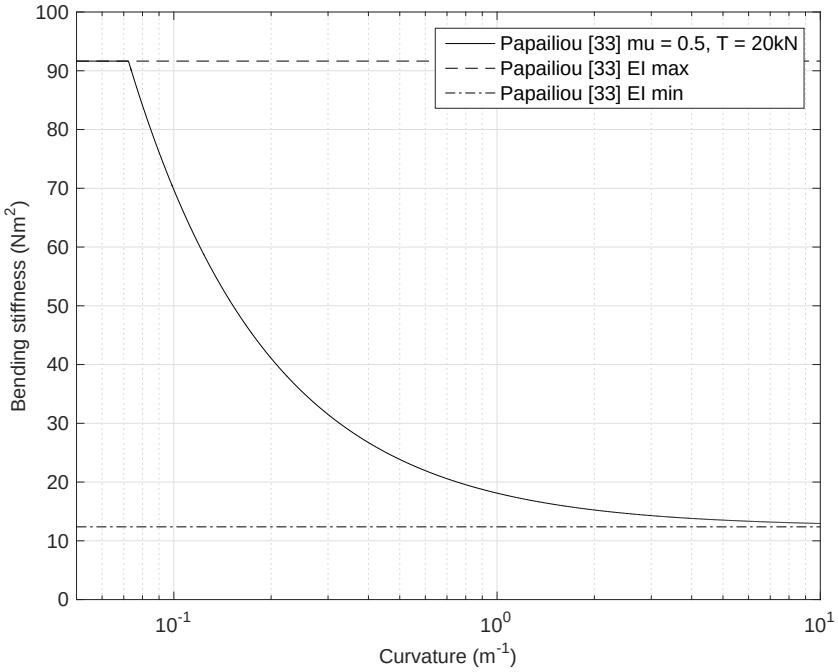

Figure 3.4: Bending stiffness as a function of cable curvature according to Papailiou [33]

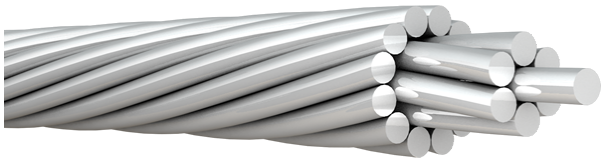

Figure 3.5: Spiral rope: Transmission line conductor cable (ACSR) [21]

between each wire layer which leads to frictional forces countering the bending moment. Frictional forces in combination with tensile forces result in the discussed stick-slip behaviour.

As can be seen in figure 3.4, there is a large difference between the analytically derived maximum and minimum bending stiffness. In fact; $\frac{EI_{max}}{EI_{min}} = 7.40$, when taking into account the simple strand described in appendix A. Assumptions made in the model most likely cause this large difference. For example, the fact that no deformation of the wires is taken into account, pure inter layer contact and no radial contraction is assumed. The numerical model will show if this large difference between minimum and maximum bending stiffness is realistic.

At large curvatures, the analytically found bending stiffness becomes equal to its minimal value where no friction is taken into account. However, it is realistic to think that friction will still play a role in the determination of bending stiffness as even frictional coefficients for greased steel on steel contact, both static and dynamic have a value above zero. Eventually for extremely high curvatures the role of the friction coefficient will diminish. Comparison with the numerical model will show if the model by Papailiou [33] is to conservative.

Papailiou in his analytical model assumes that the geometry of the cross-section will stay the same during tensioning and bending. This is a geometrically linear approach. In reality however, this cross-section will deform under loads. This effect will influence the generated results as the direction and magnitude of the forces in the strand changes with the changing geometry. Numerical modelling will take this geometric non-linearity into account.

Tests are performed by Papailiou [34] on a single transmission line conductor. The model described in this chapter is experimentally validated using these tests and matches the data quite will for a limit curvature range. The maximum bending stiffness at low curvatures matches the analytical model very well. However, only a limited curvature range is considered so no experimental verification of the minimum bending stiffness is presented. This shows that the analytical model can be considered somewhat

correct for transmission line conductors which are spiral ropes just as a simple strand. Despite this validation, numerical models are still needed to test the assumptions made in the model, some of which have just been discussed. Generating a numerical finite element model of a simple strand could provide answers to the validity of the assumptions made in the model. Because the model is only tested against one particular wire rope configuration, it validity cannot be guaranteed.

In short, the analytical model described in this chapter works well for simple strands and multiple layered spiral strand such as transmission line conductors. For larger and more complex wire rope configurations, this model has not been verified. Assumptions made in the model will also have a more profound impact on the results when larger wire rope configurations are taken into account. Therefore numerical modelling has to be used to check the assumptions made. As the results of the analytical model for simple strands are considered plausible, results from the numerical model will be compared to those analytically generated. If comparison has been found for results considering simple strands, the numerical model can be expended to larger wire rope configurations.

4

Bending stiffness: Numerical analysis

Analytical models such as those of Costello [7] and Velinsky [47] neglect non-linear effects, like friction and contact between wires. These models can be used to quickly determine preliminary results for difficult strand structures and large wire diameters. [32] For the behaviour of cables under tension and/or torsion loads, these analytical models can be used as non-linear effects do not play a significant role. When looking at bending combined with tension for simple or multilayer strands, the model by Papailiou [33] can be used to quickly generate values.

The model by Papailiou [33] is described in chapter 3 and is used to find a relationship between bending stiffness and curvature for different tensions, curvatures and lay angles. In the evaluation all assumptions which will effect the results have been mentioned. It was stated that numerical modelling is needed to check the assumptions made in the analytical model and to expand to larger and more complex wire rope configurations.

Finite element methods are numerical methods that approximate solutions of mathematical problems. By using this method, for example the bending of beams can be modelled. This is done by subdivision of the beam into smaller parts, which is called a mesh (figure 4.1). These simpler parts are called elements abiding certain element equations. By systematically recombining all local element equations, a global set of equations is derived and so the desired behaviour of the global system can be calculated. Initial conditions and boundary conditions are needed for the original set-up to obtain a numerical answer.

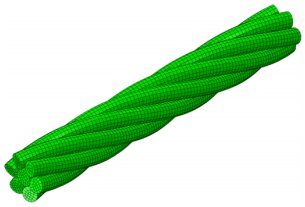

Figure 4.1: A finite element mesh of cable core [55]

Setting up a model using the finite element method divides the problem into simpler parts, the will result in several advantages:

1. FEM can handle very complex geometry
2. Relativity easy representation of the total solutions
3. Local effects can be captured more easily

However, there is also a downside to modelling with FEM. Because of the subdivision of the geometry into smaller parts, the solutions will be approximated and they always have to be checked. Used FEM software could have errors in execution of the finite element method. Although these disadvantages are severe the most common error is the one made by the user.

Presently, finite element methods which focus on the behaviour of wire ropes under bending or axial loading are increasingly being found in literature. Already many papers exist on the 3D modelling of wire ropes and strands such as in the paper by Stanova et al. [43]. One can say that the preparations to model the bending behaviour of steel wire ropes have been done but the execution has yet to be performed.

When setting up numerical models, it is wise to start simple. By expanding the model gradually and performing checks in the process, bugs and flaws can be detected without losing valuable time. When taking wire rope modelling into account, this process can be made clear easily, because wire ropes are made out of different components.

First a model of a simple wire rope configuration (figure 4.2a) is constructed. This model consists of a core wire with six helically wound wires around it. A sensitivity analysis will be performed on this relatively simple model to determine the correct settings and parameters needed to ensure its results reliable.

After the sensitivity analysis has been carried out, the model can be expanded by adding more wires to the configuration to form for example an Independent Wire Rope Core (figure 4.2b), or a complete steel wire rope (figure 4.2c). The details of the geometry of the models seen in figure 4.2 can be found in appendix A.

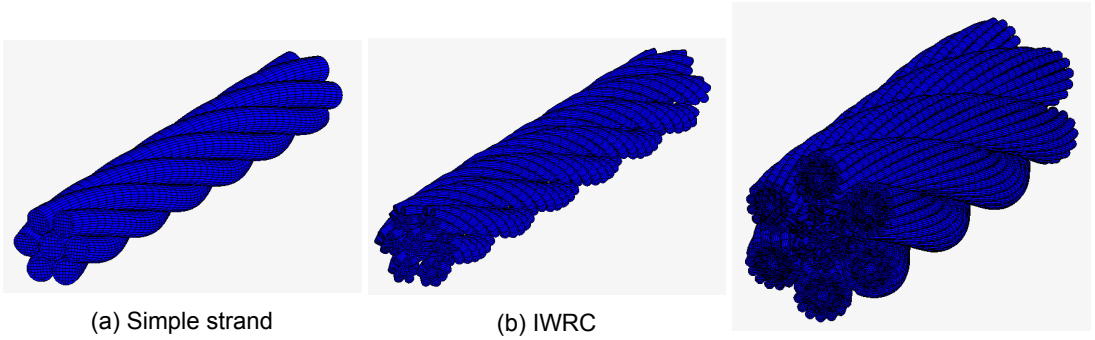

(a) Simple strand (b) IWRC (c) 6x36WS+IWRC

Figure 4.2: Meshes of different wire rope configurations

In the next chapter a comparison between analytically and numerically determined values will be made. The analytical model from Papailiou [33] described in chapter 3 will be used to compare the numerical model to. The bending stiffness will be determined as a function of the tension and curvature respectively on and off the cable. This is of importance to the practical implementation of the acquired results, as a beam will be modelled with a state-dependent bending stiffness depending on these parameters.

4.1. Numerical model set-up

The numerical model is set-up using the program Marc Mentat, where Mentat is the user interface where the kinematic model and mesh is generated. Marc is the computational engine which computes the result of the analysis. This programme is chosen because of its ability to calculate non-linear frictional problems accurately. [27]

The numerical model set-up consists of four categories: Geometry, element properties, contact and boundary conditions. The first section will focus on the method of defining the geometry of different cable configurations in Marc. Element properties are quickly addressed afterwards with a more extensive explanation of their content in appendix E. Different kinds of contact configurations will be taken into account after which the same is done for different boundary conditions. In the end of this section the standard way of analysing the bending behaviour of a cable configuration in Marc will be shown.

4.1.1. Geometry

Modelling the cable section used for the analysis starts with a sketch of the cross-section of the wire generated in the CAD drawing program Inventor. [1] After the sketch is imported into Mentat, a planer mesh of the cross section is generated.

A kinematic model of the centrelines of all wires in the strand section is constructed in Matlab (figure 4.3) using the Frenet-Serret equations explained in appendix B. This kinematic model will be translated to Python programming language, so that it can be read by Mentat. This 'input file' uses the Python based commands in Mentat to generate a 3D model from the already drawn 2D cross section. By choosing this method of constructing a model in Mentat it is easier to construct different geometries and different cables configurations quickly.

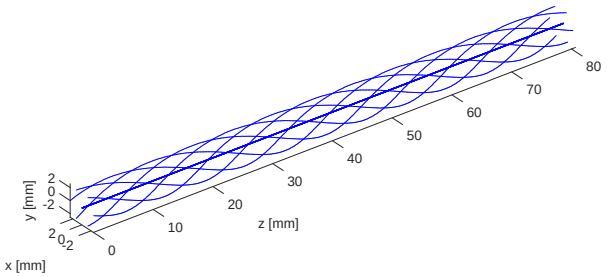

Figure 4.3: Centrelines wire in strand section

After the cross-section is imported into Mentat, the generated Python file will first rotate the wire cross-sections to the appropriate configuration is realised. Afterwards the planer elements of which the sections exist will be expanded helically and straight for the wires and the core along the z axis respectively to generate 3D solid elements.

4.1.2. Element properties

The chosen element type for these solid elements is Hex 8. This is an eight-node, isoperimetrical, arbitrary hexahedral element. According to the element library of Marc [29], this element type is the preferred choice when conducting a contact analysis. Material properties corresponding with steel are added to these elements and can be found in table 4.1.

Table 4.1: Element properties

Parameter	Unit	Value
Young's modulus	[Gpa]	188
Poissons ratio	[-]	0.3

More information on this element can be found in appendix section E.1 where the orientation and usage is discussed.

4.1.3. Contact

Different kinds of contact have been discussed in section 2.1 as interlayer, intralayer and mixed contact. All these contact modes will be analysed in the numerical analysis to display the differences between these modes while comparing the results to that of the analytical model. In the standard numerical analysis contact between all wires is considered as that is the most realistic approach. Appendix section E.3 will elaborate on the exact method of detecting contact in Marc.

4.1.4. Boundary conditions

Now that the geometry of the model and the rules for contact are implemented into Marc, boundary conditions have to be applied to the model. The method of restraining the model described in this section is not the only way to imply boundary conditions. Multiple sets of boundary conditions will be described and compared in section 4.4. However, it has been found that the standard method, which will be described in this section provides the best and most reliable answers. In this report this set-up is called the 'standard model'.

Standard model:
Two reference nodes are created on the centreline of the cable at both ends. These nodes are rigidly connected to all nodes located at the end of the cable. Boundary conditions are then applied to this

single node as can be seen in figure 4.4.

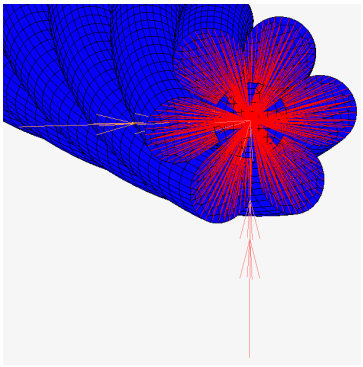

Figure 4.4: Nodes at the end of the strand, rigidly connected to a reference node with boundary conditions

The loading of the cable consists of two parts, the tensioning and bending part as is illustrated in figure 4.5. In the first part, the two reference nodes will be restrained in all degrees of freedom except the translation direction of the cable while an axial force will be build up on both ends. The middle of the centre wire of the cable will be restricted from moving in axial direction so that an axial force can be built up.

(a) Tensioning (b) Bending

Figure 4.5: Loading case

When the tension reaches its prescribed maximum value, both ends will be restrained in all directions except the rotation along the neutral axis of the cross-sections at both ends. A moment will be applied gradually on both sides while the ends of the cable will be held in place.

4.2. Data processing

The model created is a simple strand model consisting of one core wire and six wires in the first layer (figure 4.2a). The geometric and material properties of the simple strand can be found in table 4.2 as well as in appendix A. These properties are chosen because they are widely used in papers concerning the bending behaviour of steel wire ropes.

Table 4.2: Geometric and material properties simple strand

Parameter	Unit	Value
Core wire diameter	[mm]	3.94
Helical wire diameter	[mm]	3.73
Lay angle	[deg]	17.03
Pitch length	[mm]	78.67
Cable length	[mm]	80
Young's modulus	[GPa]	188
Poisson's ratio	[-]	0.3

Three different situation will be considered in this thesis:

- Fully bonded: Contacting nodes will be bonded together so that no relative movement is allowed
- Frictionless model: A friction coefficient of zero will be taken into account

- Friction (standard) model: A friction coefficient between contacting surfaces higher than zero will be taken into account

Wire ropes have their maximum bending stiffness when the cable has a curvature of zero, or a value close to zero. When wires inside a wire rope start slipping, the value for the bending stiffness of that strand will decrease. With a further increase in curvature, the bending stiffness will decrease even further until it will eventually level out and assume a constant value which is equal to the minimum bending stiffness. In most analytical models such as the model described by Papailiou [33] in the previous chapter, it is assumed that the minimum bending stiffness will not depend on the friction coefficient or applied tension.

In this thesis, the contribution to the bending stiffness due to mechanisms in the rope will be isolated and presented. In reality, increased tension on a rope will also stiffen it in bending. However, this is a contribution from the tension and not of the rope itself. This can be explained by thinking of a small hemp rope which has almost no bending stiffness. When tensioning the rope, it will be more resistant to bending. This is due to the tension on the rope and not due to a change in its internal parameters. When bending stiffness is mentioned in this thesis it refers to the change in the internal parameter of the rope.

4.2.1. Curvature

It is assumed that the curvature of the strand is constant over its length when bending the rope using the model set-up described in section 4.1. This assumption is not entirely valid because of the applied boundary conditions during the bending part of the analysis. These boundary conditions will have the effect that the centreline of the strand will not fit perfectly on a circle fitting when bend. The validity of this assumption will also depend on the length of the model. When considering large model lengths, the moment exerted on the ends will not be enough to bend the middle part of the rope. This effect can be seen in figure 4.6.

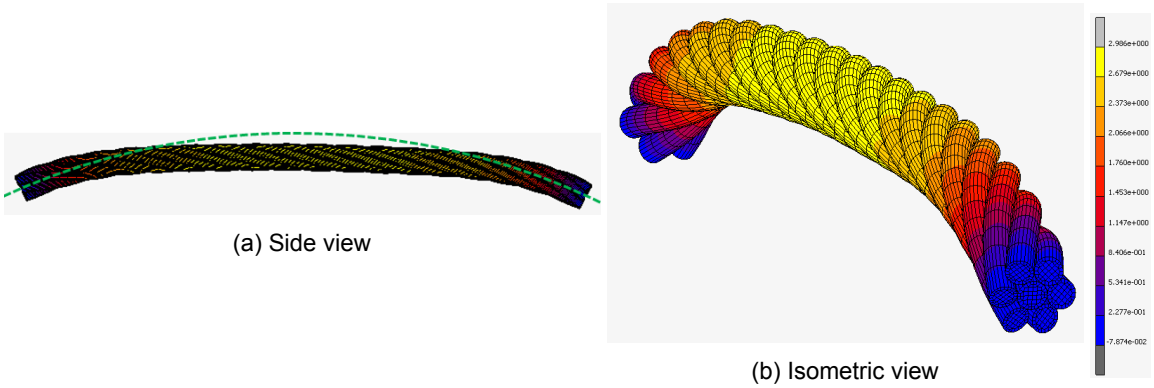

(a) Side view

(b) Isometric view

Figure 4.6: Model length of three strand rotations. Legend displays the deflection in vertical direction in millimetres.

It is obvious that the curvature in this bent rope is not constant over its length as the middle part of the rope still contains wires in stick and is still horizontal (figure 4.6a). The aforementioned assumption, that the centreline of the rope will fit on a circle fitting will not be valid when considering this model length. By reducing the length of the model, this assumption will become approximately valid as can be seen in figure 4.7. The green dotted line represents the circle fitting corresponding to the cable curvature. It can be seen that the rope in figure 4.7 matches the circle fitting better than the rope in figure 4.6. A pitch length of one will be used in further analysis so that constant curvature along the strand length can be considered.

The curvature of the rope is determined by measuring the rotation of the core at the ends (θ) which is defined as in figure 4.8.

To calculate the curvature of the strand, the curvature radius ρ has to be calculated. By making use of the aforementioned assumption of a circle fitting and assuming that the length of the cable is

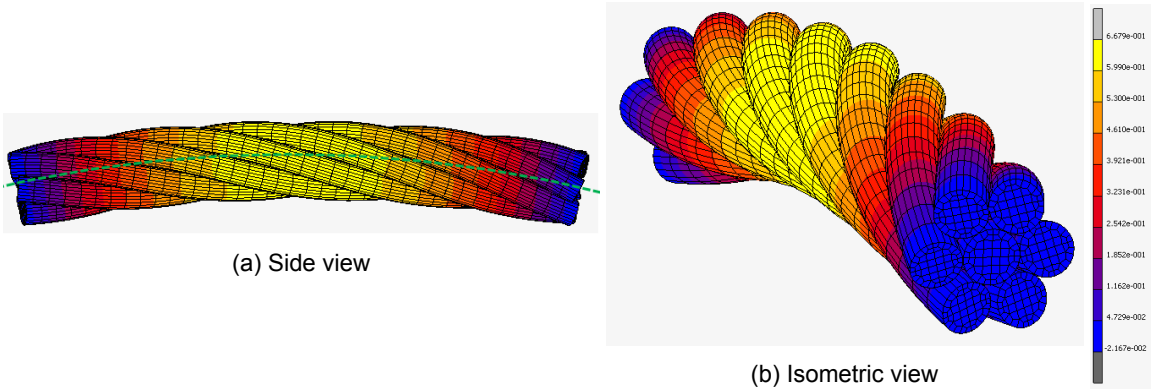

(a) Side view

(b) Isometric view

Figure 4.7: Model length of one strand rotation. Legend displays the deflection in vertical direction in millimetres.

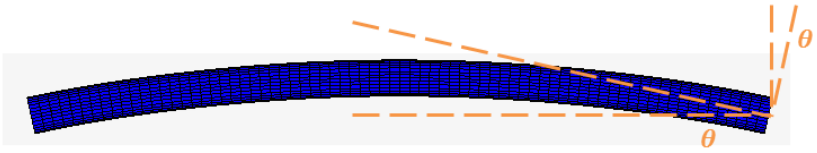

Figure 4.8: Side view of the rope showing only the core wire where θ is equal to the angle of rotation

constant before and after tensioning and bending, strand curvature is equal to

$$\beta = \theta \quad \text{(parallel lines)} \tag{4.1a}$$

$$\rho = \frac{L_{\text{straight}}}{2 \sin \beta}. \tag{4.1b}$$

The variables are defined as in figure 4.9. L_{straight} is equal to the shortest distance between the two ends of the strand. Due to the boundary conditions applied to the model, this distance will not change when bending the wire rope.

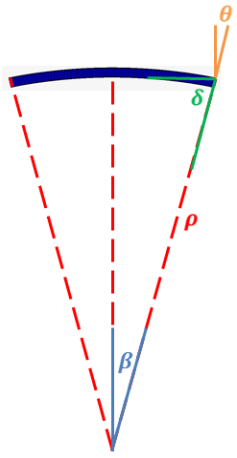

Figure 4.9: Radius of curvature ρ

4.2.2. Bending stiffness

Now that the curvature radius of the rope is known under different loading conditions more can be said of the relations between bending stiffness and bending moment. In the finite element analysis described

in this chapter, the bending stiffness will be derived using the method described in this section. The equation describing beam curvature can be approximated by,

$$EI = \frac{M}{\kappa} \tag{4.2}$$

where M is the bending moment and EI is the bending stiffness of the rope. The curvature κ is equal to

$$\kappa = \frac{1}{\rho} \tag{4.3}$$

the inverse of the previously defined radius of curvature. There are different methods of defining bending stiffness. Dastous [8] for example defined the bending stiffness relation for a beam as follows:

$$EI = \frac{dM}{d\kappa}. \tag{4.4}$$

Because of inter wire friction in a wire rope, the relation between bending stiffness, curvature and the bending moment will be more complex. Using equation 4.4 to come to a relationship for the bending stiffness will lead to a staircase shaped $EI - \kappa$ relation, instead of a continuously decreasing one. [55] Equation 4.2 will be used as a basis to construct a relationship for the state-dependent bending stiffness which will be presented at the end of this section.

According to beam theory with large axial tension [3], the force and moment equilibrium in the cross sections of a wire rope will lead to,

$$\frac{dV}{dx_3} + N\frac{d^2u_1}{dx_3^2} - p_3\frac{du_1}{dx_3} + p_1 = \rho A a_1 \tag{4.5a}$$

$$\frac{dN}{dx_3} + p_3 = 0 \tag{4.5b}$$

$$\frac{dM_2}{dx_3} + V = 0 \tag{4.5c}$$

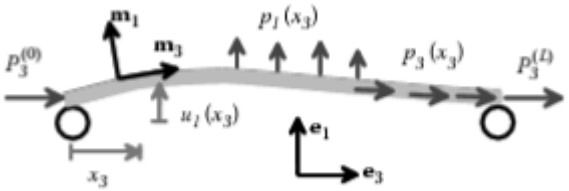

Figure 4.10: Beam subjected to transverse and axial loading [3]

where V, M and N are the cross-sectional forces and moments respectively equal to the cross-sectional shear force, bending moment and axial force. The variables p_1 and p_3 are equal to the distributed forces identities in respectively the transverse and axial direction, where u_1 and u_3 symbolize these directions, which can be seen in figure 4.10. Inertia terms will not be taken into account in this analysis. Therefore, $\rho A a_1$ in equation 4.5a will be zero. The curvature of the vector in the direction of the beam is equal to

$$\kappa = \frac{d^2u_1}{dx_3^2}. \tag{4.6}$$

In the case of wire rope bending, the bending stiffness will be dependent on curvature. Therefore, when combining the equation above with equation 4.2 the moment curvature relation can be written as

$$M = \kappa EI(\kappa) = \frac{d^2u_1}{dx_3^2} EI(\kappa). \tag{4.7}$$

Where $EI(\kappa)$ is the state-dependent bending stiffness dependent on curvature. Combining equations 4.5 with 4.7 the following equation can be derived:

$$\frac{d^2}{dx_3^2}\left(\frac{d^2u_1}{dx_3^2}EI(\kappa)\right)+p_3\frac{du_1}{dx_3}=T\frac{d^2u_1}{dx_3^2}+p_2. \tag{4.8}$$

Equation 4.8 can be worked out when selecting correct boundary conditions. When considering an axially loaded cable with a pair of bending moments M at both ends of the strand just as has been described in section 4.1.4 the following boundary conditions are present: [55]

$$u_1|_0=u_1|_L=0 \tag{4.9a}$$

$$\frac{d^2u_1}{dx_3^2}EI(\kappa)\Big|_0=\frac{d^2u_1}{dx_3^2}EI(\kappa)\Big|_L=M \tag{4.9b}$$

$$p_1=p_3=0. \tag{4.9c}$$

If EI is constant over the length of the rope then the solution of equation 4.8 is,

$$M=\frac{\left(1+\exp\left(L\sqrt{\frac{T}{EI}}\right)\right)\sqrt{TEI}}{\exp\left(L\sqrt{\frac{T}{EI}}\right)-1}\theta \tag{4.10}$$

where T is equal to the axial tension as is illustrated in figure 4.5. The rotation angle at the ends θ is in a direct relationship with κ for a cable with constant curvature. Combining equation 4.1 with 4.3 will give

$$\theta=\frac{\pi}{2}-\arctan\frac{L}{2\kappa}. \tag{4.11}$$

A relation between the bending moment M and the curvature κ of the strand is realized as can be seen in figure 4.11a and in equation 4.12.

$$M=\frac{\left(1+\exp\left(L\sqrt{\frac{T}{EI}}\right)\right)\sqrt{TEI}}{\exp\left(L\sqrt{\frac{T}{EI}}\right)-1}\left(\frac{\pi}{2}-\arctan\frac{L}{2\kappa}\right) \tag{4.12}$$

By imposing a bending moment on the rope and measuring the angle of rotation at the ends, the bending stiffness of the rope can be derived via equation 4.10 or 4.12, results of this can be seen in figure 4.11b.

4.3. Geometric (non)linear effect

As previously mentioned in section 4.1.4, the model is tensioned first before bending. After the tensioning is completed, the ends will be restricted from all movement except one rotation which allows for bending around one axis while keeping the axial force in the rope model. Because of this restriction in axial direction, the axial force on the rope will increase when the strand assumes relatively high curvatures. This is due to the geometric nonlinearity of the system.

When assuming a geometrically linear system, equations of motion are formulated in the initial state of the system. These equations are not updated when the model deforms. This assumption causes errors which can be considered insignificant for small strains or curvature changes. However, for larger deformations, these errors cannot be neglected.

The analytical linear equation for a beam simply supported at both ends loaded by a uniformly distributed load ω(N/m) over its whole length as is shown in figure 4.13 is defined by

$$\delta_{max}=\frac{5\omega l^4}{384EI}. \tag{4.13}$$

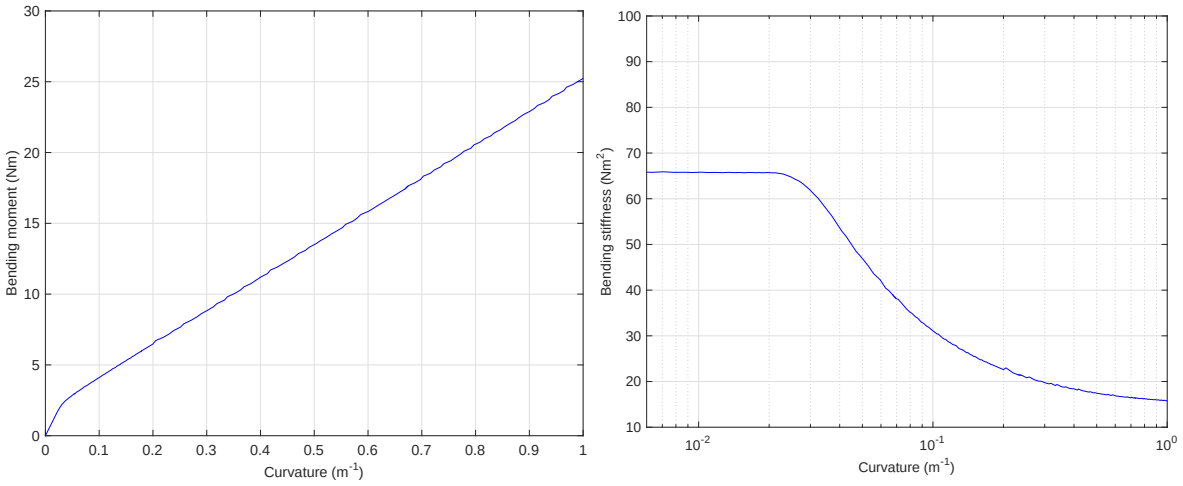

(a) Bending moment (b) Bending stiffness

Figure 4.11: Bending moment and stiffness against curvature of a simple strand with a friction coefficient of $\mu = 0.5$ and an axial tension of $T = 20$kN

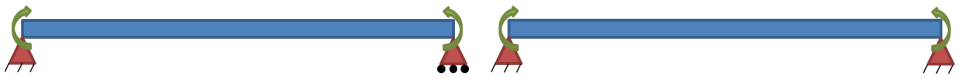

(a) Fixed and free boundary condition (b) Fixed boundary conditions

Figure 4.12: Two simple beams with different boundary conditions where figure 4.12a resembles geometrically linear behaviour while figure 4.12b generates nonlinear results. Both cylindrical beams have dimensions equal to the core wire of the simple strand described in section 4.2

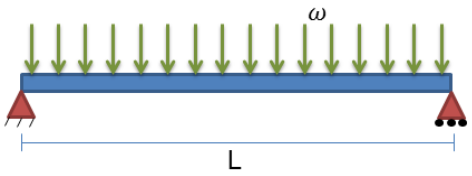

Figure 4.13: Simply supported beam of length L with distributed load ω

This equation describes the deflection of the middle point of the beam. The variable l stands is the length of the considered beam. The reaction moment at the ends can be calculated by:

$$M_{1,2} = \frac{\omega l^2}{2}. \tag{4.14}$$

When taking the examples shown in figure 4.12 and measuring the maximum defection of both models exited by the shown bending moment, differences in geometrically linear and non-linear systems modelled numerically can be explained. Both models are implemented in Marc and are compared to the analytical equation 4.13. This comparison can be seen in figure 4.14 where the numerical and analytical linear model correspond quite well. The numerically calculated non-linear model shows increasingly more deviation from the linear models after a certain curvature has been reached.

Because the numerical model of the simple strand described in this chapter uses the geometrically non-linear set-up of figure 4.12b, this deviation from the linear result can also be expected. In reality when considering cable sections far away from the ends, boundary conditions can be considered to be as in figure 4.12a. Because these boundary conditions are hard to model numerically, the set-up of figure 4.12b is used. As the models from figure 4.12 have the same dimensions as the core wire of the simple strand explained in section 4.2, they can be compared.

In figure 4.15 the relationship between bending stiffness and curvature numerically calculated for a simple strand can be seen. No friction is taken into account to isolate the contribution due to geometric

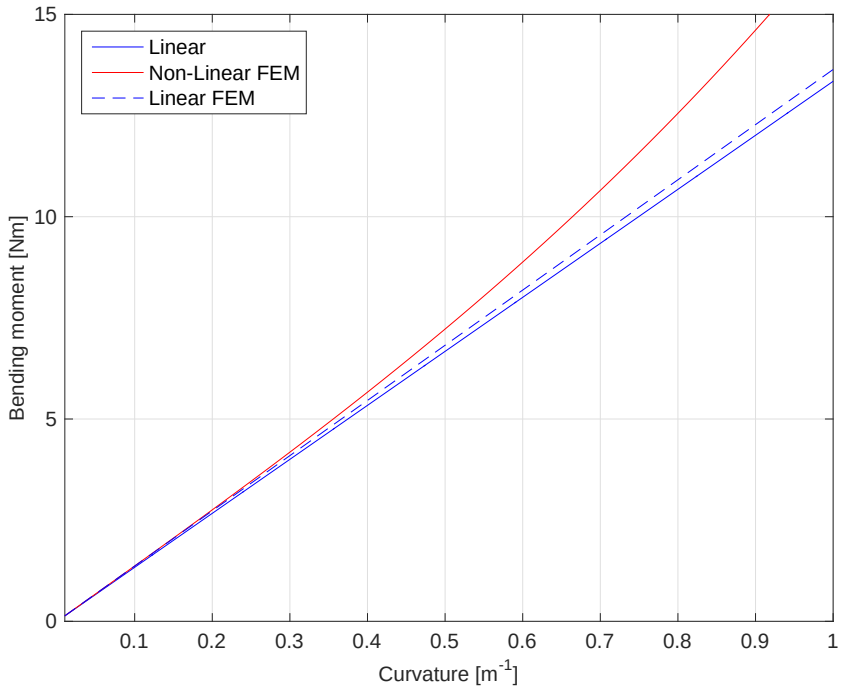

Figure 4.14: Bending moment against curvature for a geometrically linear and non-linear system

non-linearity. After a curvature of $\kappa = 0.5\text{m}^{-1}$ the results will deviate significantly from the minimum value for the bending stiffness. In figure 4.14, non-linear behaviour will deviate from the linearly derived results around the same curvature of $\kappa = 0.5\text{m}^{-1}$. Therefore it can be stated that after this curvature, bending stiffness results are not reliable any more.

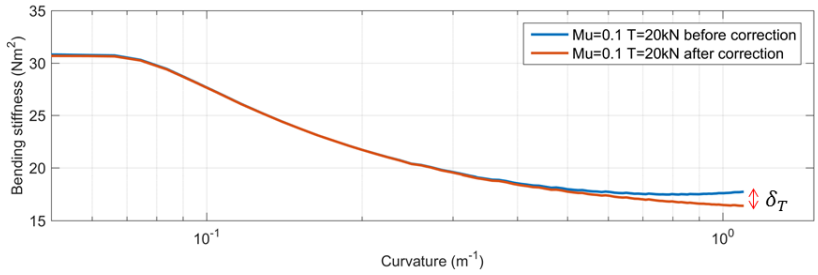

Figure 4.15: Relationship between bending stiffness and curvature for a frictionless model

To be able to conclude anything about the bending stiffness of a simple strand at higher curvatures, some sort of correction has to take place. To isolate the effect of friction on the bending stiffness, a frictionless analysis has to be performed and compared to the analysis with friction. In reality the value for the bending stiffness for a frictionless analysis should be constant. However, from figure 4.15 can be concluded that this is not the case.

When running a model with friction the change in bending stiffness arises from two different parameters; stick-slip and due to geometric non-linearity. The stick-slip contribution is considered to be dominant until a curvature of $\kappa = 0.5\text{m}^{-1}$ is reached. After this curvature, geometric non-linearity will influence the found bending stiffness. To remove this contribution, a frictionless model is constructed for each set-up while afterwards, the difference δ_t shown in figure 4.15 is subtracted from the found bending stiffness in the corresponding model with friction. An example of this correction can be seen in figure 4.16. This way the effect of geometric non-linearity is removed from the analysis and the effect of friction on the bending stiffness is isolated.

Note that this technique is not fully trustworthy. The assumption that the contribution of geometrical non-linearity to the bending stiffness of frictionless and models with friction is equal is not fully true.

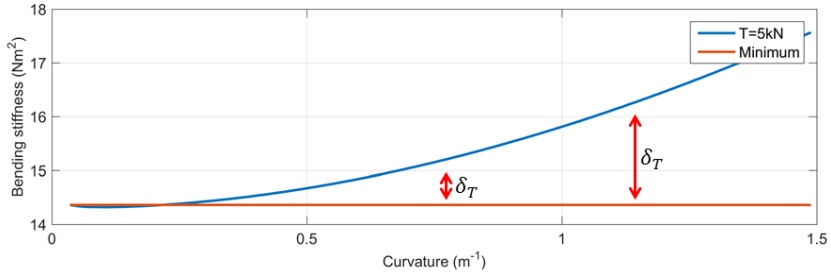

Figure 4.16: Correcting the relationship between bending stiffness and curvature for axial restriction

Results for the bending stiffness for curvatures higher than $\kappa = 0.5\text{m}^{-1}$ are corrected but cannot be fully trusted.

When changing the length of the model, the effect that geometric non-linearity has on the model outcome is different as can be seen in figure 4.17. When reducing the length of the model, the effect is not noticable for the investigated curvature range as can be found in figure 4.17a. For larger model lengths, the effect geometric non-linearity has on the model outcome will increase.

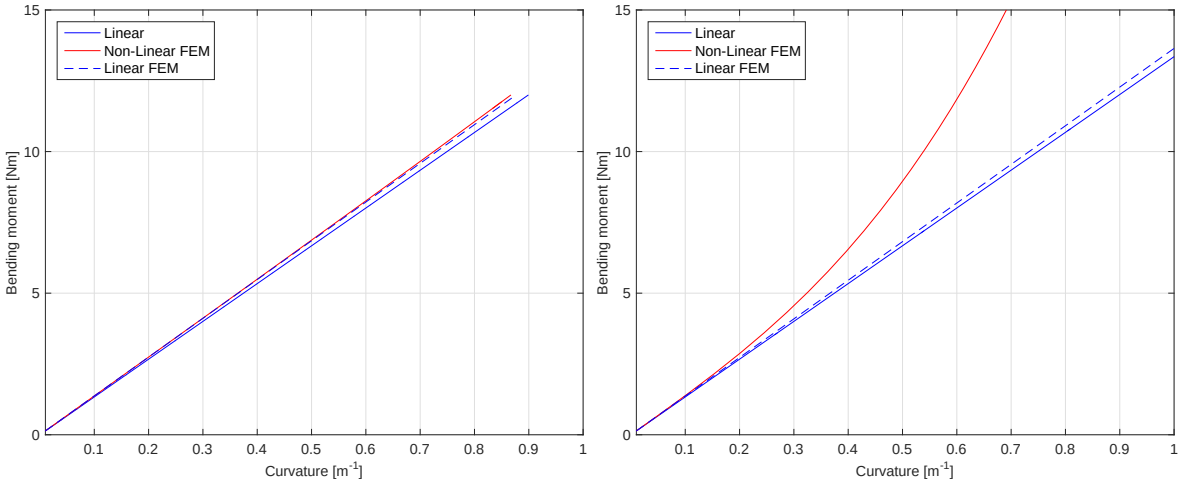

(a) Model length of 40 cm

(b) Model length of 120 cm

Figure 4.17: Bending moment against curvature for a geometrically linear and non-linear system

4.4. Sensitivity study

Now that the numerical model and the post processing method is fully described a sensitivity study has to be performed to check the impact of changing certain input parameters. The numerical model consists of a wide variety of parameters, and many relationships between the input and the output of the model exist. There is a difference in the impact of these variables on the output of the model. A sensitivity analysis will help show how the uncertainty of output of the numerical model. Increased understanding of the relationships between input and output can result in uncertainty reduction. This is done by the identification of input parameters which cause significant uncertainty in the outcome of the model. Research into these specific parameters results in a more robust model.

Parameters with no significant influence on the output can be filtered out to reduce the complexity of the model and possibly reduce computational time. Incorrect relations can be identified by encountering unexpected relations between certain inputs and outputs.

For this study a simple strand model is used as computational expense will be a significant problem when executing the sensitivity analysis on different parameters of the numerical model. The model will take 10 to 20 minutes to run in its most simple form. When changing the level of detail of the model by increasing the amount of elements, computational time will increase as can be seen in figure 4.18.

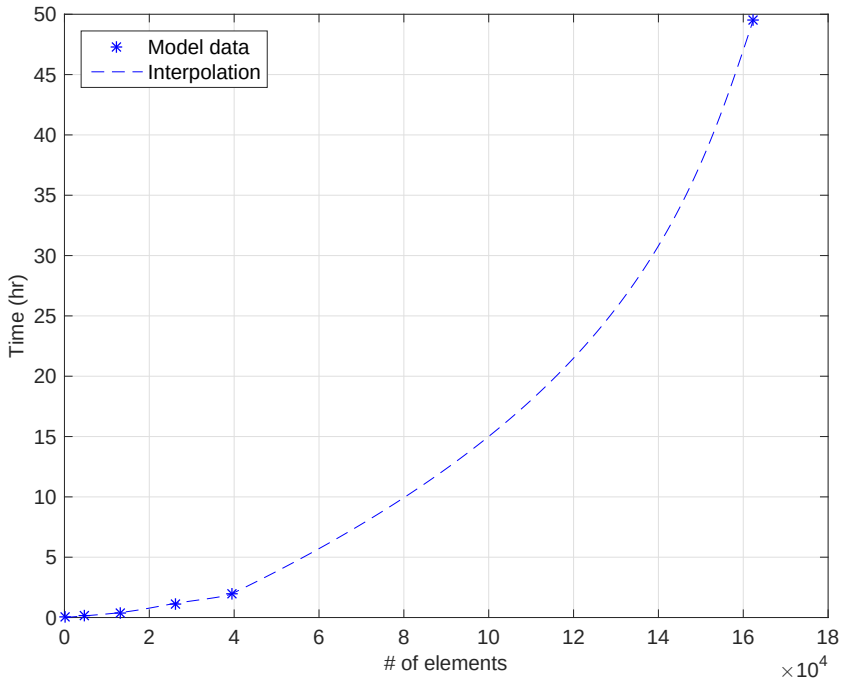

Figure 4.18: The amount of elements in a mesh against the computational time needed for an analysis

When comparing different settings and conditions, it is of importance to select a mesh size which corresponds with reliable results and with preferably low computational time. As one can expect, these two parameters do not go hand in hand. In the next section, different mesh sizes will be analysed along with the mesh size chosen for all the analyses in this thesis.

4.4.1. Mesh size

The first investigation topic of the sensitivity study is the element or mesh size. A mesh is a name for the collection of nodes and elements of which a finite element model exists. The size of a mesh is important to the degree of detail of the model. However, an increased mesh size will have a negative effect on computational time as can be seen in table 4.3.

Table 4.3: Mesh sizes and corresponding computational time for a standard simple strand model with a tension of $T = 20$kN and a friction coefficient of $\mu = 0.5$

Model name	Elements [-]	Nodes [-]	Computational time [s]
Very very coarse	4704	6477	490
Very coarse	13104	17082	1475
Coarse	26068	32552	4206
Fine	39368	48827	7040
Very Fine	162400	192761	178465

As mentioned before, mesh size also has an influence on the degree of detail of the model and of its results. The simple strand model defined in section 4.2 is constructed with the different mesh sizes seen in table 4.3. The results of the analysis of these models can be found in figure 4.20 where the horizontal dotted lines correspond with the fully bonded model where all wires are glued together. The continuous lines represent the model with friction, where all wires touch and can move relative to each other. The analytical model by Papailiou [33] is also shown so the numerical results can be compared to the theoretical one.

The difference between the fully bonded models with different mesh sizes in figure 4.20 is due to the way Marc determines contact and due to the element type chosen for the model. In appendix E the element type and contact detection techniques Marc uses can be found. The normal and friction

stress vector (when looking at the standard friction models) direction is dependent on the element size, as the normal vector of an element (figure 4.19) also describes the direction of the normal force. If the mesh is coarse and so the element size is large, than the normal stress vector from contact body one and two are definitely not perfectly opposite to each other as can be seen in figure 4.19a. When increasing the number of elements in the wire cross-section the normal vectors will align better as can be seen in figure 4.19b. When these factors are more aligned, a more representative value for the bending stiffness in the fully bonded models can be found. However, it cannot be confirmed that with an infinitely fine mesh the bending stiffness during stick will match the analytically generated one but the results generated in figure 4.20 show that with increasing mesh size the bending stiffness for the fully bonded models will go up.

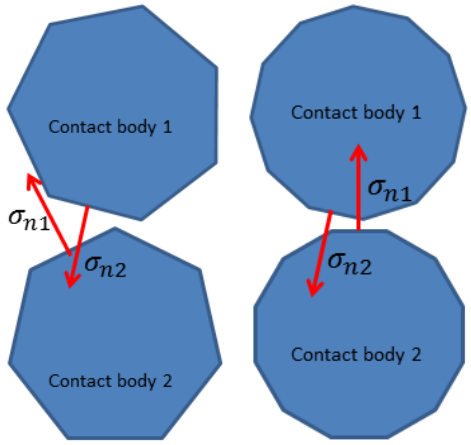

(a) Contact detection coarse mesh (b) Contact detection fine mesh

Figure 4.19: Contact detection and normal stress direction vector

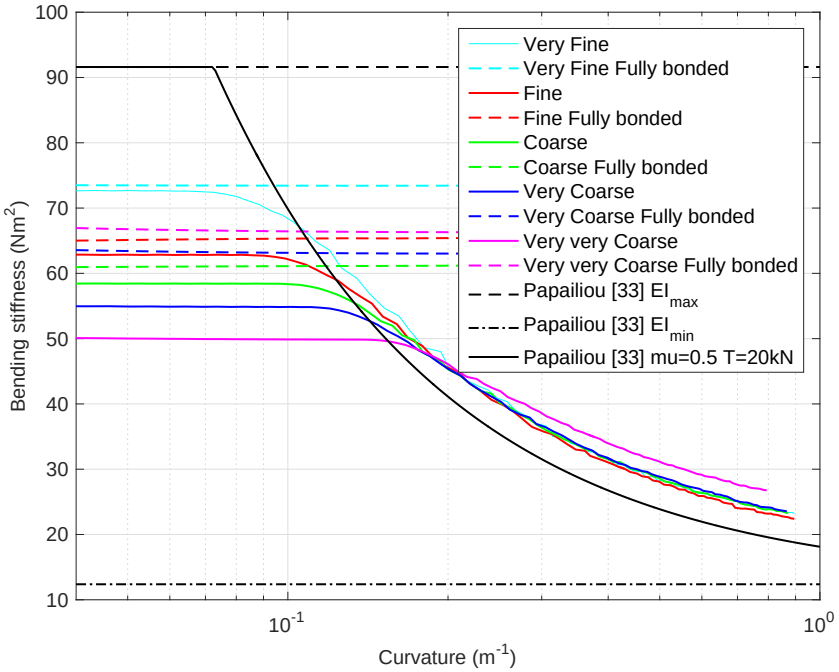

Figure 4.20: Bending stiffness as a function off curvature for different mesh size. All models are analysed with a axial tension of $T = 20$kN, all analysis with friction use a friction coefficient of $\mu = 0.5$

A few things can be concluded from figure 4.20 about the continuous lines describing stick-slip

behaviour:

- The first section of each line is horizontal and describes a regime where all wires stick to each other
- With increased detail of the mesh, the bending stiffness at low curvatures describing stick increases
- The difference between the fully bonded model and its corresponding stick-slip model decrease with increasing model complexity
- Models approximately behave the same for high curvatures

Computational time needed to run the very fine model is quite large (50hr) while for example running a very coarse model costs around half an hour. The most detailed model shows the best results. Therefore, a consideration between desired level of detail and computational time has to be made. The fine model is chosen for the bulk of further analyses as it shows a relative good initial comparison between the maximum bending stiffness of the fully bonded model and the stick-slip model and its computational time is relatively low compared to that of the very fine model.

4.4.2. Friction

Regarding the results for the very fine model (light blue) in the previous section, it can be noticed that the results for the fully bonded and the frictional (standard) model are quite close together. Other models display a difference between the fully bonded and the frictional variant. At first it can be concluded that the reason for this is the element size and due to the effect explained and illustrated in figure 4.19. However, further studies towards the method Marc calculates stick slip behaviour have shown that this is not the only reason. The method used to model friction will also have an impact on the magnitude of the bending stiffness during stick. The actual physics of friction and the numerical representation of it continues to be topics of research. [28] For the numerical model a Coulomb friction model has been used which can be represented by the following equations,

$$|f_t| < \mu f_n \quad \text{stick} \tag{4.15a}$$

$$f_t = -\mu f_n \cdot t \quad \text{slip} \tag{4.15b}$$

where f_t is the tangential (friction) force, f_n is the normal force and t is the tangential vector in the direction of the relative velocity. The discontinuity in equations 4.15 for the friction value may easily cause numerical difficulties. Marc can use different methods that deal with this problem. For example a bilinear friction model, where stick and slip conditions correspond to reversible (elastic) and permanent (plastic) relative displacements, respectively. Because of this assumption to resolve the discontinuity in the Coulomb model, numerical errors arise in the results of the analysis. Due to the allowed elastic movement during stick the measured bending stiffness will not be realistic. The ”frictional stiffness” corresponding to this elastic relative displacement is dependent on the element size and thus also has an influence on the measured bending stiffness. This explains the fact that the bending stiffness during stick for the standard models increases with higher mesh sizes. The details of what is stated here is further explained in detail and can be found in appendix E.3. The method of analysing the bending stiffness correctly, which will be used in this thesis is explained in section 4.4.2 where the parameters on which this frictional stiffness depend will be varied. The standard model is considered correct if the horizontal plateau in the graph displaying the maximum bending stiffness during stick matches the value generated by the corresponding fully bonded model.

For higher curvatures, the bilinear model and the Coulomb model described in equations 4.15 behave in the same way and so no significant dissimilarities between outcomes of different mesh sizes are found.

When changing the value for the friction coefficient, it is expected that the maximum bending stiffness at low curvatures will not change as wires are still in the sticking phase. When looking at figure 4.21 it can be seen that this is not the case. The bending stiffness at low curvatures will decrease for lower friction coefficients.

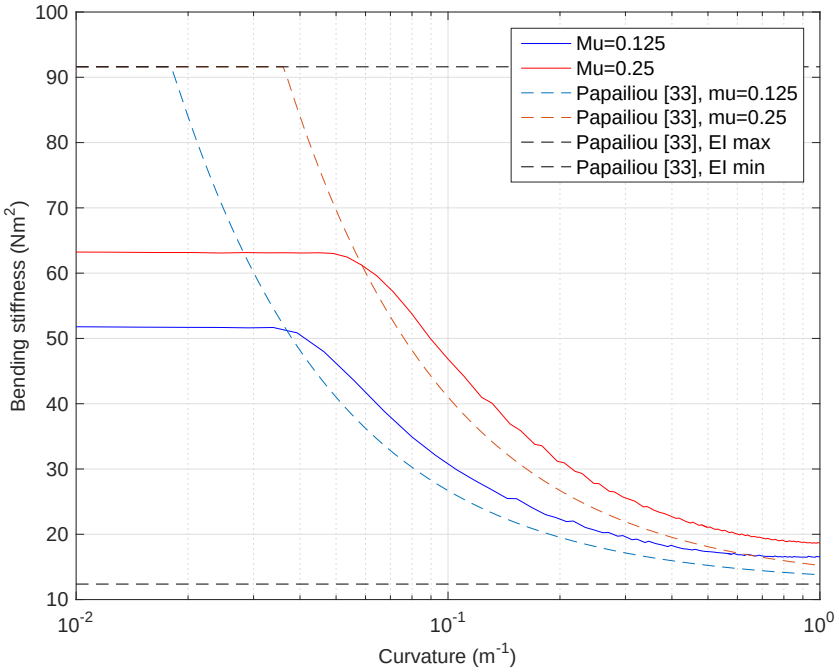

Figure 4.21: Variation of friction coefficient using a very fine model using a axial tension of $T = 20$kN.

This has to do with the way Marc solves friction problems which has been addressed previously in this section. The friction coefficient has an influence on the ”frictional stiffness” previously introduced. How this influence can be calculated is shown in appendix E.3. The main outcome of the analysis shown in appendix E.3 is that the so called slip threshold (δ) has to be adjusted when the friction coefficient changes to make sure that the frictional stiffness during stick stays the same when using different friction coefficients. The slip threshold describes a distance which is smaller than the average element edge length. It defines a section of elastic relative displacement where the frictional stiffness will be used to define the resistance to external forces.

The bending stiffness value during stick has to match the value found when running the fully bonded models. As the bending stiffness found during stick is dependent on this frictional stiffness, the slip threshold has to be adjusted when choosing a friction coefficient so it will match the required maximum bending stiffness defined by the fully bonded models. This adjusting of the slip threshold to match the correct value of the bending stiffness can be seen in figure 4.22.

The curve corresponding with a δ value of 1.5mm is found to match the fully bonded model best when looking at the maximum bending stiffness at low curvatures. All simulations in figure 4.22 are run using a friction coefficient of $\mu = 0.5$. When using other friction coefficients, the δ value has to be adjusted. How this is done can be found in appendix E.3.

The default value of the slip threshold is $\delta_{default} = 0.0025 L_{edge}$, where L_{edge} is the average edge length of the mesh. Using the fine model this results in $\delta_{default} = 0.0018$m $= 1.8$mm. For a model using $T = 20$kN and $\mu = 0.5$ a slip threshold of $\delta = 1.5$mm has to be used to make the model behave as it should. Because a friction coefficient of $\mu = 0.5$ is not realistic for steel wire ropes, a value of $\mu = 0.125$ is used. Because the frictional stiffness (equation 4.16) has to remain equal,

$$C_{fric} = \frac{\mu F_n}{\delta} \tag{4.16}$$

the slip threshold has to reduce by the same factor as the friction coefficient to keep C_{fric} constant. As is determined in section 4.4.6, the same will be done for a change in tension. This will result in the slip thresholds and their percentage from the default value seen in table 4.4.

In the third case in table 4.4, a slip threshold has to be chosen which is 10.44 percent lower than the default value. A reduction in slip threshold will result in the need for smaller load steps to reduce the numerical instability generated by the slip threshold reduction thus increasing computational time significantly.

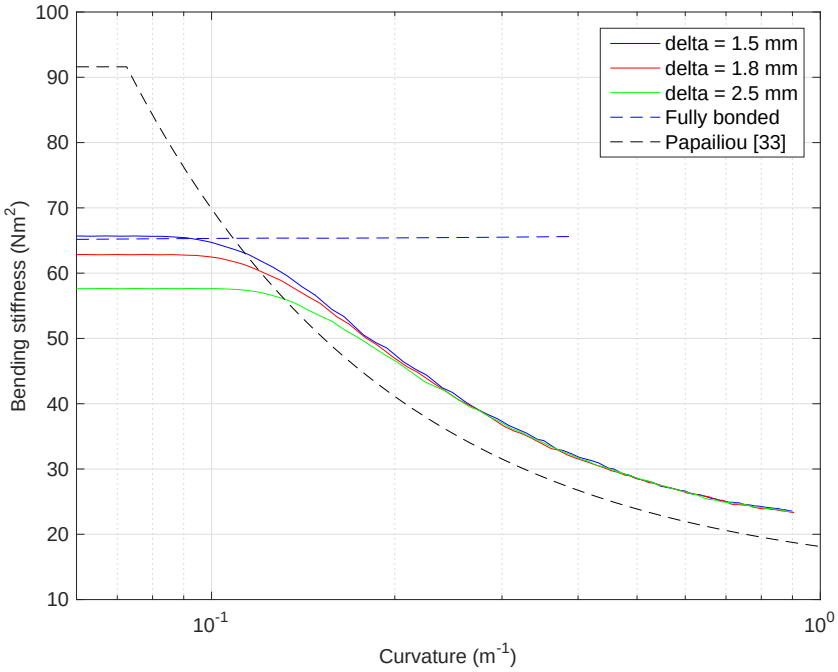

Figure 4.22: Variation of the slip threshold using a fine model using a axial tension of $T = 20$kN and a friction coefficient of $\mu = 0.5$

Table 4.4: Standard model with different parameters using different slip threshold values to match to the fully bonded model

-	Tension [N]	Friction coefficient [-]	Slip threshold [mm]	percentage of default [%]
1	20000	0.5	1.5	83.33
2	20000	0.125	0.375	20.83
3	10000	0.125	0.188	10.44

4.4.3. Load step determination

The transition from stick to slip is hard to model numerically as it is somewhat of an abrupt change. The abruptness is made smooth by the program as will be explained in section 4.4.2 but will still require detail to model correctly. Because of this fact, the load step will be varied when the model progresses so that the load step size can be reduced where needed without heavily increasing computational time. The analysis will be divided into three parts, the tensioning, stick to slip transitions regions, and the slipping part. After the tensioning part the results can be seen in figure E.2. The load steps that have been taken into account for a simple strand model with a fine mesh can be seen in table 4.5. Noticeable are the smaller load steps in the transition and slip part where the former contains the lowest load step. This is due to the aforementioned abrupt change in bending stiffness as can be seen in figure E.2. Note that when an even more abrupt change from stick to slip is seen, the load steps shown in table 4.5 will be reduced until a smooth transition in the results is seen.

Table 4.5: Different load steps per analysis region for a simple strand model with a fine mesh with a tension of $T = 20$kN and a friction coefficient of $\mu = 0.5$

Analysis part	Load step [s]
Tension	0.01
Transition	0.002
Slip	0.008

Determining the correct load step is also important because of the non-linear behaviour of the strand in the slip regime. When the load step selected is to large, the program reacts to abruptly to the change

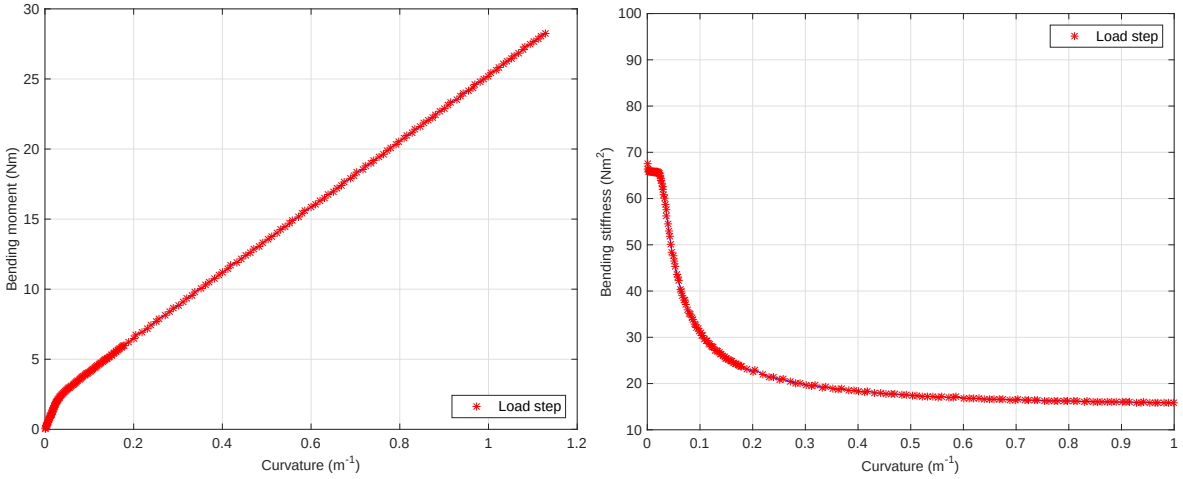

(a) Bending moment (b) Bending stiffness

Figure 4.23: Load step variation for a simple strand model with a fine mesh with a tension of $T = 20$kN and a friction coefficient of $\mu = 0.5$

in load resulting in outliers when compared to results from analysis ran with a smaller load step. In appendix section E.2 results of different analysis using other load steps have been shown. Again, the load steps shown in table 4.5 for the slip part are reduced when uncertainties are found in the results.

4.4.4. Boundary and initial conditions

In section 4.1.4 the boundary conditions are explained which have been implemented into the standard model, for clarity these will be summarized in this section.

The standard model loading characteristic is divided into two parts, tensioning and bending where the axial forces and bending moments are exerted on two reference nodes located on each end of the strand. All nodes at the end of a strand are rigidly connected to that one reference node. To properly map the bending stiffness due to the bending of the strand, friction is only allowed in the second or bending part.

Other set-ups of boundary and input conditions can be realized and compared to the standard model. This will show which model set-up is the most realistic and which model should be used for further analysis. Five different model set-ups have been developed, the first two will consist of the standard model and the all friction model. Both models have the same boundary conditions: all nodes at the ends have been rigidly connected to a reference node where the tension and bending loads will be applied but have different input parameters. The last three models have the same input parameters as the standard model but differ in boundary condition set-ups.

1. *Standard:* Only friction during bending is allowed, friction during tensioning is assumed to be zero
2. *All friction:* Friction is allowed during both tensioning and bending
3. *Free translation:* Movement in axial direction of the strand between wires and between wire and core is allowed as can be seen in figure 4.24a
4. *Free rotation:* Movement in rotational direction of the strand between wires and core is allowed as can be seen in figure 4.24b
5. *Free translation and rotation:* Movement in axial and rotational direction of the strand between wire and between wire and core is allowed as can be seen in figure 4.24c

When comparing the standard with the All friction model in figure 4.25a, it can be concluded that the All friction model displaces a more compliant response. This can be explained due to the fact that during the tensioning of the strand, the All friction model generates friction between wires. This pre-existing friction on the onset of bending makes it easier for the wires to slip and also reduces the bending stiffness during the stick regime. In order to rule out the effect of pre-existing friction so that

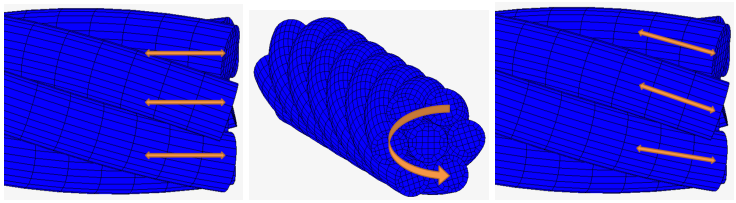

(a) Free translation (b) Free rotation (c) Free translation and rotation

Figure 4.24: Alternate boundary condition set-ups

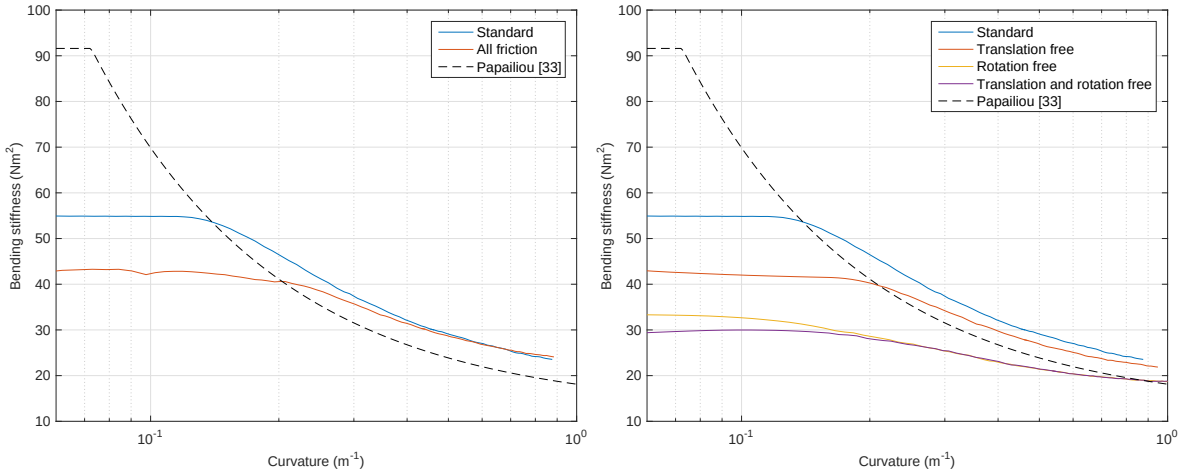

(a) Standard and all friction model

(b) Standard model compared to alternate boundary conditions set-ups which can be found in figure 4.24

Figure 4.25: Boundary condition analysis, all very coarse models are calculated with $\mu = 0.5$ and $T = 20$kN

solely the effect of the bending can be taken into account, following analysis have been performed with the method of the standard model with only friction during bending.

The models that allow for different movements at the boundaries displayed in figure 4.25b also show more compliant movement than the standard model. Energy will be dissipated due to the allowed movement of the individual wires in the strand. The more the wires are allowed to move at the boundaries, the lower the bending stiffness. The ends of wire ropes are clamped at thus displaying the restrictions set for the standard model, however over the length of the rope different wire rope components can slightly move relatively to one another which resembles the models with allowed movement. This movement however is not entirely free such as is the case with the models 3, 4 and 5.

The problem with these models allowing movement is the numerical calculation of the friction. As is briefly explained in section 4.4.1, the conditions for slipping depend on the mesh size and orientation of the mesh. When allowing movement at the ends, the calculation of the friction on the mesh is more difficult and a more detailed mesh size and load step are needed. However, changing the mesh size has an influence on the bending behaviour as has been seen in section 4.4.1. Changing the mesh size will impact the results. To properly compare results, constant mesh sizes have to be used. This causes some numerical instabilities as can be seen in figure 4.25b.

It seems like the standard model due to its boundary conditions isolates the effect of the inter wire friction on the state-dependent bending stiffness. This model set-up will be used to compute the state-dependent bending stiffness shown in this thesis.

4.4.5. Modelled length

During the bending tests performed by Raoof [35] is was concluded that the slip of wires in a wire rope start at the neutral axis of bending. In the numerical model a limited length of the simple strand can be constructed. Wires inside the strand cross the neutral axis only with a spacing of $60°$ times the pitch

length separated from each other. In figure 4.26 different strand lengths are shown with the same lay angle. The locations of different wires inside the strand crossing the neutral bending axis are indicated. It is expected that slip will propagate from these locations outward in both directions.

It has to be noted that the maximum bending stiffness found for the models with different lengths shown in figure 4.27 cannot be compared. This is due to the fact that the maximum bending stiffness for the fully bonded models is dependent on the element size which is not constant throughout the models. The parameters defining the frictional stiffness during stick, explained in appendix section E.3 is adjusted individually for each model so that the maximum bending stiffness during stick will match the value found in the corresponding fully bonded model. It is assumed that all models shown in 4.26 with have approximately equal values for the maximum bending stiffness if the element sizes were equal.

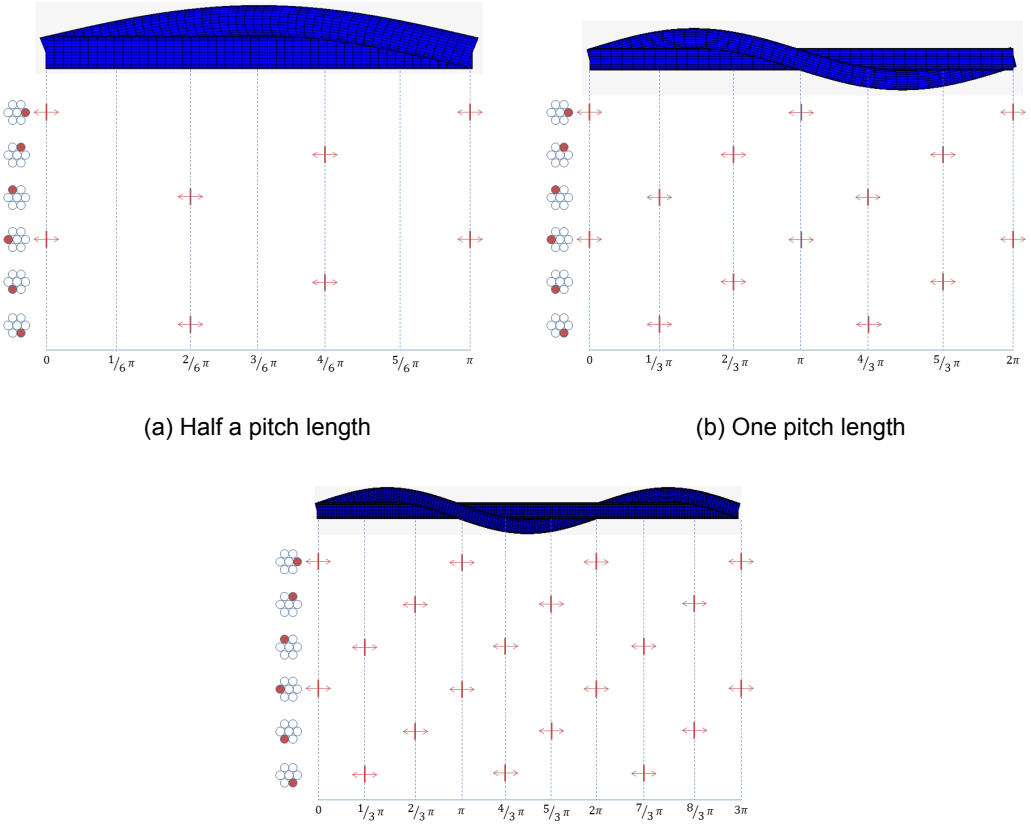

(a) Half a pitch length

(b) One pitch length

(c) One and a half pitch length

Figure 4.26: Slip starting locations for multiple lengths of a simple strand with equal lay angle

When looking at figure 4.26a where half a pitch length has been modelled, it can be seen that two wires cross the neutral bending plane at the ends of the model. All nodes at the ends are connected to a reference node which is restricted in all movement except the rotation in the direction of the moment. Due to this boundary condition, wires will not slip close to the ends of the strand. Therefore, only four wires will slip while bending this model. This will result in a higher bending stiffness for larger curvatures as not all wires will slip. This effect can be seen in figure 4.27 where the bending stiffness is shown for different curvatures for all model lengths shown in figure 4.26.

The results for a pitch length of one and that of one and a half show similar results. This is because the pitch length is long enough so that all wire can show slip behaviour as is schematically shown in figures 4.26b and 4.26c. However, the bending stiffness found for the one and a half pitch lengths is again slightly higher than that of the one pitch length model for high curvatures. This is because of the previously explained phenomenon in section 4.2 where it is explained that when a model gets to long, the middle of the strand will not slip. This will results in a larger bending stiffness than expected because the assumption that the bended strand is on a circle is no longer valid and wires in the middel of the strand will still be in sticking condition. However, with this model length, this effect is still quite

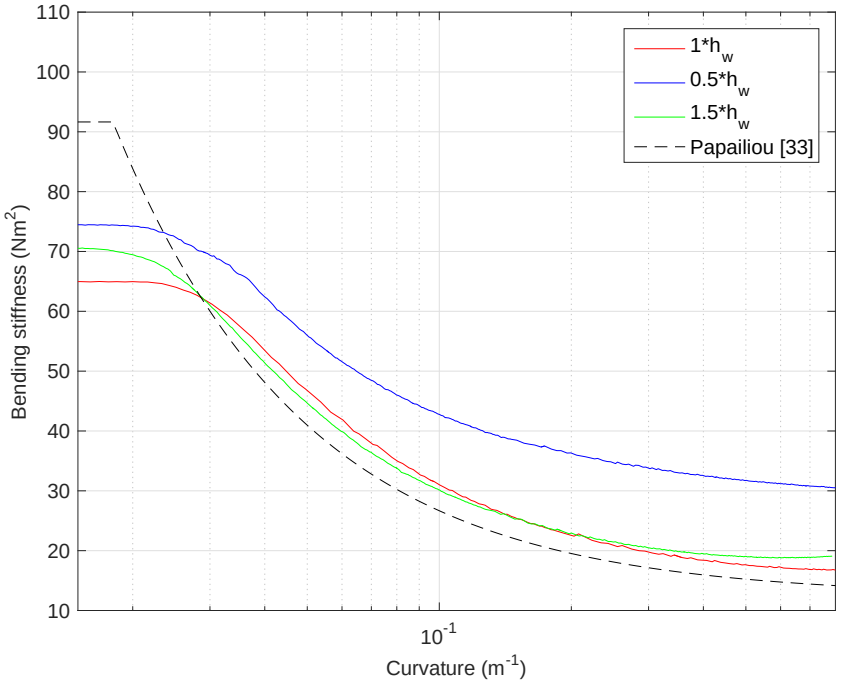

Figure 4.27: Bending stiffness for standard models with model length variation using simple strands with the same lay angle

small so the results from the model with a pitch length of one and that of one and half are approximately the same.

It can be concluded that the one pitch length model is long enough so that when bent, all wires will be able to slip along their length. The model is considered short enough so that the middle part of the strand will also show slip causing the assumption that the bent strand can be projected on a circle to be valid. This last remark is strengthened by the fact that the one pitch length strand also has two wires that pass the neutral bending axis in the middle of the cable thus starting slip from that location onwards.

4.4.6. Tension

The effect described in the previous section defining the way Marc solves frictional problems, also has an effect on the bending stiffness during stick when varying the tension on the strand. In appendix E.3 it is explained that the friction coefficient and the normal force on the element have an effect on the frictional stiffness during stick. As has been shown in section 4.4.2, adjusting the slip threshold when changing the friction coefficient is sufficient to make sure that the bending stiffness during stick will remain the same when other frictional coefficients are used.

However in the case of varying tension, it is more complicated as the normal force influencing the frictional stiffness is not directly determined by the tension but is also dependent on the lay angle and the orientation of the wires. Another difference is the fact that the frictional coefficient is constant throughout the analysis while the normal force on the elements will continually change due to the applied external forces thus effecting the frictional stiffness and therefore effecting the bending stiffness during stick.

It is important to state that the bending stiffness of the strand during stick is not expected to change when different pretensions are used. As can be seen when modelling the strand as a beam following the Euler-Bernoulli equations with pretension:

$$\rho A\ddot{w} + EIw'''' - Tw'' = 0 \tag{4.17}$$

The term Tw'' will take the extra bending resistance due to a higher pretension into account while the material bending stiffness parameter will stay the same. Consider for example a simple string with hardly any bending stiffness loaded with tension. Apply a point load perpendicular to the string halfway along the length. When increasing the tension, it will become harder to bend the string using the point

load. This is not because the bending stiffness of the string is increased, in fact it is still the same as it was before. It is due to extra tension that is added in the system described by T in equation 4.17.

Wire ropes during stick will behave the same way as the string does in the aforementioned example. This can be seen in figure 4.28 where different tensions are applied to a simple strand with a fully bonded and a standard frictional model. The maximum bending stiffness that has been found for different curvatures for the fully bonded model will stay the same. This corresponds to the findings stated in this section.

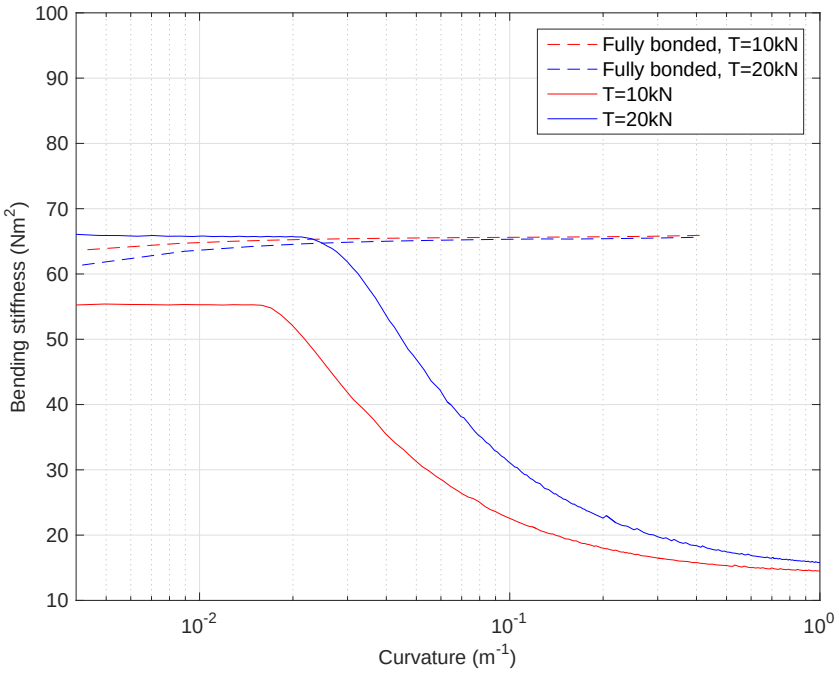

Figure 4.28: Fully bonded and frictional models using a friction coefficient of $\mu = 0.125$ for different tension levels

In figure 4.28 also the standard frictional model change under different tension levels is shown. When examining the effect of varying tension while keeping the slip threshold constant, it can be stated that the effect is similar to the effect of changing friction coefficient which was seen in figure 4.21. Although the effect of the tension forces on the normal force determining the frictional stiffness during stick are more complicated than that of the friction coefficient, the results seem similar. Therefore changing the slip threshold could again keep the frictional stiffness similar for different tension levels. In figure 4.29 different slip threshold values for a standard model with a constant tension are shown. It can be seen that when decreasing the slip threshold value even further, the horizontal plateau of the standard model with match the fully bonded model.

It can be seen in figure 4.29 that by decreasing the slip threshold the bending stiffness during stick will go up and with therefore eventually match the fully bonded model. If these values match the model is considered well represented. During the slipping phase the influence of the slip threshold will no longer have an influence and all models will behave similarly.

4.5. Model expansion

Steel wire ropes used in the offshore industry consist of more complex wire rope configurations. Wires describing double helical paths in the outer layers are present in these more complex configurations. When solving these models using Marc [27], problems with mesh size can be expected especially with more wires and thus contact bodies as has been seen in figure 4.20. In the same figure is is shown that the shape of the curve corresponds quite well with the model by Papailiou [33] although the extremes of the numerical model are more nuanced when compared with the analytical model.

The difficulties with setting up a numerical model for larger wire ropes configurations are caused by several components, which will be addressed with a coarse mesh model consisting of 67228 elements. The mesh used is shown in figure 4.30. While performing the same method of measuring the bending

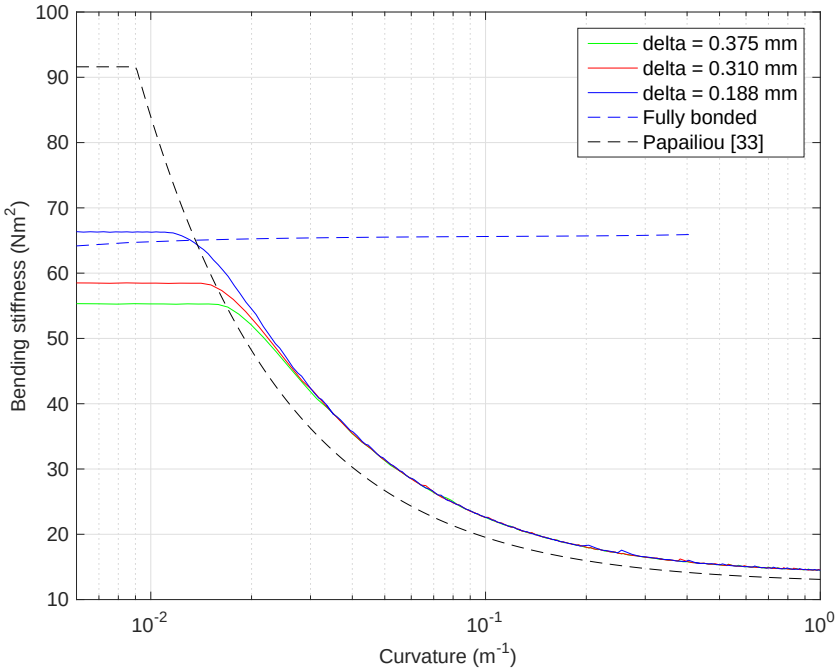

Figure 4.29: Models with changing slip threshold δ while keeping tension at $T = 10$kN and friction at $\mu = 0.125$

moment as is described in section 4.1 the following relationship has been found between bending stiffness and curvature (figure 4.31).

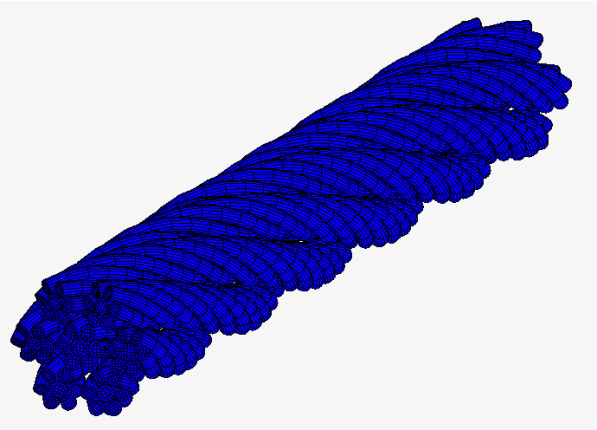

Figure 4.30: Mesh of the coarse IWRC model

When comparing figure 4.31 with for example figure 4.20 it can be concluded that there is no clear horizontal part of a curve in figure 4.31 which indicates full stick. The minimum and maximum theoretical values calculated using C are far removed from the numerically determined ones. The curve in figure 4.31 does however show stick slip behaviour as after a certain curvature the bending stiffness will drop towards a constant value.

High computational time

Modelling more complex geometries in Marc can provide numerical uncertainties because of the presence of multiple wires and thus contact bodies and because of the way Marc calculates friction which is briefly explained in section 4.4.1. Large computational time is needed to run a model such as an IWRC with a configuration as is described in appendix A. The large number of elements and the small load step which are necessary to come to a stable solution are the main contributions towards this high computational time.

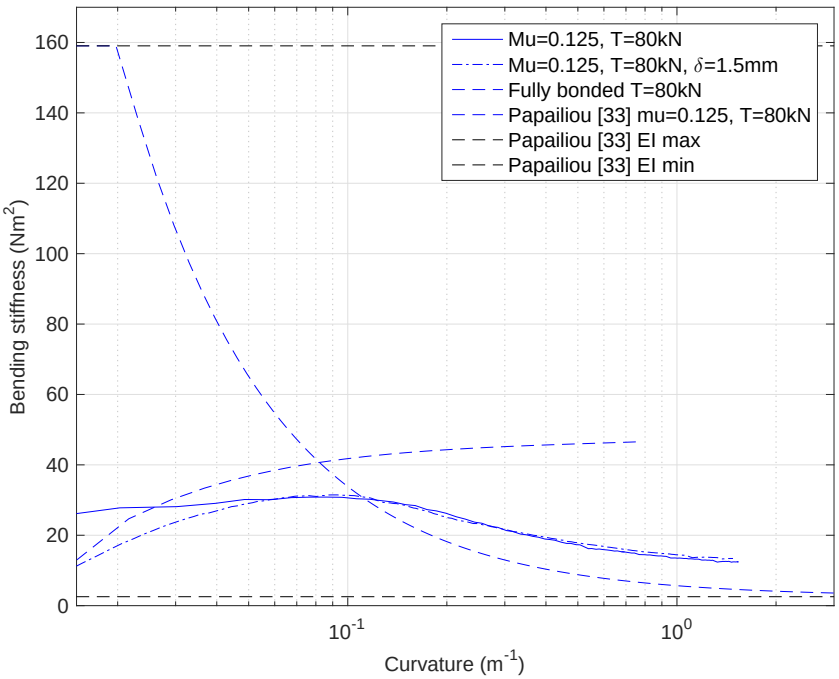

Figure 4.31: Relationship between bending stiffness and curvature for an IWRC

Radial contraction limitation

The first part of the graph corresponding with low curvatures in figure 4.31 can be explained by the fact that some wires are not touching each other somewhere over their length at the onset of bending. This is due to the boundary conditions placed upon the model restricting the radial contraction of the ends of the IWRC. This effect can be seen in figure 4.32 where in figure 4.32a the side view of the model in initial condition is shown. Because of the rigid connection between the nodes at the ends of the IWRC and the reference node no radial contraction is allowed. Figure 4.32b shows a exaggerated situation after tensioning where it can be seen that all wires in the middle of the model touch while at the ends the initial configuration is still maintained. Wires will not achieve perfect line contact along their entire length thus resulting in a non equal distribution of the normal forces between wires. Therefore the bending stiffness at the onset of bending is quite uncertain as the loads and contact conditions near the boundaries differ from the situation in the middle of the model. After certain deformation and movement during bending, wires will settle and a more reliable response is found as can be seen in figure 4.31 for somewhat higher curvatures.

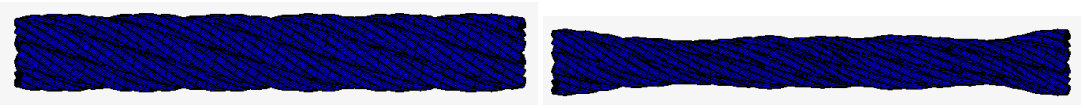

(a) Initial configuration (b) After tensioning

Figure 4.32: Exaggerated visualisation of the radial contraction limitation in larger wire rope configurations

Slip threshold

The way Marc determines friction explained in appendix E.3 also has an influence on this varying bending stiffness during stick. The size of the elements in all wires of the IWRC are not the same while the slip threshold for all elements is equal. This results in the fact that the frictional stiffness between elements is not the same throughout the model which will result in a non constant bending stiffness during stick.

When decreasing the slip threshold as has been done in this chapter for simple strands the resistance during stick should increase. As however can be seen in figure 4.31, bending stiffness during stick decreases and it takes some time or curvature of the cable until it reaches its maximum value. In

the case of the simple strand model the slip threshold was also equal for all elements while the element edge size was not. However, differences due to the low number of different wires are very small and no serious issue arises. In the IWRC, differences between wire diameters are larger and thus reducing the slip threshold has a different effect on the elements of different contact bodies.

Model length

The model length influences the found results. Taking to much strand rotations into account will result in the maintaining of stick in the middle of the strand when bending, as has been shown in section 4.2. This is not the desired effect as it will increase the found bending stiffness. When considering a to short model, not all wires will start slipping as is explained in more detail in section 4.4.5.

When considering larger wire rope configurations such as an IWRC with double helical wires in the outer strands, more parameters play a role. For the results shown in this section an IWRC as in figure 4.30 is taken into account. The strands accomplishes one full rotation while the wires in those strands make four rotations. The wires in the core strand make two rotations all within the same model. Due to these differences in winding lengths, it is difficult to find the ideal model length. A to short model will prevent wires from slipping while a to long model will prevent wires from slipping in the middle of the model. This problem increases for even larger wire rope configurations.

Modelling the correct bending stiffness while taking all these mentioned challenges into account is time consuming and challenging. The simple strand model is chosen and elaborated on in this thesis as results are generated more quickly.

4.6. Evaluation

This chapter has treated the method used to model different wire rope configurations into the FEM program Marc. The simple strand model is discussed elaborately along with the method of calculating the bending stiffness dependent on parameters such as curvature, tension and friction coefficient. The method of finding the bending stiffness can be divided into the following steps:

1. Create an input file for an arbitrary wire rope configuration using Matlab
2. Construct the wire rope cross sectional configuration in Marc or import it directly from Inventor
3. Use the input file to construct the mesh
4. Choose settings and boundary conditions corresponding to the desired analysis (fully bonded, frictionless or standard)
5. Run the fully bonded and standard model and compare the results for the maximum bending stiffness
6. Adjust the slip threshold so that the maximum bending stiffness from the standard model matches the fully bonded model
7. Run the frictionless model and use the results to correct the bending stiffness found for large curvatures due to geometric non-linearity
8. When parameters such as friction coefficient, tension or element size are changed, the slip threshold has to change accordingly

In the sensitivity study some aspects of the program Marc are described and it is discussed how they influence the results. One main challenge with modelling friction was found when changing the values for the friction coefficient and the tension. The maximum bending stiffness during stick was not influenced by the variation of the friction coefficient or tension. This is an unrealistic result and is caused by the slip threshold value determining the frictional coefficient which has an impact on the bending stiffness during stick. Adjusting this slip threshold according to the parameters used resulted in models which behaved representatively and which could be used in further analysis. However, reducing the slip threshold value will result in higher computational time because of the smaller load step that has to be chosen. Lowering the slip threshold will result in a more sudden change between

stick and slip thus resulting in numerical instability. By reducing the time step, this instability can be resolved. In appendix section E.3, the effect of reducing the slip threshold is shown.

The preliminary study performed in this chapter does show very promising results as the numerical model clearly resembles the analytical model by Papailiou [33] for simple strands. When looking at multiple layers in section 4.5, the resemblances are still there for higher curvatures but for lower curvatures they correlate much less. As computational time needed for these more complex models are substantial, only basic results are shown. However, the findings in this chapter are promising. With time and increasing computer capacity, numerical modelling for these more complex wire rope geometries is certainly possible.

For further research into the validity of the assumptions by Papailiou [33] and into the bending behaviour of helical wound ropes, a simple strand with a configuration as in appendix A is used. This is done because of its simplicity. This reduces computational and model fine-tuning time considerably. When it is shown that it is possible to model the state-dependent bending stiffness for simple strands, the conditions required for model expansion can be discussed.

5

Results

This chapter will focus on the results generated by the numerical model explained in chapter 4. The results will be compared to that of the analytical model described in chapter 3. Some of the assumptions made in the analytical model by Papailiou [33] will be discussed in this chapter. The standard model described in section 4.1.4 is used for the analyses with a fine meshed simple strand model (table 4.3). The used load step will vary depending on the input as some input parameters require a smaller load step to be able to deliver reliable results.

In section 5.1 the assumption of pure interlayer contact will be checked. Differences between all aforementioned contact modes: interlayer, intralayer and mixed will be shown.

In section 5.2 the friction coefficient will be varied. This is of importance as the friction coefficient in steel wire ropes is hard to determine and will change over time. Lubricant will seep out of the wire rope because of repeated tensioning and bending thus increasing the friction coefficient. [10] As it is uncertain what the axial coefficient is, its effect on the bending stiffness has to be monitored.

The effect of tension on the bending behaviour of wire ropes is an important parameter to monitor as the tension varies along a vertically suspended wire rope due to its self weight. Section 5.3 will display and evaluate the effect of tension.

Lay angle variation and tension differences along a wire rope are caused by one another. Section 5.4 will show the impact of different lay angles on the bending stiffness at different curvatures.

The chapter will end with a discussion of the results and an overall comparison of the analytical and numerical models. Use of both models for large wire rope configurations will be discussed.

5.1. Contact

The three different contact modes implemented in the numerical model are: interlayer, intralayer and mixed contact. A more detailed description of how contact is determined in Marc will be shown in appendix E.3.

The black dotted line in figure 5.1a represents the analytical solution defined in chapter 3 and is used as a reference. In the analytical solution, the contact is assumed to be solely interlayer.

In figure 5.1a the result can be seen for a simple strand with a lay angle of $17°$. This lay angle is high enough to let the wires in the first layer of the strand touch each other in the undisturbed situation. If only interlayer contact is allowed, a reduction in bending stiffness at low curvatures is seen while comparing with the intralayer or mixed contact conditions. Intralayer contact resembles the mixed contact quite well for a simple strand with a lay angle of $17°$ as can be seen in figure 5.1a.

This is completely different when looking at the results of a simple strand with a lay angle of $9°$ in figure 5.1b. Wires only make interlayer contact in the undisturbed situation. This is in agreement with the assumption made in the analytical model. At lower curvatures, the results from the intralayer contact condition show lower values for the bending stiffness. Interlayer contact and mixed contact show exactly the same results thus indicating that throughout the model only interlayer contact is present.

The assumption by Papailiou [33] that only interlayer contact is present can be considered correct for low lay angles. When in the undisturbed situation, intralayer contact is available, this assumption

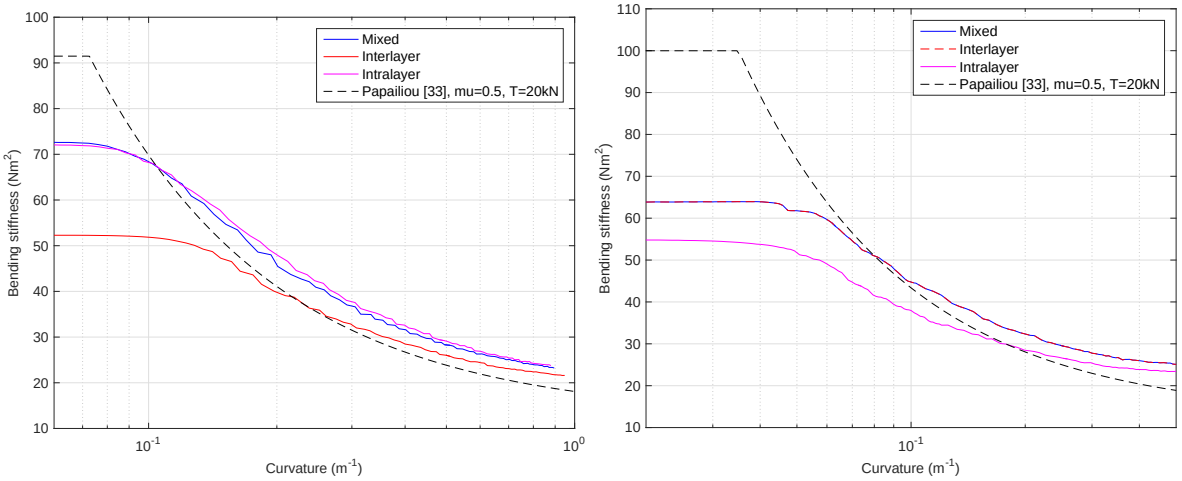

(a) Lay angle = 17°

(b) Lay angle = 9°

Figure 5.1: Relationship between bending stiffness and curvature while using different contact modes for a simple strand with lay angels of 9° and 17°

will not be correct for low curvatures of the strand. At higher curvatures, the difference between the the mixed and interlayer results will diminish.

5.2. Friction coefficient

After numerically validating the model for friction variation in section 4.4.2, this section focusses on the effect of changing the friction coefficient while mapping the change in bending behaviour. The uncertainty of input parameters like the friction coefficient of lubricated steel on steel contact is quite high. [41] Therefore, the effect of different friction coefficients is measured in this section.

As the determination of the friction coefficient between wires in a wire rope can be uncertain, the outcome of a model and experimentally determined results can be as well. Figure 5.2 displays the effect of a different friction coefficient on the outcome of the model while keeping the tension constant. The analytical results display a stiffer response in lower curvature ranges and a more compliant response at higher curvatures than those numerically generated. The slope during stick is higher and the slope of the graph in slip is smaller than that of the numerical model. It can be seen from the graph that with an increasing friction coefficient, slip will start at higher curvatures both in the analytical and numerical model.

Figure 5.3 displays the relation between curvature and bending stiffness. When comparing the analytical and the numerical model, similarities and dissimilarities can be seen when only focussing on the effect of the friction coefficient. The dissimilarity at low curvatures can be explained by the level of detail of the mesh as has been explained in section 4.4.1.

The moment of slip calculated by the numerical model starts at higher curvatures than the moment of slip from the analytical model. However, this is not representative as the analytical model starts with a higher bending stiffness during stick. The moment of slip generated by the numerical model does match with the predicted curvature described by the analytical model as can be seen in figure 5.3. The transition from stick to slip is less abrupt in the numerical model as at the start of slipping, not all wires have slipped over their entire length. As the curvature increases, the rest of the wire length will slip and thus decrease the bending stiffness gradually.

The shape of the curve at larger curvatures is similar for both models apart from the fact that the numerically generated value is slightly higher than that of the analytical model. The friction coefficient in the numerical model seems to have an influence on the bending stiffness at high curvatures. However this statement could be false due to the fact that the numerical model is corrected for geometric non-linearity which is explained in section 4.3. It was found that values generated for curvatures higher than $\kappa = 0.5\text{m}^{-1}$ can be unreliable. The correction reduces the non-linear effect. However, it cannot be assured that the values found at these high curvatures are completely reliable.

Curvatures higher than $\kappa = 1\text{m}^{-1}$ are considered quite large. These curvature are hard to model

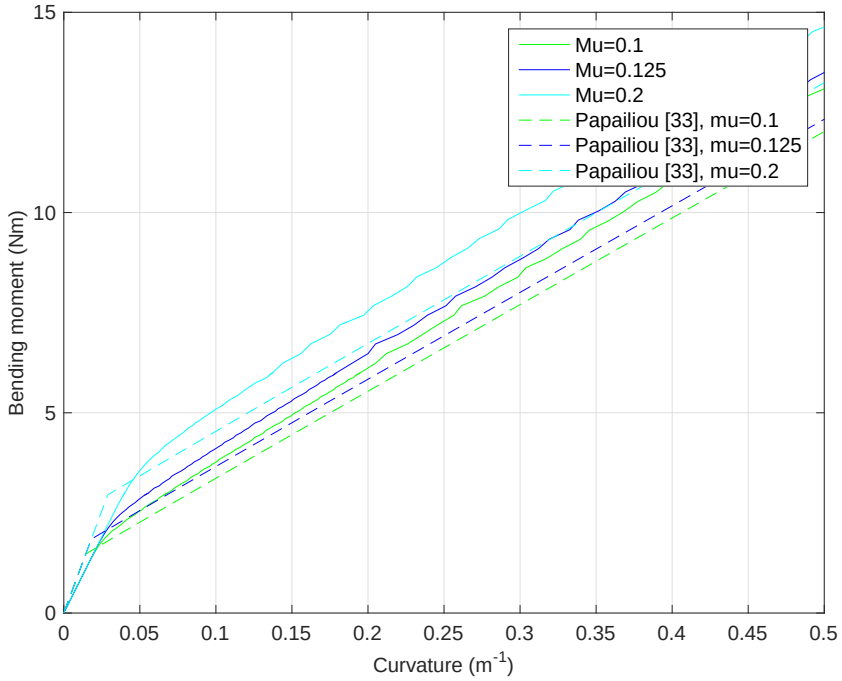

Figure 5.2: Relationship between curvature and bending moment with varying friction coefficient while maintaining a constant axial force of $T = 20\text{kN}$

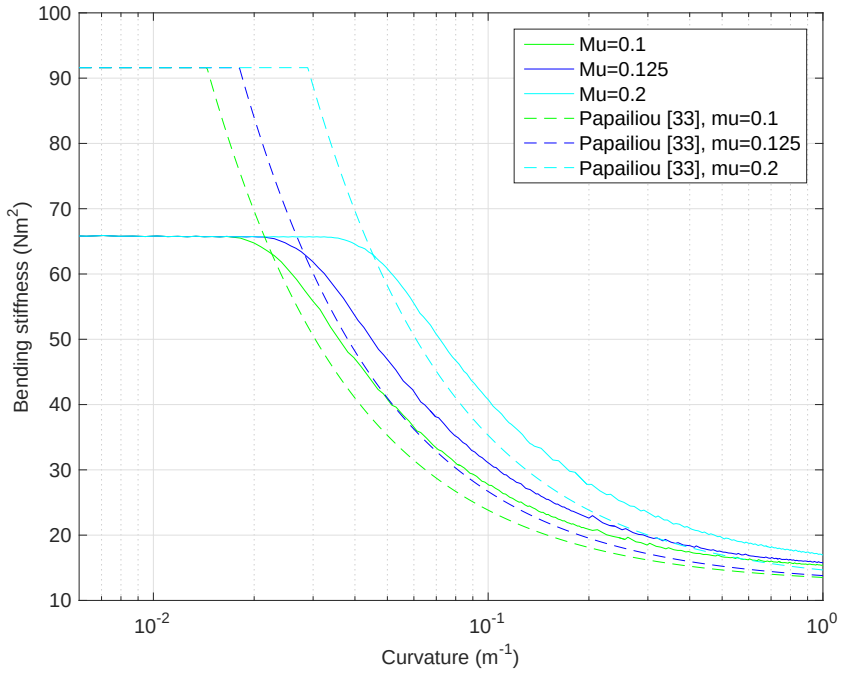

Figure 5.3: Relationship between curvature and bending stiffness with varying friction coefficient while maintaining a constant axial force of $T = 20\text{kN}$

numerically due to the geometric non-linearity of the model set-up. It can therefore not be stated that the bending stiffness reaches the analytical minimum independent of the friction coefficient. These curvatures are not likely to be found in reality, so it can be stated that the minimum bending stiffness is not reached when using a wire rope in practice. However, the value for the bending stiffness at a curvature of $\kappa = 1\text{m}^{-1}$ is almost equal to the theoretical minimum value. This statement will be investigated in the practical implementation of the next chapter.

It can be concluded that with a variation in the friction coefficient both models behave in the same manor except for large curvatures. At these curvatures, the numerical model shows a dependency on the coefficient of friction while the analytical model does not. Another conclusion is that the higher friction coefficient will generally result in a higher slipping curvature which indicates the starting point of slip. After the slipping curvature is reached values for the bending stiffness for larger friction coefficients will be higher.

5.3. Tension

Tension has an effect on bending stiffness which is found to be somewhat similar to that of the friction coefficient. Slip of the wires inside the strand will start at higher curvatures with increased tension, just as with an increased friction coefficient. The bending stiffness at high curvatures will be higher for strands with a higher axial tension according to both the analytical and numerical model. Eventually, the bending stiffness will drop to the theoretical minimum value according to the analytical model. For the same reasons as in section 5.2, the same cannot be stated for the numerical model. However, curvatures higher than $\kappa = 1\text{m}^{-1}$ are not likely to occur.

The analytical model does take into account that with increasing tension, wires will slip at higher curvatures as can be seen in figure 5.5.

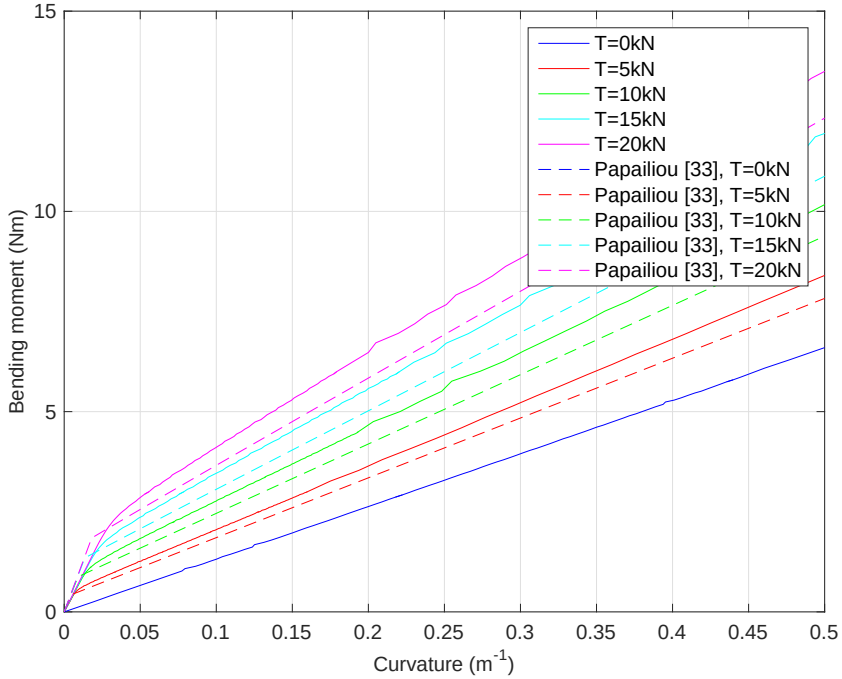

Figure 5.4: Relationship between curvature and bending moment with varying axial tension while maintaining a constant friction coefficient of $\mu = 0.125$

It can be seen in figure 5.5 that the bending stiffness of all models during stick is not entirely equal to each other as they should be. This is due to the load step and slip threshold change which is needed to ensure comparable results. Section 4.4.6 has provided more information into this phenomenon. The results shown in the figures 5.4 and 5.5 do show good resemblance with the analytical model derived by Papailiou [33].

The observed change in relationship between bending stiffness and curvature for different tension levels shown in this section can be translated to the situation of a steel wire rope in an A&R operation. When vertically used in large water depths, the tension at the bottom of the cable will be low while the tension at the top will be high. According to figure 5.5, the bending stiffness over the whole curvature range in the slip and transition regime will be lower when considering low tension. Taking this into account in the aforementioned situation, a lower bending stiffness will be found in the lower parts of the wire rope. However, this does not necessary have to be the case. The results shown in this section are for a simple strand with a constant lay angle. In reality, the lay angle will change because of the

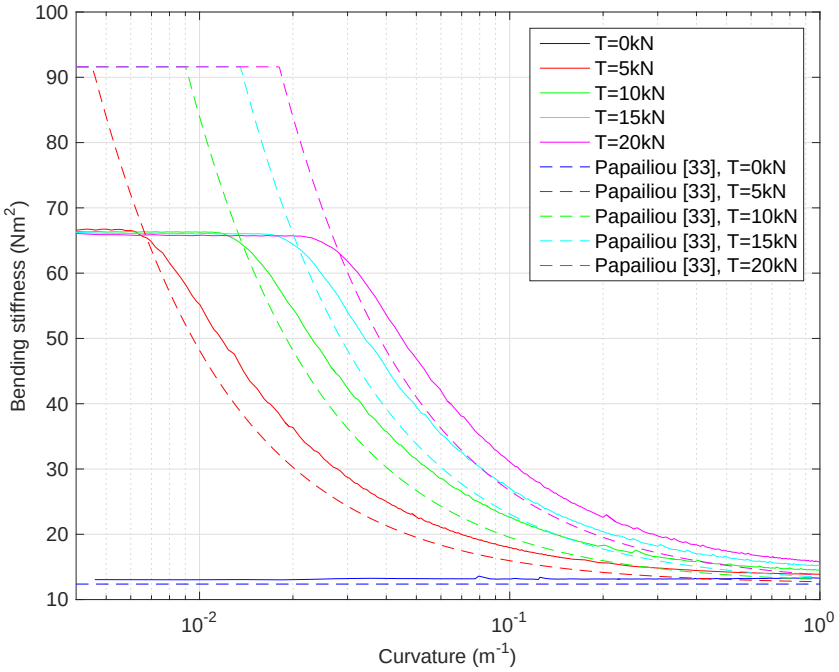

Figure 5.5: Relationship between curvature and bending stiffness with varying axial tension while maintaining a constant friction coefficient of $\mu = 0.125$

applied tension and helical geometry as has been explained before. Therefore the conclusion that the bending stiffness over the whole curvature range will drop when lower tension is considered is not yet justified when considering an A&R wire rope used in large water depth. Lay angle variation has to be taken into account. This effect will be discussed in section 5.4.

5.4. Lay angle

The model by Costello [7] has been used to display the relation between axial tension and torsion of a simple strand. Using the numerical model generated in section 4 the approach by Costello [7] can be verified. Figure 5.6 displays the tension torsion relationship according to Costello [7] and the numerical model. Because Costello [7] does not take friction into account, the numerical model is run with and without friction to see the difference between the results.

Both the frictionless and friction models correspond quite well with the analytically generated result. It can be seen in figure 5.6 that friction influences the numerical result but the deviation from the frictionless result can be considered small. It can be concluded that the model by Costello [7] corresponds quite well with the numerically generated numerical model and can therefore be used in further analysis.

Now that the relationship between tension and torsion is analysed, the torque in a wire rope used in A&R operations can be derived. Because the lay angle of a wire rope section located halfway along the vertically suspended length does not change, the torque can be derived in this location. This torque is then equal along the whole length of the vertically suspended cable.

The effect of axial torsion coupling on the bending behaviour of wire ropes is not of a direct nature. Due to the effect that the lay angle of wire ropes will change over their length, bending behaviour will change accordingly. Bending stiffness of wire ropes is not only dependent on tension, friction coefficient and curvature but also on the lay angle of the rope or strand.

As can be seen in figure 5.7 while using the analytical model by Papailiou [33] the minimum bending stiffness corresponding with high curvatures does not change significantly when considering different lay angles. The maximum bending stiffness corresponding with lower curvatures does show changes when different lay angles are considered. Higher values for the stiffness are found if lower lay angles are considered.

However, when increasing the curvature the opposite occurs. The value for the stiffness will be less

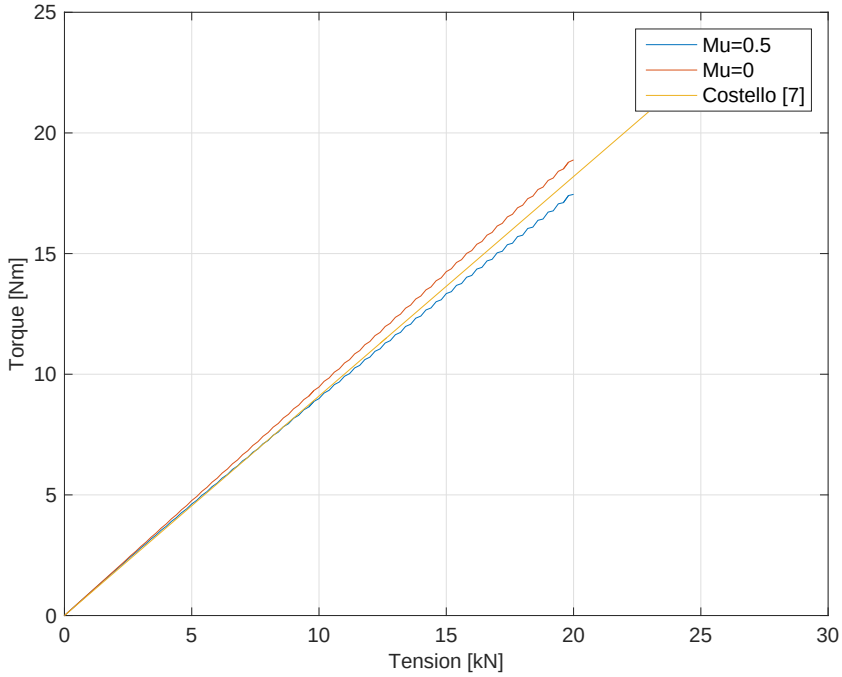

Figure 5.6: Axial-torsion relationship of a simple strand according to the FEM model and Costello [7]

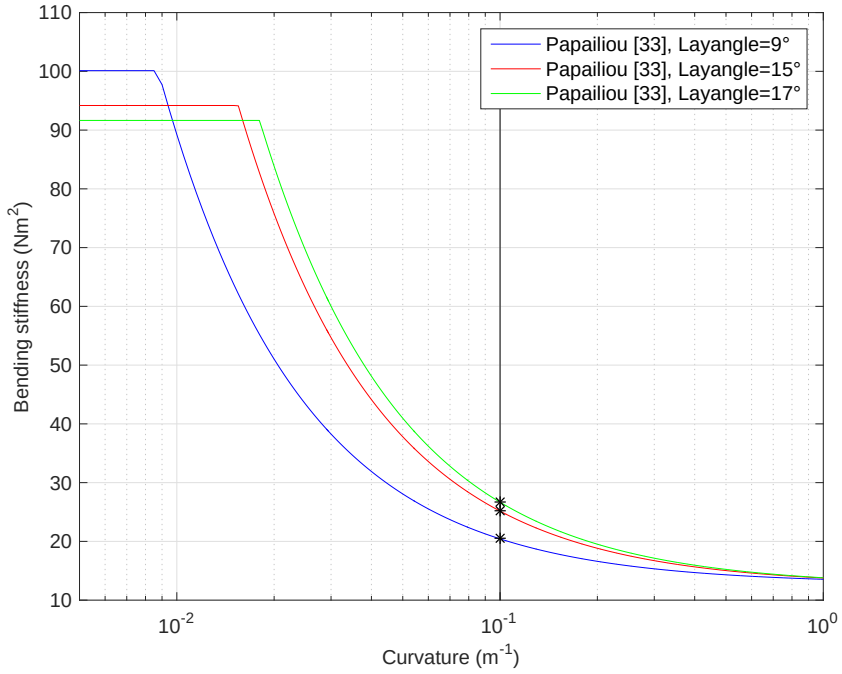

Figure 5.7: Relationship between bending stiffness and curvature with different lay angles and keeping tension constant. The simple strand in appendix A is used in the model by Papailiou [33]

for lower lay angles after the slipping curvature has been reached. This is shown in figure 5.7 by the difference in bending stiffness when considering the same curvature and different lay angles.

When considering for example a vertically suspended wire rope from an offshore vessel in multiple kilometres water depth, the tension will vary along the rope length as well as the lay angle. In these situations, the middle of the cable will not experience lay angles change [49]. In fact, this point is located a bit below the middle of the cable but for simplicity the middle is assumed.

When for example a simple strand in appendix A is used with a lay angle of $\alpha = 12°$ and the tension

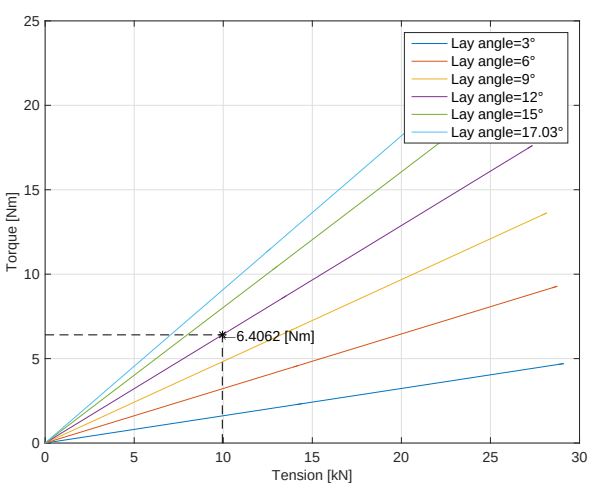

(a) Relationship between torsion and tension for different lay angles

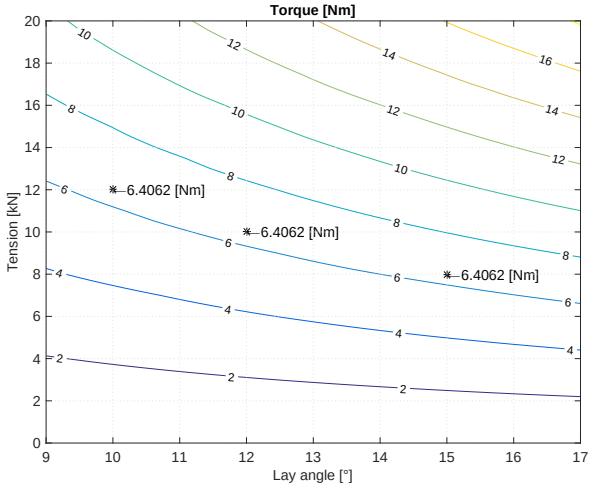

(b) Relation between tension and lay angle showing lines with constant torque according to the model by Costello [7] elaborated on in appendix D

in the middle of the cable is found to be $T = 10$kN, figure 5.8a provides a torsion value of approximately $M_t = 6.41$Nm. The value for the torsion has to be constant throughout the cable while the tension varies. Figure 5.8b can be used to select the values for the changing lay angle when assuming that at the top of the cable the tension is equal to $T = 12$kN and at the bottom $T = 8$kN. With constant torque the lay angles are respectively $\alpha = 10°$ and $\alpha = 15°$. With the same difference in tension of $\Delta T = 2$kN between top and bottom, non equal differences in lay angle are found as can be seen in figure 5.8b. Lowering tension will result in a larger change of lay angle then increasing tension with the same magnitude.

In the regions close to the seabed, where mechanisms such as hockling will occur due to higher curvatures, lay angle variation will play a prominent role. Because of the low tension and constant torque over the length of the cable, lay angles will increase at the lower regions of the cable. In figure 5.7 it was concluded that a strand in its stick regime will have a lower bending stiffness if larger lay angles are considered. However, when looking at larger curvatures, larger lay angles will cause the strand to become stiffer en so more resistant to bending.

While modelling different lay angles in Marc, the pitch length of the model will vary with different lay angles due to the fact that one full strand rotation is taken into account for each model. The mesh size is dependent on the length and so the element size is as well. The slip threshold value that influences the bending stiffness during stick is dependent on the size of the elements and therefore has to be adjusted for each model so that they can be compared. This has been done according to the same strategy used in the sensitivity analysis in 4.4.

In figure 5.9 similarities between the numerical and analytical model can be seen. The maximum bending stiffness found for the numerical models is again lower than the analytically derived ones due to the mesh size. When decreasing the lay angle, both models display stiffer behaviour in low curvature regions and softer behaviour at higher curvatures. For even higher curvatures, the bending stiffness for lower lay angles will again be higher than that of higher lay angles. This is due to the geometric non-linear effect. Because this effect has a different influence when different model lengths are considered, differences in the outcome at higher curvatures can be found.

5.5. Evaluation

In section 2.1 multiple modelling considerations where stated which are the governing assumptions describing a wire rope model. The modelling considerations for the analytical model have been shown in table 5.1. In this evaluation the assumptions made in the analytical model and in the numerical model are compared. Information from chapter 3, 4 and 5 are used.

Boundary conditions such as clamping forces are neglected in in the analytical model. The analytical model uses infinite long wires, while in the numerical model only one pitch length is considered. It is found that increasing the length of the numerical model generates problems with determining the

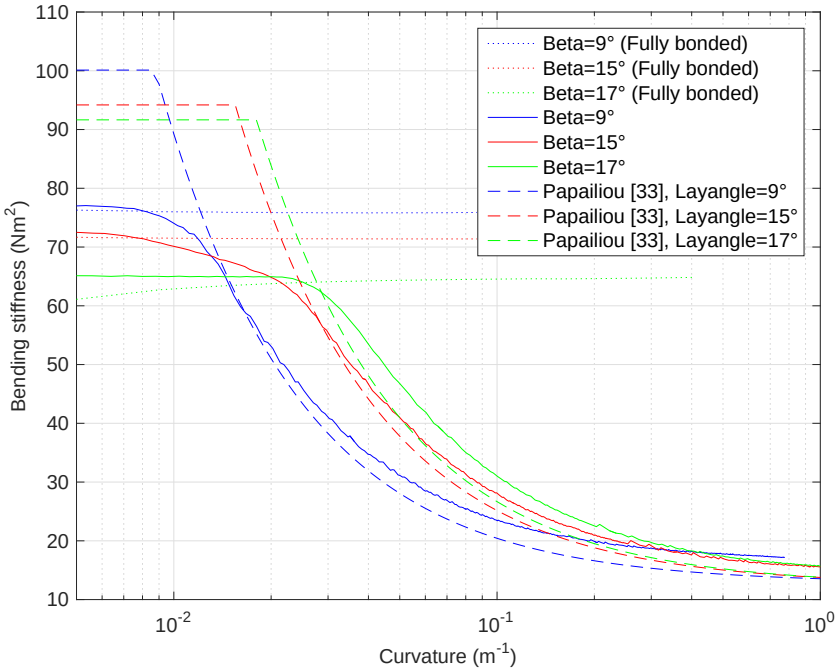

Figure 5.9: Change of lay angle comparison using a friction coefficient of $\mu = 0.125$ and a tension of $T = 20$kN

Table 5.1: Modelling considerations Papailiou [33]

Modelling consideration	
Boundary conditions	Clamping forces are neglected, long wire considered so that boundary conditions can be neglected.
Inter wire contact	Purely interlayer contact is assumed
Wire cross sectional geometry	Cross sectional geometry change is partly taken into account
Radial contraction	Radial contraction is neglected
Additional wire forces and moments	Wires are assumed to be subjected to additional wire forces and moments
Friction regimes	Interwire friction is taken into account
Lay angle	The lay angle is assumed constant over the length of the wire during bending
Material	Material is assumed to be linear elastic

curvature of the strand as the centre line can no longer assumed to be on a circle as is shown in 4.2. Sticking of the wires in the middle of the strand increases the resistance towards bending. The effect of geometric non-linearity also effects the found bending stiffness. Increasing the length of the model is found to decrease the reliability of the results.

Inter wire contact in the analytical model is considered to be interlayer while in the numerical model contact between all wires is taken into account. As is seen in section 5.1, low lay angles correspond to a more interlayer contact while larger lay angles are more similar to models considering intralayer contact. Therefore, by assuming that in all wire rope configurations only interlayer contact is present, reliability issues arise when working with higher lay angles.

Wire cross sectional geometry changes in the numerical model are taken into account. The correctness of the wire cross sectional geometry will depend on the level of detail of the mesh. In a finer mesh, the kidney shaped cross section of a wire perpendicular to the strand axis is more pronounced. In the analytical model, wire cross sections are corrected for the lay angle. However, the kidney shape shown in figure 2.2 is not taken into account. This is considered correct when low lay angles are considered as the shape of the cross section will be elliptical. When larger lay angles are considered, the kidney shape will be more pronounced thus leading to reliability issues due to the assumption made in the analytical model.

Radial contraction is neglected in the analytical model while in the numerical model it is taken into account. Mostly due to the tensioning part of the analysis, the wire will experience radial contraction which could influence the found results. This radial contraction is taken into account along the model length, except for the boundaries. Because of the movement restriction of all nodes connected to the reference node, no radial contraction is allowed. This feature is a problem when looking at models with

more wires such as an IWRC. Wires will not have perfect contact along their length when tensioned which can lead to uncertainties when bending an axially loaded strand as has been seen in section 4.5.

Additional wire forces and moments are all taken into account in the numerical model. The analytical model uses axial tension, frictional, normal and shear forces. Forces due to the deformation of wire rope material are not taken into account.

Friction regimes are part of both the analytical and numerical models. However, the numerical model describes the transition region, which is located between the stick and slip regimes in more detail. The analytical model displays a more sudden change in bending stiffness when the so called critical curvature is reached. Papailiou [33] showed methods to describe the transition region in more detail. However, this method has many uncertainties and so it will not be discussed in this thesis.

The lay angle is assumed to be constant over the length of the cable. This is done in both the numerical and analytical model. It is shown in section 5.4 that, the lay angle will influence the bending stiffness parameter when vertically suspended cables used in for example A&R operations are considered. The assumption that for small cable sections the lay angle under tension and bending loads will stay constant is correct. However, one must take into account that when using longer cables, lay angle variation will have an effect on the bending behaviour.

Material using the thin-rod modelling method by [33] is linear elastic. The numerical model uses a geometrically non-linear model with elasto-plastic materials using a large strain analysis.

As can be concluded from the comparison described above, many differences are present between the analytical and numerical model. However, both models do show similar bending behaviour. The fact that the maximum bending stiffness in the numerical model is always lower than the one analytically found cannot be explained using the differences in assumptions described above. It is found that it has more to do with the numerical way of modelling friction and the level of detail of the mesh. As the value for the maximum bending stiffness is mostly influenced by these numerical parameters, nothing can be said about the influence of the assumptions used in both models.

The more detailed and smooth transition region shown in the numerical model is assumed to be realistic as the transition from stick to slip is not supposed to be an instantaneous development. Slip will not start at the same time along the length of the strand but it will gradually develop. The assumption that there is a critical curvature and a sudden shift from stick to slip as is the case in the analytical model is therefore not correct.

At higher curvatures, there is a difference between both models, however it is not very significant. It seems to be that the numerically found value is still influenced by the friction coefficient and tension as was also found by Zhang and Ostoja-Starzewski [55]. This statement is still not entirely certain as this difference could also be due to the geometric non-linearity of the model.

When combining the results of this chapter, something can be said about the bending stiffness dependent on lay angle, tension, friction coefficient and curvature. For a simple strand with a realistic friction coefficient of $\mu = 0.125$ and a lay angle of $\alpha = 17°$ as is much used in literature, the bending stiffness according to the numerical model can be described as in figure 5.10.

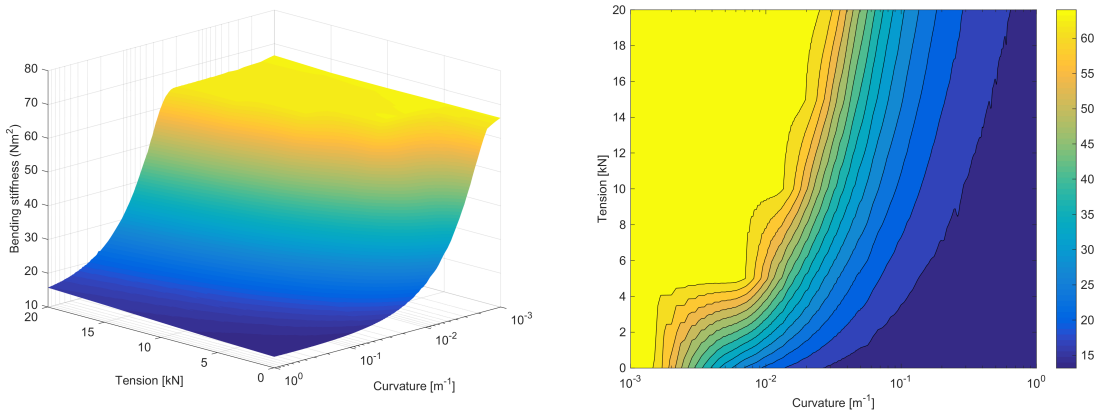

(a) 3D graph (b) Contour plot

Figure 5.10: Simple strand model with a lay angle of $\alpha = 17°$ with varying tension and curvature

Overall there seems to be good comparison between the analytical and numerical models for simple strands as has been shown in this chapter. After modification of the numerical method that determines friction by adjusting the slip threshold, the behaviour of the numerical model is as expected. However, especially at low tension levels, the slip threshold has to become so low that numerical difficulties prevent a well simulated result. Results from the numerical model at lower tension levels are therefore more uncertain than those generated with higher tensions. Figure 5.10b shows that the value for the maximum bending stiffness stays constant for low curvatures at any tension value. The non-continuous development of the maximum bending stiffness border when lowering the tension seen in figure 5.10 is due to the interpolation technique that is used. This interpolation technique is explained in appendix F. A model with a tension of 1 kN is used as the lowest tension level. This is due to the fact that the slip threshold value becomes very low at lower tension levels. Therefore numerical modelling does no longer provide reliable results.

Model expansion using both the analytical and numerical model have shown to be quite a challenge. When looking at the numerical model results, a stick slip behaviour can be seen. However, at lower curvatures, results seem unstable due to the large amount of wires which need to settle first before they can fully resist the applied external load. The similarity between the analytically and numerically found results is less than the comparison found between the results for a simple strand. The different diameters of the modelled wires in a IWRC and thus element sizes of which they consist, are the main problem of this more complex wire rope configurations. As friction modelling in Marc [27], depends on the average size of the elements, problems occur when a certain element largely deviates from the average value which is the case in the IWRC model constructed in this report. Calculating the bending stiffness variation for IWRC's however is possible. In chapter 7, recommendations will be presented how to realise correct friction modelling in Marc.

The results shown in this chapter describe the impact of the change of one particular parameter while trying to keep all other parameters constant. This is a perfect way of checking the influence of one parameter and comparing the numerically found relationship to the analytical one. However, in reality if a parameter such as for example tension changes, the value for the lay angle will change as well which will have an impact on the bending behaviour of the researched strand or wire rope. In figure 5.10, the lay angle is constant and independent from tension resulting in unusable results for the practical implementation.

In chapter 6 a critical situation during an A&R operation will be simulated using the relationship calculated from the analytical and the numerical model. All parameters that change during this practical study are taken into account.

6

Practical implementation: Beam model simulation

In previous chapters the state-dependent bending stiffness of steel wire ropes has been calculated using the analytical model by Papailiou [33] and the numerical model developed in this thesis. Different parameters are varied to study and compare the response of both models. The results from the numerical model are used to check the assumptions made in the analytical model. It has been found that the numerical model resembles the analytical model quite well.

This chapter will focus on the impact of using both models for a simulation of a situation that could occur during A&R operations. A criterion for loop formation is developed. Parameters which influence this criterion will be monitored during the simulation.

First, an introduction to critical situations during A&R operations will be presented along with a schematic visualisation of the model set-up. The next section will cover the vessel motions used for the analysis. The effect of these motions on the stinger tip will be discussed. Since it is assumed that the top of the A&R wire rope is located here. The modelling technique and strategy will be discussed in the next section. Input parameters, explanation of subroutines and interpolation techniques are discussed here. The chapter will end with a discussion on results and an evaluation.

6.1. Introduction

During abandonment and recovery operations (figure 6.1) a critical situation can occur when the pipeline is located on the seabed with the A&R wire rope connected to the ship. This situation becomes dangerous when the pipelay vessel is above the pipeline and experiences heave motions. This situation occurs when moving towards the location of the pipeline for retrieval or when laying the pipeline down for abandonment. The main reason for the situation to become critical is because of the vertical motions that the vessel experiences due to wind and waves. This induces curvature in the wire rope which will reduce the bending stiffness. This effect could lead to loop formation or hockling in wire rope sections. This mechanism most likely occurs near the seabed where the wire rope has the lowest tension and is forced to bend. As has been found in chapter 4, adding curvature to wire ropes whilst having a low tension will decrease their bending stiffness significantly.

Normally decreasing the bending stiffness of wire ropes would not be that much of a problem. However, when combining the reduced bending stiffness with a high torque and low tension, problems arise. Hockling or loop formation is a phenomenon that occurs when helically wounded ropes are bent while they contain torsional energy. Because of the helical shape of wire ropes, they generate this torsional energy when loaded axially. This axial force on the wire rope is generated by its own weight, the load it carries and due to the vessel motions.

Downward vessel motions could introduce slack in wire rope sections close to the seabed. This increased curvature will reduce the bending stiffness of the wire rope section significantly. With the constant self-weight of the cable, axial tension and therefore the torque in the cable make it easier for the cable to form loops or to hockle.

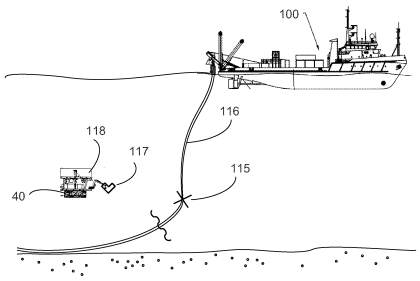

Figure 6.1: Abandonment and recovery operation [45]

To simulate the reduction of the bending stiffness due to vessel motions in A&R operations, a 2D beam model has been developed. The model will be used to calculate the shape of the wire rope due to vertical movement of the vessel while monitoring all parameters which could trigger loop formation or hockling. This simplified model has been illustrated in figure 6.2a and has been implemented in Marc [27] resulting in the model displayed in figure 6.2b. The wire rope has been divided into several beam elements so that the variation of certain parameters along the length can be monitored. The beam model is put under a slight angle, to avoid numerical instabilities.

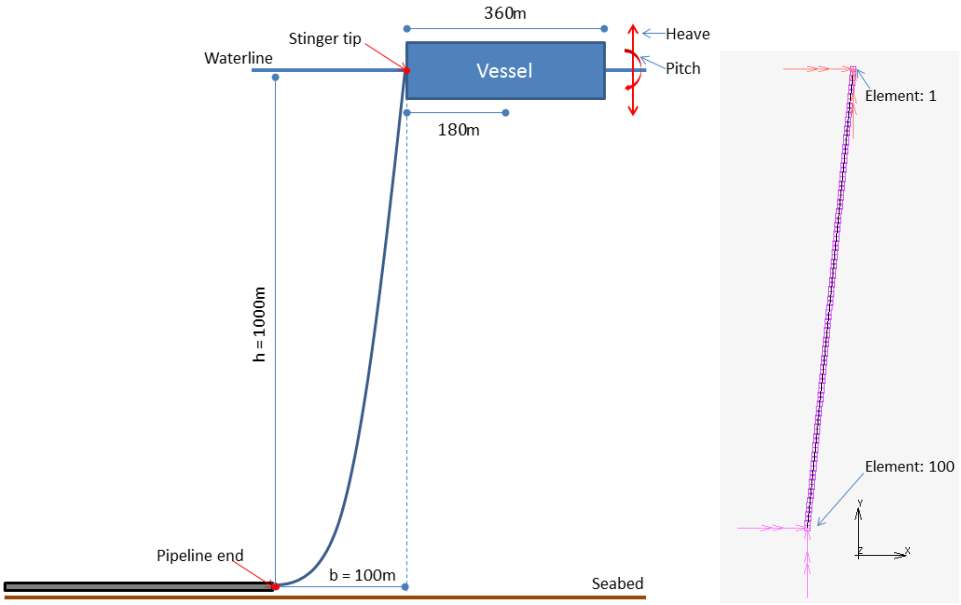

(a) Schematic visualisation

(b) Implementation of the simplified model in Marc [27]

Figure 6.2: Simple model of critical abandonment and recovery situation

6.2. Vessel motions

Response amplitude operators (RAO's) from the Solitaire (a ship from Allseas, figure 6.3) are used to calculate the vessel motions which will lead to the vertical displacement of the stinger tip over time. These values will be taken into account for the analysis shown in this chapter. Since this chapter is about developing a beam model with a state-dependent bending stiffness, no extensive study towards the vessel motions has been done. The values for the accelerations of the vessel only serve as an indication. Therefore, no further explanation into the working method of the program used to come up with the RAO's is given.

It is chosen to analyse the vessel motions for two particular wave approach angles, periods and

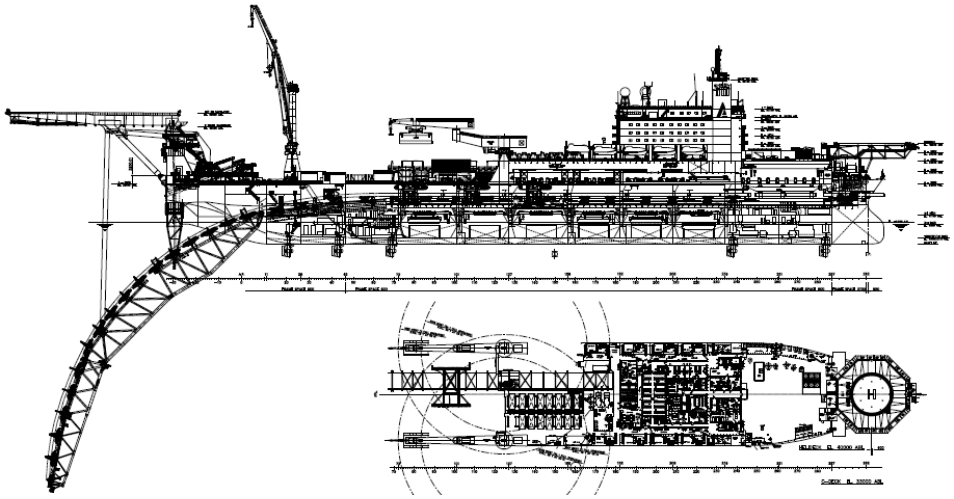

Figure 6.3: Solitaire

Table 6.1: Two different wave characteristics are taken into account for the calculation of the vessel motions

Description	Symbol [unit]	Case 1	Case 2
Significant wave height	H_s[m]	1	1.5
Wave frequency	f[rad^{-1}]	0.1	0.350
Wave approach angle	θ[°]	30	90

heights. The parameters for the two corresponding wave states can be found in table 6.1. The RAO's corresponding to these wave characteristics can be found in table 6.2.

Case	Surge		Sway		Heave		Roll		Pitch		Yaw	
	Amp	ϕ	Amp	ϕ	Amp	ϕ	Amp	ϕ	Amp	ϕ	Amp	ϕ
1	1.0407	89.85	0.5948	89.93	0.9975	0.00	0.0506	64.18	0.0604	-90.81	0.0310	-161.77
2	0.0012	138.14	0.9223	89.33	1.0099	0.01	1.1267	-103.55	0.0062	-173.65	0.0103	-82.95

Table 6.2: RAO's of the Solitaire in sea states described by the two cases in table 6.1. The amplitudes are dimensionless and the phase angles ϕ are in degrees. [17]

To calculate the actual wave amplitude the RAO amplitudes from table 6.2 have to be multiplied by the significant wave height corresponding to that particular case. Both the centre of gravity (CoG) and the location of the stinger tip of the vessel are assumed to be located exactly on the heart line of the ship. The overall length of the ship is approximately equal to 360m. By assuming that the CoG is located exactly in the middle of the ship, the distance from the CoG to the stinger tip will be equal to $\frac{360}{2} = 180$m. Only heave and pitch motions will contribute towards the vertical movement of the stinger tip. For the two cases described in table 6.1 this will result in the vertical motions of the stinger tip as presented in figure 6.4.

6.3. Variable bending stiffness

In chapter 3 and chapter 4 analytical and numerical models are given to calculate the state-dependent bending stiffness of simple strands. However, the results from these chapters are so that only one parameter is changed per analysis. This is a good method to map the influence from a certain parameter. In reality multiple parameters change simultaneously when bending a wire rope.

To be able to use the information about the bending stiffness developed in chapter 3 and 4 in a beam simulation, a strategy has to be made which will be explained in this section.

The constant torque over the length of the rope in an A&R operation has to be calculated first. This can be done using the theory from Costello [7] which resembles the results generated from the

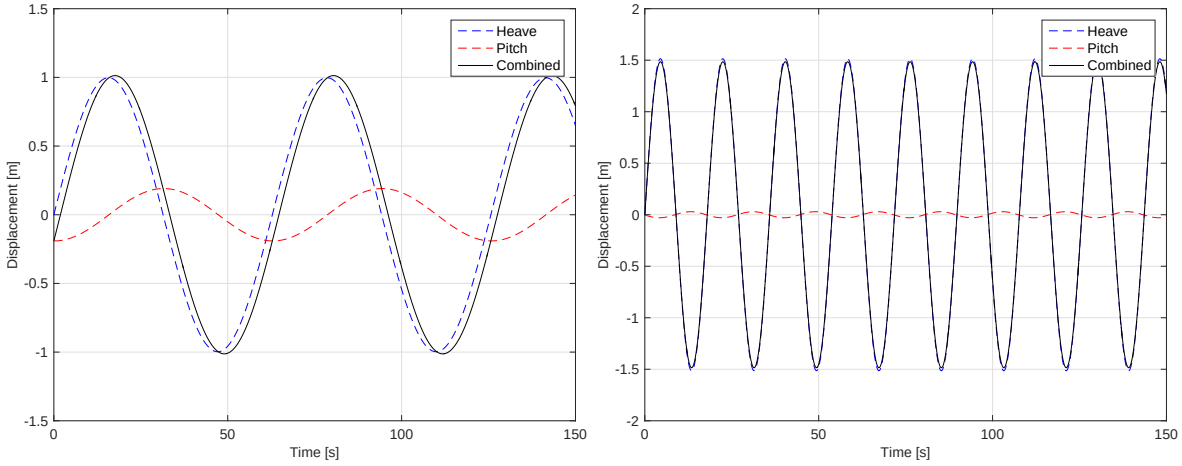

(a) Case 1 (b) Case 2

Figure 6.4: Vertical motion of the stinger tip for the two cases described in table 6.1 using the RAO's from table 6.2

numerical model quite well as was seen in section 5.4. When the torque is known, the lay angle variation along the rope length can be determined. Torque is constant over the wire rope length while the tension is highest at the top and lowest at the bottom. Using these parameters, lay angles will be low at the top and high at the bottom of the wire rope. Now that the lay angle and torque of a wire rope section are known something can be said about the bending stiffness of that section of rope. The curvature and tension of that section is an output of the beam model and are used to adapt the bending stiffness, using the results from the numerical model generated in the previous chapter.

To be able to use this strategy, multiple models combining different parameters have to be analysed. Fine simple strand models have been run for the following tension levels: $T = 1, 5, 10, 15$ and 20kN. The lay angels that are modelled are the following: $\alpha = 9°$ and $\alpha = 17°$. At $\alpha = 17°$ all wires will be in contact with each other, while at $\alpha = 9°$ only radial contact is possible. The friction coefficient is considered constant using the simulation.

A lay angle of $\alpha = 12°$ is used as the original lay angle of the simple strand. According to Costello [7], the relation between tension and torsion for a simple strand with a lay angle of $\alpha = 12°$ can be described as follows,

$$M_t = 6.44e^{-4}T \tag{6.1}$$

where M_t is equal to the torque and T is the tension. The method to calculated this value by Costello [7] is shown in appendix D. The constant value in equation 6.1 is equal to the gradient of the curve in figure 5.6 corresponding to a lay angle of $\alpha = 12°$. According to Verreet [50], the lay angle of the rope located in the middle and at both ends of the rope will not change. The constant torque over the whole cable length can be calculated in the location where the lay angle is known, such as in the middle. Equation 6.1 together with the present tension will provide the value for the torque.

Now that the constant torque is calculated and the tension distribution over the cable length is known, the lay angle can be determined. The method from section 5.4 gives the lay angles at different tension levels while keeping the torque constant. Lay angle, tension and curvature values can now be used to determine the bending stiffness of a wire rope section during the A&R simulation.

An initial offset of 100m in horizontal direction between the two ends of the vertically suspended cable is implemented to prevent numerical problems with buckling. The total water depth is selected to be 1000m as is presented in figure 6.2. The initial length of the cable will be $L_{cable} = \sqrt{100^2 + 1000^2} = 1005$m. The cable is modelled as a collection of multiple beam elements with a state-dependent bending stiffness.

In the first 50 seconds of the simulation, pretension and gravity will be gradually introduced to avoid numerical instabilities. First, the beam model is tensioned by applying a positive vertical displacement to the top node during the first 25 seconds. In the next 25 seconds, the gravity will be introduced. During the increase of gravity, the top node will vertically displaced towards its starting position which is determined by the vessel motions from figure 6.4. After all these initial conditions are satisfied, a

sinusoidal movement simulating the vertical movement of the stinger tip is applied to the top node. The development of this displacement and that of the gravity increase is presented in figure 6.5.

A static and dynamic analysis will be performed. In this case, a static analysis is an analysis where the inertial effects are neglected and a static equilibrium is found for each increment. A time step of $\Delta t = 1$s is taken into account for the static analysis, resulting in 200 increments for a simulation that lasts 200 seconds. In the dynamic analysis, inertial effect are taken in to account. The time step for the dynamic analysis will be equal to $\Delta t = 0.5$s.

The top node simulating the stinger tip will be displaced according to the vessel motions as for example can be seen in figure 6.5a. The increase of the gravity will be presented in figure 6.5b. For the gravity a maximum value of $g_{max} = 9.81\text{ms}^{-2}$ is assumed. For the displacement of the top node a maximum value of $d_{max} = 1.01$m is found for case 1. The maximum displacement for case 2 is equal to $d_{max} = 1.48$m.

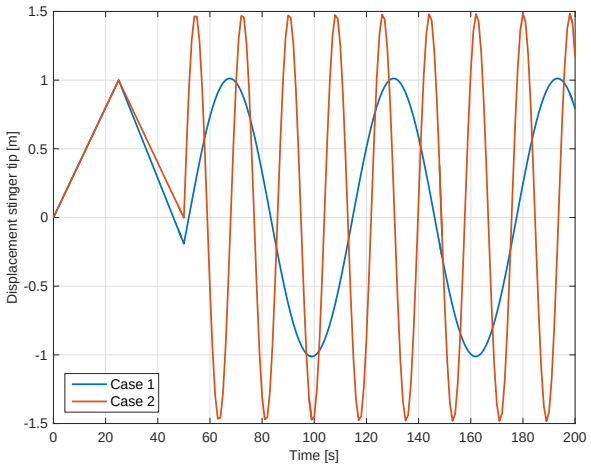

(a) Displacement of the top node for both vessel motion cases

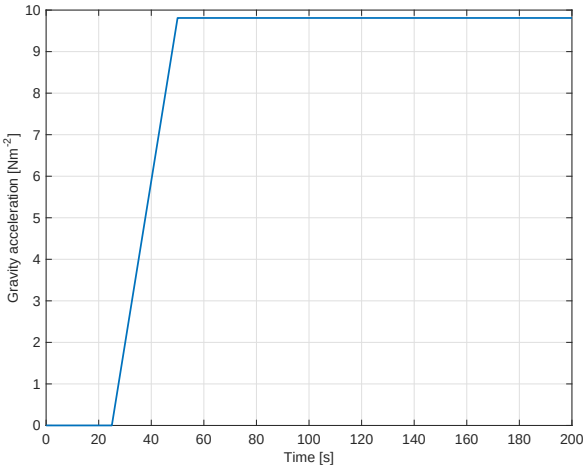

(b) Increase of the gravity loads

Figure 6.5: Development of the external loads on the beam model over the specified time range

6.3.1. Subroutines

Three simulations are performed with different methods to determine the bending stiffness of the elements of the beam model. In the first simulation the bending stiffness is considered independent of curvature and equal to the minimum bending stiffness as calculated by Papailiou [33]. The second simulation will assume that the bending stiffness is a function of curvature, tension and lay angle and that it will behave according to the analytical model by Papailiou [33] described in chapter 3. The third and last simulation will include the relationship between bending stiffness and curvature as is generated by the numerical model described in this report in chapter 4.

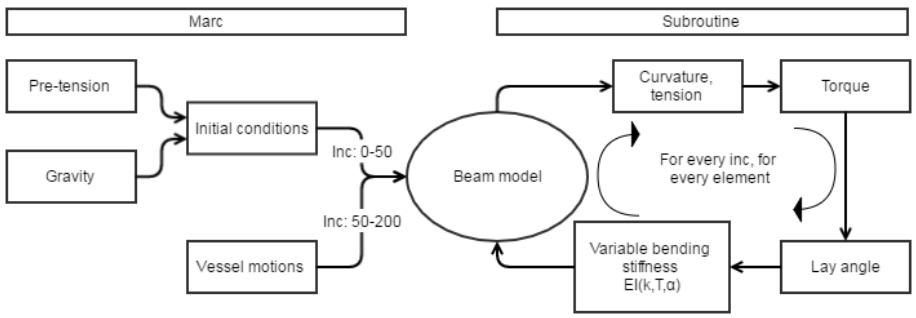

Figure 6.6: Simulation flowchart

To change the bending stiffness of beam elements, so called subroutines are used in Marc [27]. These subroutines allow the user to solve non standard problems of a wide variety. The subroutine illustrated by the flowchart in figure 6.6 is used to change the bending stiffness of the modelled beam sections during the simulation. The bending stiffness is considered equal over the length of the modelled beam element.

The vertical displacement of the top node simulating the vertical movement of the stinger tip shown in figure 6.5 will cause the cable model to deform. Tension and curvature of the elements is calculated by Marc and will be sent to the subroutine.

In the subroutine torque along the cable length is calculated. Together with the tension, the lay angle per element can be determined. Information about the tension, curvature and lay angle of an element is enough to provide a value for the bending stiffness. The element properties are changed to incorporate this calculated bending stiffness property. This process will repeat itself for every element for each increment.

6.3.2. Interpolation

Not all combinations of parameters are calculated using the numerical model. Therefore, interpolation is needed. When using the analytical model no interpolation is needed as it uses explicit expressions to describe the relation between parameters.

The numerical model is only run for a finite amount of parameter combinations. These combinations can be found in table 6.3. To acquire the bending stiffness belonging to certain parameters which satisfy the following conditions $9° \leq \alpha \leq 17°$ and $0\text{N} \leq T \leq 20\text{kN}$ interpolation has to be used. The values found for a tension of zero are assumed equal to the ones found for a tension of $T = 1\text{kN}$. This is because the slip threshold has to become so low that it is not possible to solve the analysis numerically. The values for the curvature are in the range $0\text{m}^{-1} \leq \kappa \leq 1.67\text{m}^{-1}$.

Table 6.3: Numerical model analysis defined by combinations of input parameters

Combination	Lay angle (°)	Tension (kN)
1	9	0 (1 kN)
2	9	5
3	9	10
4	9	15
5	9	20
6	17	0 (1 kN)
7	17	5
8	17	10
9	17	15
10	17	20

For each combination shown in table 6.3, piecewise cubic interpolation is used to interpolate the relationship between bending stiffness and curvature. The curvature range is interpolated with a variable interval where the first part has a small interval which is increased in the second part. The reason for this is that the first part of the relation displays the transition from stick to slip. Therefore a smaller interval is chosen so that more detail can be captured. All models have completed the transition region if a curvature of $\kappa = 0.05\text{m}^{-1}$ is reached, so this curvature will mark the end of the first part and the beginning of the second. Three dimensional interpolation using the griddata function in Matlab is used to come up with values for the bending stiffness depending on curvature, lay angle and tension with the intervals and range of values which are shown in table 6.4.

The interpolated data is exported to a text file which can be read by the subroutine controlling the bending resisting properties of the beam elements. However data has to be interpolated further in the subroutine as the values for the lay angle, tension and curvature do not exactly match the values from the interpolated data. This is done by trilinear interpolation which is a multivariate interpolation performed on a three-dimensional regular grid. The state-dependent bending stiffness corresponding with the output from the beam analysis in Marc will be used to find the interpolated value for the bending stiffness. For further information about the interpolation technique being used, appendix F can be consulted.

Table 6.4: Parameter ranges and interval value used for interpolation

Parameter	Unit	Range	Step size
Curvature	[m]	$0 \leq \kappa_1 < 0.05, 0.05 \leq \kappa_2 \leq 1.67$	$0.0005, 0.016$
Tension	[kN]	$0(1\text{kN}) \leq T \leq 20$	2.5
Lay angle	[°]	$9 \leq \alpha \leq 17$	1

6.4. Loop formation

The occurrence of loops in wire ropes is dependent on multiple parameters such as the tension, torque and the bending stiffness. With the beam model described in this chapter, parameters can be monitored continuously along the length of the cable. In this section, a strategy is presented to be able to determine the critical combination of values which could result in loop formation.

The Greenhill formula [14] is commonly used to determine a critical tension or tension threshold. When a wire rope is tensioned with a force above this value, no loop formation can occur. The equation 6.2 gives the tension threshold from Greenhill [14], which is a function of the torque on and bending stiffness of the wire rope.

$$F_{crit} = \frac{M_t^2}{mEI} \tag{6.2}$$

Here F_{crit} is the critical tension or tension threshold, M_t the torque, m the Greenhill constant and EI the bending stiffness of the rope. The Greenhill constant is conservatively chosen to be equal to $m = 2$, as is described by Ross [40]. The tension threshold value for the simple strand described in this thesis is quite low. This is due to the low self-weight of the strand. If larger wire ropes are considered, high tensions and a higher torque will be present in the cable. As torque has a quadratic influence on the tension threshold value in equation 6.2, the critical value will increase exponentially with increasing self-weight of the wire rope.

As the bending stiffness over the cable length varies, the value for the tension threshold does as well. The bending stiffness is lowest when looking at elements close to the seabed. The tension threshold will therefore be highest and thus critical in this location because of the influence of the bending stiffness in equation 6.2. The maximum found tension threshold for the static simulation is found to be equal to $F_{crit} = 2.90\text{N}$.

6.5. Results

The results of the simulations will be shown using two methods. The first method will show the variation of the involved parameters along the length of the cable fixed in time. The moment in time where the parameters are the most critical is at $t = 180\text{s}$ for case 1 and at $t = 190\text{s}$ for case 2. These moments in time correspond with the highest negative vertical displacement of the top node in both cases.

The second method will show the parameter variation of one particular element during the simulation. An element at the bottom end of the cable is taken into account. Element number 99 is chosen, which is the second-to-last element of the cable. The first and last element are shown in the simplified model as presented in figure 6.2b. Element 99 is chosen instead of element 100 because it does show lay angle variations where the lay angle of element 100 is fixed.

Note that the influence of hysteresis on the bending behaviour is not taken into account during the simulations. The effect of taking hysteresis into account during a simulation is discussed in appendix G.

6.5.1. Static: case 1

The input parameters for the vertical displacement of the top node for case 1 and case 2 can be found in figure 6.5a. The movement for case 1 is quite calm compared to that of case 2. At $t = 180\text{s}$, the maximum negative displacement of the top node is realized. Interesting parameters along the length of the cable are shown in figure 6.7 at this location in time. Bending stiffness, tension, lay angle, torque and curvature variations along the cable length can be found in this figure.

Method 1: $t = 180s$: The bending stiffness is considerably reduced at the beginning and at the end of the cable as can be seen in figure 6.7a. This is mainly due to the increase in curvature at these

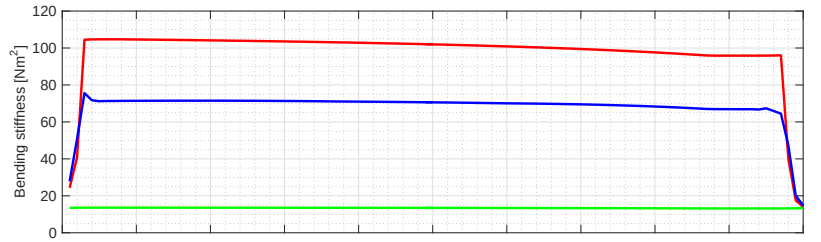

(a) Bending stiffness

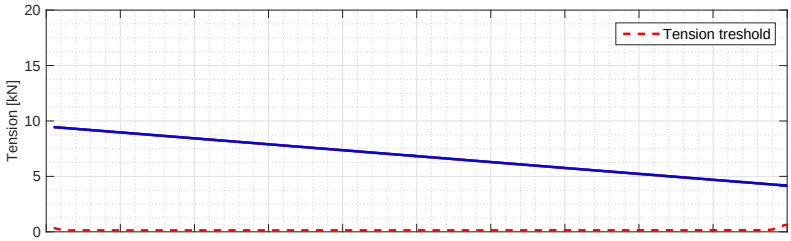

(b) Tension

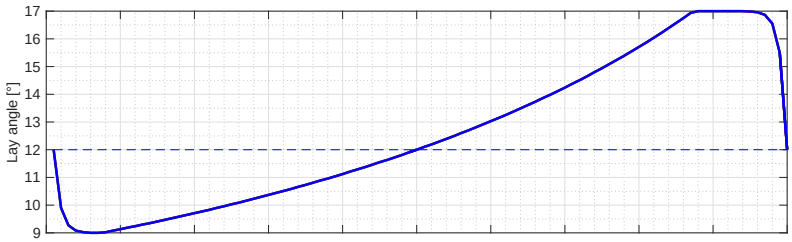

(c) Lay angle

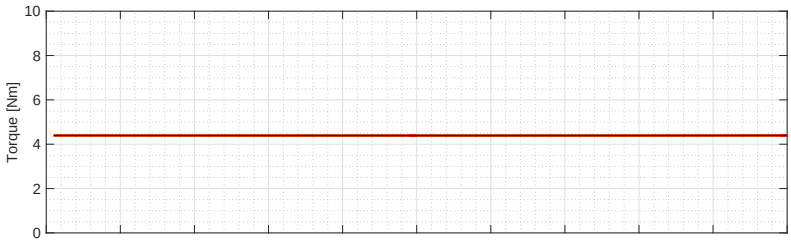

(d) Torque

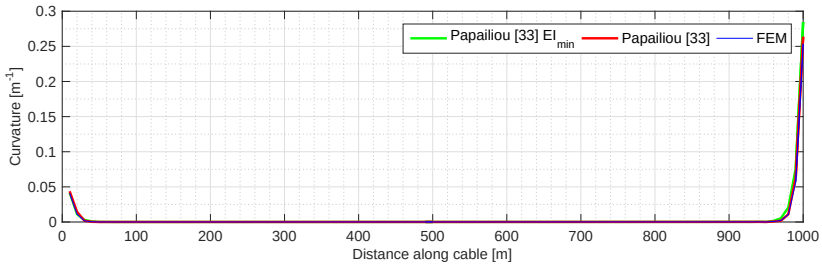

(e) Curvature

Figure 6.7: Various parameters monitored along the length of the cable using the input from case 1 shown in figure 6.5a at increment number 180

locations as can be seen in figure 6.7e. A negative slope can be seen when looking at the bending stiffness progression along the cable length. This is due to the lay angle variation seen in figure 6.7c.

Increasing lay angle corresponds with a lower bending stiffness for small curvatures. Because the curvatures are very close to zero for the majority of the cable length, this downward slope is seen.

Tension variation along the cable length can be seen in figure 6.7b. Tension is highest at the top of the cable and lowest at the bottom. This tension variation does not have an effect on the maximum bending stiffness during stick but has influence when wires start slipping, which is the case at the ends of the cable. The tension threshold is found to be lower than the minimum tension reached in any cable section. In fact $T_{min} = 4.16$kN while the tension threshold is equal to $F_{crit} = 2.90$N. According to Greenhill [14] no loops will be formed over the cable length.

The lay angle varies quite a lot over the cable length as can be seen in figure 6.7c. In the middle and at the ends, the lay angle is equal to the initial lay angle of $\alpha = 12°$. An exponential function is used to force the lay angle to become equal to this value at the ends. Therefore the lay angle values for cable lengths lower than 50 m and higher than 950 m will increase and decrease exponentially to the initial lay angle respectively. It is assumed that the lay angle cannot be larger than $17°$. At this lay angle, all the wires in the outer layer will be in contact with each other.

The torque will be constant over the length of the wire rope as is presented in figure 6.7d.

Method 2: Element 99: The parameters corresponding with the second-to-last element can be found in figure 6.8. All increments are shown. The first 50 increments are used to implement the gravity loads and the initial displacement of the top node. Afterwards vertical motions of the stinger tip will describe the displacement of the top node.

The bending stiffness shown in figure 6.8a drops when gravity is introduced into the model (from increment 25 until 50). The bending stiffness of the element is almost equal to the theoretical minimum value because of the tension drop which can be seen in figure 6.8b combined with the increased curvature of the element in figure 6.8e. Afterwards, the top node is moved upwards thus increasing tension and reducing curvature. When the tension is increased the bending stiffness will follow. This is only the case when the wire rope is in the slipping state. During stick, tension differences will not effect the bending stiffness property of the wire rope. The tension at the time range $50\text{s} < t \leq 200\text{s}$ will have a minimum of $T = 1.35$kN while the tension threshold has a maximum value of $F_{crit} = 1.32$N, so no loop formation will occur during the simulation.

The lay angle will decrease when the tension on the element increases as can be seen by comparing figures 6.8b and 6.8c. The tension on the element will again be high enough to unlay the wires of the strand. The maximum lay angle of around $\alpha = 15.5°$ in figure 6.8c is because of the exponential function used to force the lay angle to become equal to $\alpha = 12°$ at the ends. As the element considered here is the second-to-last, a slightly higher lay angles will be considered limit.

The torque variation is shown in figure 6.8d. The torque, together with the bending stiffness define the tension threshold which can be calculated by equation 6.2. As the torque has a linear relationship with the tension, the graphs are of a similar shape. The tension threshold value of $T_{crit} = 2.90$N is not exceeded in this simulation so no loop formation will occur. This was expected as a low torque is developed in the simple strand due to its size and shape resulting in a low tension threshold calculated by equation 6.2.

6.5.2. Dynamic: case 1

In figure 6.9, the results from the dynamic analysis of case 1 are shown. Only the variation of the parameters over time for element number 99 are shown as the variation along the cable at one time step is quite comparable to the results from the static analysis in figure 6.8.

The global variation of the parameters is quite similar to that of the static analysis shown in the previous chapter. The fluctuating response is due to inertial effects that are part of the dynamic simulation. Due to this fluctuation, maximum en minimum values of the parameters will be higher and lower respectively. This observation causes the dynamic model to be more conservative than the static model.

6.5.3. Case 2

The results found for case 2 resemble that of case 1 shown in section 6.5.1 and 6.5.2. The same conclusions can be deducted from the results. As the figures are quite large to display, the results for case 2 can be found in appendix H.

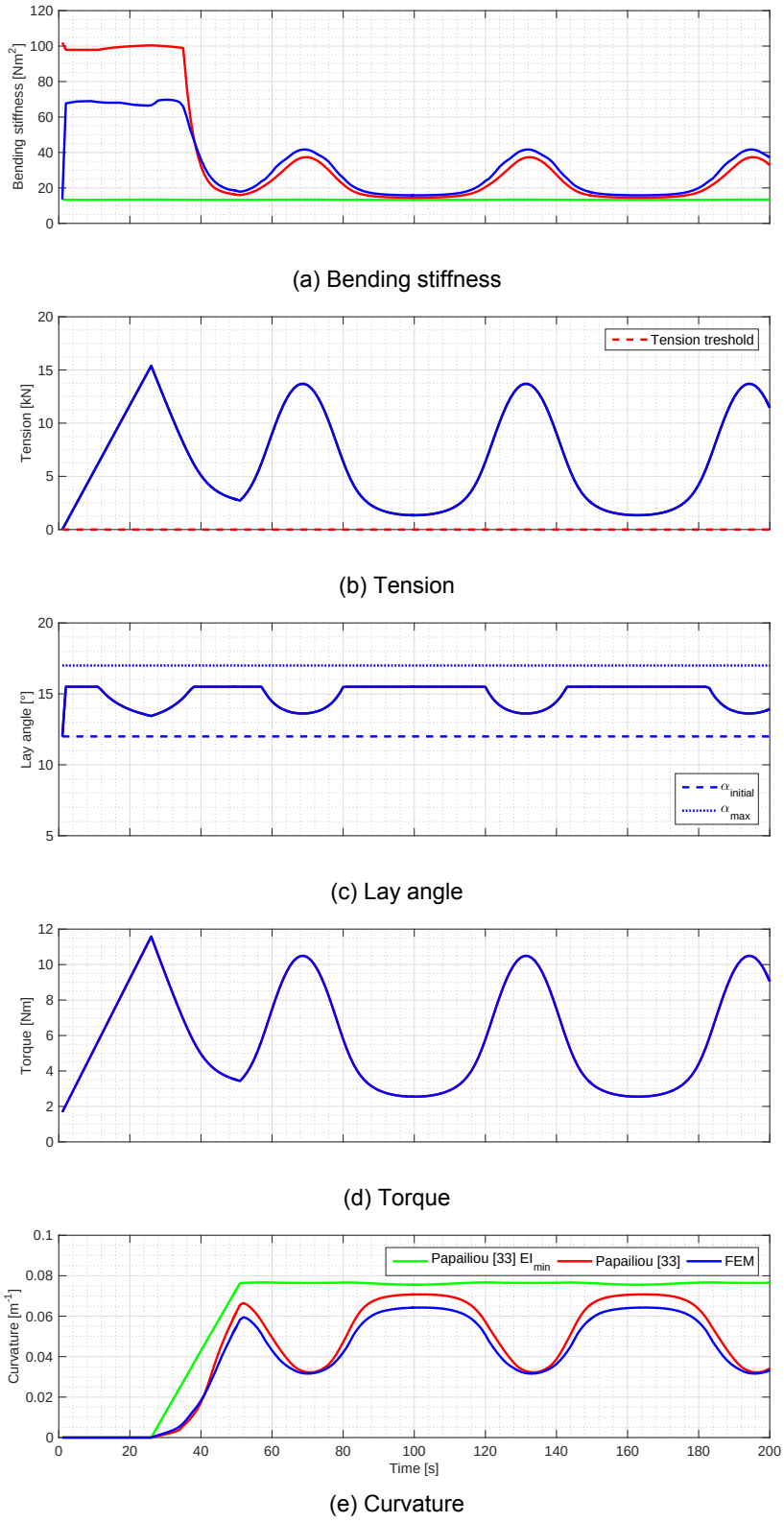

(a) Bending stiffness

(b) Tension

(c) Lay angle

(d) Torque

(e) Curvature

Figure 6.8: Various parameters monitored for all cable increments using the input from case 1 shown in figure 6.5a for element number 99 (closest to the seabed)

6.6. Evaluation

In this chapter an implementation of the models developed in this thesis describing the state-dependent bending stiffness is discussed. Results are generated by the creation of a beam model in Marc using

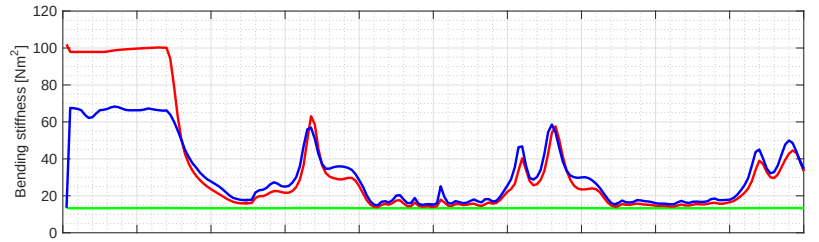

(a) Bending stiffness

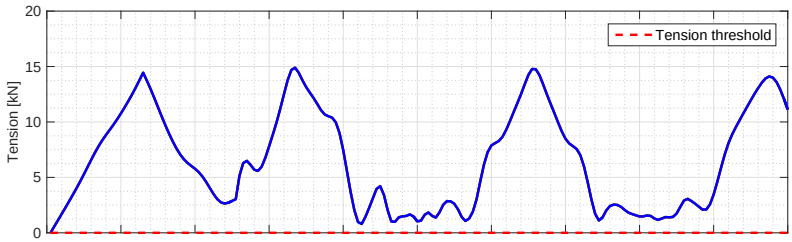

(b) Tension

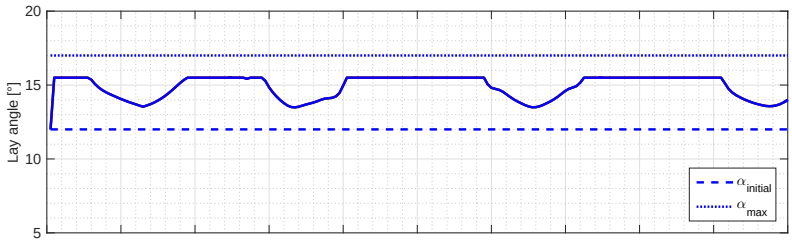

(c) Lay angle

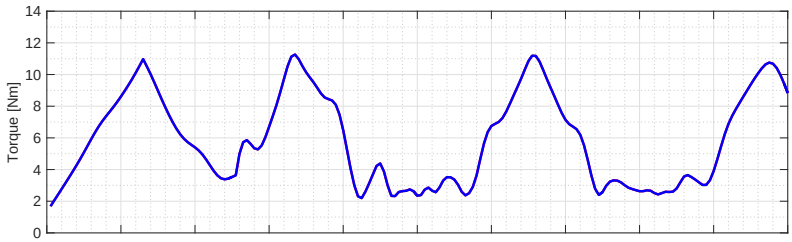

(d) Torque

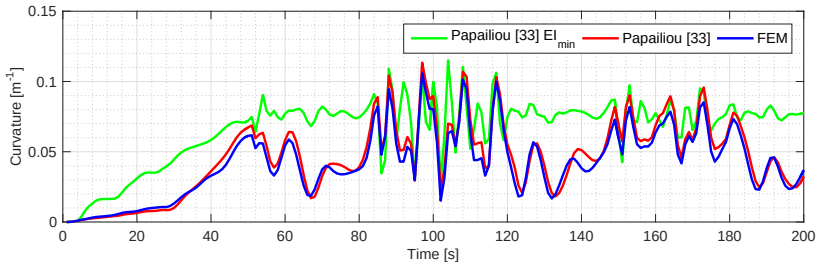

(e) Curvature

Figure 6.9: Various parameters monitored for all cable increments using the input from case 1 shown in figure 6.5a for element number 99 (closest to the seabed)

subroutines to implement the state-dependent bending stiffness for each beam element.

The 2D model has been developed in Marc using multiple beam elements connected to each other

to simulate a wire rope. The bottom node, which resembles the seabed is restricted from all movement except rotation around one axis. The top node has the same rotational degree of freedom and is allowed to move vertically.

Vessel motions are roughly derived using selected wave characteristics and corresponding RAO's. The Solitaire is used for the determination of these parameters. These wave characteristic are not considered critical for the analysis, they just serve as an example to show that the numerical model provides reliable results.

The method used to implement the results from the analytic and numerical model to vary the bending stiffness of these beam elements is described. A designed subroutine makes it possible to vary the bending stiffness property of beam elements during the simulation. Because not all combinations of parameters needed to derive a value for the bending stiffness have been analysed in this thesis, interpolation is needed. When analysing the results for a tension level of zero, slip threshold values have to be so low that the results become unreliable. The results from an analysis with zero tension have been selected to be equal to the results of an analysis with 1 kN tension which could be numerically modelled. The bending stiffness of slack cable sections will be slightly overestimated due to this assumption.

Both a static and dynamic simulation has been performed. The parameter variation along the cable length for all a certain increment has been shown. The variation of parameters of a certain element along different increments/time steps are also analysed. It can be concluded that the bending stiffness at the bottom end of the cable is significantly lower than in for example the middle section. This is due to the increased curvature at that cable section. When observing the bending stiffness variation over time at the bottom end of the cable, sinusoidal variations are seen depending on the displacement of the top node. In the dynamic analysis inertial effects cause the output to fluctuate which results in a more irregular curve.

This chapter has shown that a wire rope can be modelled as a simple beam model with a state-dependent bending stiffness. A&R operations can be simulated using this model. All parameters which are needed to define the loop formation criterion can be monitored during the simulation. With this information an indication, based on the tension threshold criterion described by Greenhill [14] concerning loop formation can be made. This will show the impact that the state-dependent bending stiffness has on the critical tension value that is used to design equipment for A&R operations.

7

Conclusions and recommendations

The main objective of this work is to *describe the bending behaviour of steel wire ropes and its impact on A&R operations*. The conclusions concerning this objective are presented in this chapter and are divide into four parts, each with associated questions which served as a guidance throughout the thesis. These four parts are repeated, along with the accompanying conclusions and recommendations, ranked in order of importance.

It can be stated that the main objective of this thesis has been achieved for simple wire configurations. The bending behaviour of these configurations has been numerically modelled. However, for larger and more complex steel wire ropes, more computational time and effort is needed.

A numerical model has been developed in this thesis to describe the state-dependent bending stiffness of steel wire ropes. The results have been compared with the analytical model from Papailiou [33]. The latter model shows good resemblance with experimental results found by the same author. However, the model is limited to simple stands or spiral ropes. Results from the numerical model match the analytically generated ones reasonably well for simple strands. Hence, the used model strategy can be considered plausible and could be used for other wire rope compositions.

A beam model with a state-dependent bending stiffness simulating a vertically suspended steel wire rope has been developed. This model is used to simulate situations which can occur during an A&R operation. The impact of the state-dependent bending stiffness on the model outcome has been discussed.

7.1. Conclusions

1. *Create an overview of all available research on wire rope modelling*

- After an extensive literature study the model by Papailiou [33] has been chosen to represent the state-dependent bending stiffness of simple strands analytically. According to the author, the state-dependent bending stiffness can be divided into three regimes; stick, transition and slip. It is concluded that the calculated bending behaviour for simple strands matches reality rather well. Therefore, these results are used to validate the numerical model developed in this thesis.

- Bending experiments to model the state-dependent bending stiffness property of wire ropes are scarce. Experiments that have been performed, involve spiral ropes instead of stranded ropes.

- Wire rope researching techniques are shifting from analytical models to finite element solutions. Analytical models are widely used for simple strands and spiral ropes. However, stranded ropes used in the offshore industry are not commonly researched using analytical models due to their complexity. Models that simulate the behaviour of stranded ropes analytically need many controversial assumptions which greatly influence the results. Numerical models using finite element methods have greater potential to deal with these more complex wire rope configurations. Computational time and performance seem to be the limiting properties concerning the feasibility of numerical models.

- Semi-continuous models have been constructed for stranded ropes in order to research their axial behaviour. However, for bending of stranded ropes, this modelling technique is not feasible. However, these models have better results compared to thin-rod models for spiral strands with a large number of wires.

2. *Elaborate and study the analytical model by Papailiou*

- The state-dependent bending stiffness of wire ropes is due to inter wire friction. In the stick regime, friction will prevent movement of the wires relative to each other, thus resulting in the maximum bending stiffness. With increased bending of the wire rope, wires will start to slip. Therefore, the bending stiffness of the rope will reduce. This mechanism will continue until all wires have slipped over their entire length resulting in the minimum bending stiffness of the rope.
- The transition region describes the start of slip of the wires, where wires will slip one after another. In the slip region, all wires will have slipped along a certain portion of their length. When curvature increases, the slip will propagate until all wires slip along their entire length.
- The maximum and minimum bending stiffness is not dependent on the tension or the friction coefficient of the rope. However, these parameters do have an influence on the curvature at which slip of the wires will commence.
- Slip of the wires will start at the locations where a wire passes the neutral bending plane of a rope.
- The use of the analytical model is limited to simple strands or spiral ropes. Adjusting the analytical model for stranded ropes requires assumptions that limit the reliability of the acquired results. This adjustment of the analytical model has been developed in this thesis. Resemblance has been found with the results from the numerically generated models.

3. *Evaluate and describe the generated numerical model*

- The analytical and numerical model results match each other reasonably well for simple strands. The analytical model gives higher values for the maximum and lower values for the minimum bending stiffness compared to the numerical model.
- The maximum bending stiffness found using fully bonded models is dependent on the level of detail of the mesh. It can be concluded that an increase in mesh size increases the found maximum value for the bending stiffness. However, it seems likely but cannot be stated that this value will eventually reach the theoretical limit.
- The element size of the numerical model has an influence on the maximum bending stiffness during stick. The bending stiffness during stick for a model with a particular lay angle is dependent on the average edge length of the mesh, tension, friction coefficient and slip threshold. As the tension and friction coefficient change for different analysis, the slip threshold has to be altered so that the found maximum bending stiffness remains unchanged.
- Altering the value for the slip threshold has consequences for the numerical feasibility of the model. Load step size has to be reduced so that results from the model are still reliable and stable, therefore increasing computational time. For certain combinations of parameters, the slip threshold is so low that no reliable numerical solution can be found.
- The numerically generated minimum bending stiffness is higher than the theoretical minimum value because of the boundary conditions of the numerical model. These prevent the wires to slip over their entire length, thus increasing the bending stiffness at large curvatures slightly.
- Geometrical non-linear effects cause incorrect results for the bending stiffness at higher curvatures. A method to compensate for this error is presented in this thesis. Using this technique, the effect of friction on the state-dependent bending stiffness is isolated by removing the contribution of the geometrical non-linear effect. The results of the analytical model for large curvatures are questionable due to geometric non-linearity. Therefore, comparing both models for high curvatures is arguable.

- Numerical modelling of the state-dependent bending stiffness of large stranded ropes requires detailed computational meshes and time. However, with the suggested modelling methodology presented in this thesis it is possible to model the bending stiffness variation of these larger stranded ropes.

4. *Implement the state-dependent bending stiffness in a wire rope model to simulate critical situations during A&R operations*

- A model is developed to simulate a vertically suspended A&R wire rope as multiple beam elements with a state-dependent bending stiffness. During the simulation, the bending stiffness is found to be close to the theoretical minimum value at wire rope sections close to the seabed. Low tension combined with torsional deformation and a high curvature at these locations are the main reason for this low bending stiffness.

- The conservative assumption that during the simulation, the bending stiffness will reach its theoretical minimum value is considered correct when a simple strand is taken into account. However, preliminary numerical results concerning the minimum bending stiffness of an IWRC show a numerically generated minimum bending stiffness which is significantly larger than the theoretical value. Therefore, it could be that previously made assumption is too conservative when larger wire ropes are considered.

- A criterion for loop formation has been introduced in the form of a tension threshold. This criterion depends on the torque in the rope and on its bending stiffness. If the tension in a wire rope is reduced below this value, loop formations will occur.

- The bending stiffness decrease during the analysis is mainly due to the low tension at lower sections of the wire rope. If sufficient tension can be maintained in the wire rope, large reductions in bending stiffness can be avoided.

7.2. Recommendations

- Segment to segment friction modelling in Marc using bilinear Coulomb friction is used in this thesis. Therefore, element size, tension and the friction coefficient have an effect on the maximum bending stiffness found using this model. As this effect is unwanted, it can be countered by adjusting the slip threshold factor. However, for larger wire rope configurations, this becomes more difficult. As the element size in different contact bodies differ more for larger wire ropes, segment to segment friction modelling could prove to be unreliable. This is because the slip threshold is equal for all contact bodies in a mesh while the element size is not. Node to segment modelling in Marc should be investigated, as edge lengths do not influence important parameters needed for modelling friction.

- Previously performed experiments by Allseas into the hockling behaviour of steel wire ropes did not provide desired results. As is concluded in this thesis, bending stiffness reduction is a combination of the friction coefficient, tension, lay angle change and curvature of the wire rope. In the experiment performed by Allseas, tension was varied and lay angle change was simulated by torque variations. However, this did not provide the desired result of loop formation as no curvature was introduced in the wire rope. With zero curvature, bending stiffness values of a wire rope are at their maximum, therefore the resistance to loop formation is at its highest. Experiments should be performed with no or little tension while introducing a torque and a curvature on the wire rope. This will reduce the bending stiffness while increasing the likelihood for loop formation. The results from these experiments can provide Allseas with information about the combination of parameters at which loops will occur. The validity of the Greenhill formula could also be checked using these experiments.

- The numerical model should be expanded to stranded rope configurations which are used by Allseas, using the methodology presented in this thesis. After the state-dependent bending stiffness has been found, the developed subroutine and interpolation technique can be used to implement the bending stiffness into a beam model simulating a wire rope.

- Bending experiments with stranded ropes used for A&R operations should be performed. A test set-up should be designed which can measure the bending resistance of these ropes due to an external moment or load. The results from the experiment should be used to verify the results from the numerical model.
- For the determination of the state-dependent bending stiffness in this thesis, no initial deformations of the wires due to manufacturing and wear have been taken into account. The manufacturing process and wear of wire ropes could increase, or decrease, the contact area and normal stresses between wires, resulting in a bending stiffness which is higher or lower than the theoretical minimum value. Therefore, the effect of pre-stresses and deformations in wire ropes should be investigated using the numerical model developed in this thesis.

Bibliography

[1] Inventor Autodesk. Autodesk. *Software Corporation, San Rafael, CA*, 2016. URL http://www.autodesk.nl/products/inventor/overview.

[2] F. Blouin and A. Cardou. A study of helically reinforced cylinders under axially symmetric loads and application to strand mathematical modelling. *International journal of solids and structures*, 25(2):189–200, 1989.

[3] A.F. Bower. *Applied mechanics of solids*. CRC press, 2009.

[4] A. Cardou and C. Jolicoeur. Mechanical models of helical strands. *Applied Mechanics Reviews*, 50:1–14, 1997.

[5] Mazzella Companies. The parts list of a wire rope machine. URL https://www.mazzellacompanies.com/Catalog/Wire-Rope/Parts-List-Of-A-Wire-Rope-Machine. [Accessed 4 May 2016].

[6] G.A. Costello. Analytical investigation of wire rope. *Appl. Mech. Rev*, 31(7):897–900, 1978.

[7] G.A. Costello. *Theory of wire rope*. Springer Science & Business Media, 1997.

[8] J.B. Dastous. Nonlinear finite-element analysis of stranded conductors with variable bending stiffness using the tangent stiffness method. *IEEE Transactions on Power Delivery*, 20(1):328–338, 2005.

[9] FTL Design. History of the atlantic cable & undersea communications. URL http://atlantic-cable.com/Cables/1956TAT-1/. [Accessed 14 December 2016].

[10] K. Feyrer. *Wire ropes*. Springer, 2007.

[11] F. Foti and L. Martinelli. Mechanical modeling of metallic strands subjected to tension, torsion and bending. *International Journal of Solids and Structures*, 91:1–17, 2016.

[12] V.G.A Goss, G.H.M van der Heijden, J.M.T Thompson, and S. Neukirch. Experiments on snap buckling, hysteresis and loop formation in twisted rods. *Experimental mechanics*, 45(2):101, 2005.

[13] S. Goyal, N.C. Perkins, and C.L. Lee. Non-linear dynamic intertwining of rods with self-contact. *International Journal of Non-Linear Mechanics*, 43(1):65–73, 2008.

[14] A.G. Greenhill. On the strength of shafting when exposed both to torsion and to end thrust. *Proceedings of the Institution of Mechanical Engineers*, 34(1):182–225, 1883.

[15] M.P. Groover. *Fundamentals of Modern Manufacturing*. John Wiley & Sons, Inc, fourth edition edition, 2010.

[16] F.H. Hruska. Calculation of stresses in wire ropes. *Wire and wire products*, 26:766–767, 1951.

[17] Jumper installation analysis plem-lul 05 lorelay. Technical report i-rl-3a03.12-6520-966-a1b-017. Technical report, Allseas Engineering, 2015.

[18] W. Jiang. A general formulation of the theory of wire ropes. *Transactions of the ASME-E-Journal of Applied Mechanics*, 62(3):747–755, 1995.

[19] C. Jolicoeur. Comparative study of two semicontinuous models for wire strand analysis. *Journal of engineering mechanics*, 123(8):792–799, 1997.

[20] C. Jolicoeur and A. Cardou. Semicontinuous mathematical model for bending of multilayered wire strands. *Journal of engineering Mechanics*, 122(7):643–650, 1996.

[21] Kingwire. Acsr aluminium conductor steel reinforced. URL http://www.kingwire.com/product-catalog/bare-aluminum/acsr. [Accessed 07 October 2016].

[22] M.G. Leider. Secondary stresses in the bending of wire ropes. *Wire, May-June 1974, 24, 119-126*, 1974.

[23] IJIN Marine Limited. 6x36ws+fc/6x36ws+iwrc stainless steel wire rope. URL http://www.chinamarineropes.com/product/192569.html. [Accessed 5 May 2016].

[24] Innovation On Demand LLC. URL http://www.inod.az/wireropes.html.

[25] A.E.H. Love. *A treatise on the mathematical theory of elasticity*. Cambridge university press, 2013.

[26] M. Lutchansky. Axial stresses in armor wires of bent submarine cables. *J. Eng.*, 91(3):687–691, 1967.

[27] Marc. Msc. *Software Corporation, Santa Ana, CA*, 2016.

[28] MSC Marc. Volume a: Theory and user information. *MSC. Software Corporation*, 2016.

[29] MSC Marc. Volume b: Element library. *MSC. Software Corporation*, 2016.

[30] MSC Marc. Volume d: User subroutines and special routines. *MSC. Software Corporation*, 2016.

[31] A.H. Mimoune, A. Cardou, and A. Elchebair. Free constant curvature bending of axially preloaded strands. *Transactions of the canadian society for mechanical engineering*, 17(3):325–350, 1993.

[32] I. Páczelt and R. Beleznai. Nonlinear contact-theory for analysis of wire rope strand using high-order approximation in the fem. *Computers & Structures*, 89(11):1004–1025, 2011.

[33] K.O. Papailiou. Bending of helically twisted cables under variable bending stiffness due to internal friction, tensile force and cable curvature. *Doctor of Technical Sciences thesis, ETH, Athens, Greece*, 1995.

[34] K.O. Papailiou. On the bending stiffness of transmission line conductors. *IEEE Transactions on Power Delivery*, 12(4):1576–1588, 1997.

[35] M. Raoof. Free bending tests on large spiral strands. *Proceedings of the Institution of Civil Engineers*, 87(4):605–626, 1989.

[36] M. Raoof and T.J. Davies. Determination of the bending stiffness for a spiral strand. *The Journal of Strain Analysis for Engineering Design*, 39(1):1–13, 2004.

[37] M. Raoof and R.E. Hobbs. The bending of spiral strand and armored cables close to terminations. *J. Energy Resour. Technol.(Trans. ASME)*, 106(3):349–355, 1984.

[38] M. Raoof and R.E. Hobbs. Analysis of multilayered structural strands. *Journal of engineering Mechanics*, 114(7):1166–1182, 1988.

[39] M. Raoof and Y.P. Huang. Axial and free-bending analysis of spiral strands made simple. *Journal of engineering mechanics*, 118(12):2335–2351, 1992.

[40] A.L. Ross. Cable kinking analysis and prevention. *Journal of Engineering for Industry*, 99(1): 112–115, 1977.

[41] T.L Schmitz, J.E Action, J.C Ziegert, and W.G Sawyer. The difficulty of measuring low friction: uncertainty analysis for friction coefficient measurements. *Transactions of the ASME-F-Journal of Tribology*, 127(3):673–678, 2005.

[42] Sirtef. X-rays of a steel wire rope: Wires and strands lay. [Accessed 26 January 2017].

[43] E. Stanova, G. Fedorko, M. Fabian, and S. Kmet. Computer modelling of wire strands and ropes part i: Theory and computer implementation. *Advances in Engineering Software*, 42(6):305–315, 2011.

[44] U. Starossek. Cable dynamics-a review. *Structural Engineering International*, 4(3):171–176, 1994.

[45] A.J. Sweeney. Methods and apparatus for recovery of damaged subsea pipeline sections, November 17 2015. US Patent 9,188,246.

[46] P. Tejarat. Steel wire ropes for spin & rotation resistance. URL `http://wirerope-co.com/en/news/none-rotating`. [Accessed 18 Januari 2017].

[47] S.A. Velinsky. General nonlinear theory for complex wire rope. *International journal of mechanical sciences*, 27(7):497–507, 1985.

[48] R. Verreet. Allseas internal steel wire rope coarse, November .

[49] R. Verreet. Steel wire ropes with variable lay lengths for mining applications. *Bulletin*, 81:63–70, 2001.

[50] R. Verreet. Steel wire ropes for cranes-problems and solutions. *Casar Drahtseilwerk Saar Gmbh Internal Report*, 2002.

[51] R. Verreet and I. Ridge. Wire rope forensics. *Casar Drahtseilwerk Saar Gmbh Internal Report*, 2005.

[52] E. Xing and C. Zhou. Analysis of the bending behavior of a cable structure under microgravity. *International Journal of Mechanical Sciences*, 114:132–140, 2016.

[53] B.D. Yang, M.L. Chu, and C.H. Menq. Stick–slip–separation analysis and non-linear stiffness and damping characterization of friction contacts having variable normal load. *Journal of Sound and vibration*, 210(4):461–481, 1998.

[54] Y. Yu, X. Wang, and Z. Chen. A simplified finite element model for structural cable bending mechanism. *International Journal of Mechanical Sciences*, 113:196–210, 2016.

[55] D. Zhang and M. Ostoja-Starzewski. Finite element solutions to the bending stiffness of a single-layered helically wound cable with internal friction. *Journal of Applied Mechanics*, 83(3):031003, 2016.

A

Wire rope details

In this thesis, multiple wire rope configurations have been mentioned which are used for calculation. A Simple strand is the most common because it is a simple configuration and is mostly used throughout the thesis. More complex wire rope configurations are also used, for example a 6x36WS+IWRC or IWRC.

A.1. Strand

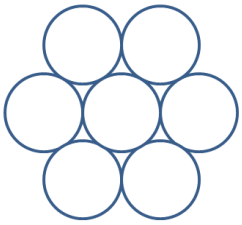

Figure A.1: Simple strand with one core wire and six outer wires

Table A.1: Geometric and material properties simple strand

Parameter	Symbol	Unit	Value
Core wire diameter	$[\delta_c]$	[mm]	3.94
Helical wire diameter	$[\delta_1]$	[mm]	3.73
Lay angle	$[\alpha]$	[deg]	17.03
Pitch length	$[h_w]$	[mm]	78.67
Cable length	$[L]$	[mm]	80
Young's modulus	$[E]$	[GPa]	188
Poisson's ratio	$[\upsilon]$	[-]	0.3

A.2. IWRC

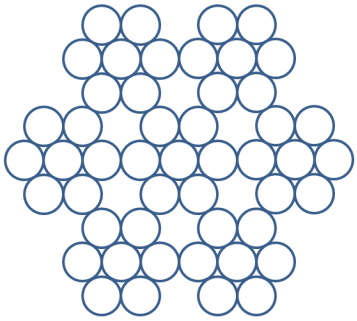

Figure A.2: Independent Wire Rope Core

Table A.2: Geometric and material properties IWRC

Parameter	Symbol	Unit	Value
Diameter of core wire in core strand	$[\delta_{c,c}]$	[mm]	1.76
Diameter of wire in first wire layer of core strand	$[\delta_{c,1}]$	[mm]	1.64
Diameter of core wire in first layer strand	$[\delta_{1,c}]$	[mm]	1.64
Diameter of wire in first wire layer of first layer strand	$[\delta_{1,1}]$	[mm]	1.47
Lay length first layer wires in core strand	$[hc_w]$	[mm]	40.32
Lay length first layer wires in first layer strands	$[h1_w]$	[mm]	40.32
Lay length first layer strand	$[hs_w]$	[mm]	89.5 - 93.1
Cable length	$[L]$	[mm]	91.15
Young's modulus	$[E]$	[GPa]	188
Poisson's ratio	$[\upsilon]$	[-]	0.3

A.3. 6x36WS+IWRC

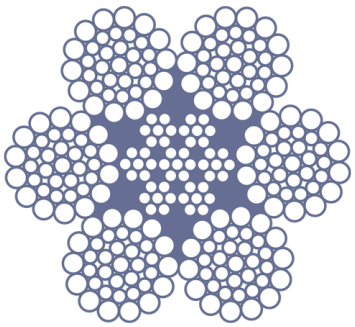

Figure A.3: Geometric and material properties 6x36WS+IWRC

Table A.3: Geometric and material properties 6x36WS+IWRC

Parameter	Symbol	Unit	Value
Diameter of core wire in core strand	$[\delta_{c,c}]$	[mm]	1.76
Diameter of wire in first wire layer of core strand	$[\delta_{c,1}]$	[mm]	1.64
Diameter of core wire in first layer strand	$[\delta_{1,c}]$	[mm]	1.64
Diameter of wire in first wire layer of first layer strand	$[\delta_{1,1}]$	[mm]	1.47
Diameter of core wire in second layer strand	$[\delta_{2,c}]$	[mm]	2.24
Diameter of wire in first wire layer of second layer strand	$[\delta_{2,1}]$	[mm]	1.96
Diameter of wire in second wire layer of second layer strand	$[\delta_{2,2}]$	[mm]	1.60
Diameter of filler wire in second wire layer of second layer strand	$[\delta_{2,2f}]$	[mm]	1.23
Diameter of wire in third wire layer of second layer strand	$[\delta_{2,3}]$	[mm]	1.64
Lay length wires in core strand	$[hc_w]$	[mm]	40.32
Lay length wires in first layer strand	$[h1_w]$	[mm]	40.32
Lay length first layer strand	$[h1_s]$	[mm]	89.5 - 93.1
Lay length wires in second layer strand	$[h2_w]$	[mm]	91.15
Lay length second layer strand	$[h2_s]$	[mm]	231.7 - 241.0
Cable length	$[L]$	[mm]	91.15
Young's modulus	$[E]$	[GPa]	188
Poisson's ratio	$[v]$	[-]	0.3

B

Frenet-Serret equations

A simple strand consists out of 1 core wire surrounded by 6 helically wound wires. The helical curve of the outer wires can be parametrized by the following equations.

$$x = \frac{r}{\tan(\alpha)} * \phi \tag{B.1a}$$

$$y = r * \cos(\phi) \tag{B.1b}$$

$$z = r * \sin(\phi) \tag{B.1c}$$

Where x, y and z described the coordinates of the centreline of the helical wire. Here, α is the lay angle of the wire in the strand and ϕ is the angle of rotation around the strand.

For more complex curves, such as those of a wire located in the outer strands of an IWRC the following parametrisation is carried out.

$$x = r * \sin(\upsilon) * \sin(\beta) + \phi * \frac{R}{\tan(\beta)} \tag{B.2a}$$

$$y = r * (\cos(\upsilon) * \cos(\phi) - \sin(\upsilon) * \cos(\beta) * \sin(\phi)) + R * \cos(\phi) \tag{B.2b}$$

$$z = r * (\cos(\upsilon) * \sin(\phi) - \sin(\upsilon) * \cos(\beta) * \cos(\phi)) + R * \sin(\phi) \tag{B.2c}$$

Here, $\upsilon = \phi \frac{R_s \tan \alpha_j}{r_j \sin \beta}$ characterizes the relation between the size of the torsion υ of a point γ around the axis of the helical wound strand and the size of the rotation ϕ of the strand around the core of the wire rope. The parameter β is equal to the lay angle of the helical strand around the core strand. r and R are the winding radii of the wire in the strand and of the strand respectively. The Frenet-Serret formulas are used to simulate the local coordinate systems, curvatures and torsion values of all wires.

$$\gamma = [x, y, z] \tag{B.3}$$

The arc length s corresponding with the swept angle ϕ:

$$s = \int_0^{\phi} \left| \frac{d\gamma(x, y, z)}{d\phi} \right| d\phi \tag{B.4}$$

Now that the curve has been parametrized by arc length, the Frenet-Serret equations can be for-

mulated.

$$T = \frac{\frac{d\gamma(x,y,z)}{ds}}{\left|\frac{d\gamma(x,y,z)}{ds}\right|} \tag{B.5a}$$

$$N = \frac{\frac{dT}{ds}}{\kappa} \tag{B.5b}$$

$$B = TxN \tag{B.5c}$$

The curvature and torsion can be derived and are needed for the equations B.6:

$$\kappa = \left|\frac{dT}{ds}\right| \tag{B.6a}$$

$$\tau = \frac{dB}{ds} * N \tag{B.6b}$$

C

Adapted thin-rod model for IWRC

Geometry and configuration of the IWRC used in this appendix can be found in appendix A. As is explained section 3.3, the model by Papailiou [33] can be used to come up with the maximum and minimum bending stiffness for IWRC configurations. For the bending stiffness in the transition region, an assumption has to be done which is explained in section 3.3. Symbols used in this appendix can be found in appendix A.

C.1. Minimum bending stiffness

According to Papailiou, the minimum bending stiffness of multiple layered strands can be defined as,

$$EI_{min,i} = n_i E_i \frac{\pi \delta_i^4}{64} \cos\beta \tag{C.1}$$

where i stands for the wire number and β is the lay angle. This equation is valid for transmission line conductors (spiral stranded ropes) as they only consist of wires in concentric layers. IWRC's do not have the same configuration and thus have to be treated differently. In full slip, the only contribution towards bending stiffness comes from the individual contribution of each wire. The problem can be separated into two parts; the bending stiffness of the core strand and that of the outer strands. The bending stiffness of the core strand can be easily calculated using the method described by Papailiou [33] for a simple strand.

$$EI_{min,corestrand} = E \frac{\pi(\delta_{c,c}^4 + 6\delta_{c,1}^4)}{64} \cos\alpha \tag{C.2}$$

The bending stiffness of the outer strand can be divided into the bending stiffness of the core wires of the outer strand and that of the wires in the strand.

$$EI_{min,outerlayerstrands} = E \frac{\pi 6 \delta_{1,c}^4}{64} \cos\beta + \frac{\pi 36 \delta_{1,1}^4}{64} \cos\beta \cos\alpha \tag{C.3}$$

Here, α is the lay angle of the wire in the strand and β is the lay angle of the strand. The total minimum bending stiffness is then equal to the sum of these values.

$$EI_{min} = EI_{min,corestrand} + EI_{min,outerlayerstrands} \tag{C.4}$$

C.2. Maximum bending stiffness

The maximum bending stiffness is calculated using Steiner's rule which stipulates that the moment of inertia of a body which is not located on the rotation axis is equal to the moment of the body itself, as if the rotation axis is located on its own rotation axis plus the area of the body times the distance from the axis. Figure C.1 is used as a visualisation of this equation C.5.

$$I_{z'} = I_z + d^2 A \tag{C.5}$$

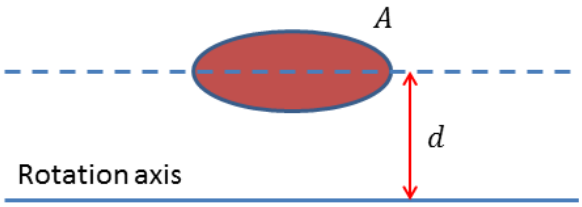

Figure C.1: Steiner's rule

This rule has to be applied to the IWRC as if all wires are glued together and thus support each other. EI_{min} corresponds with I_z in equation C.5 and EI_{stick} with the remaining d^2A. For each wire with its centreline displaced from the rotating axis shown in figure C.2 the following equations have to be performed.

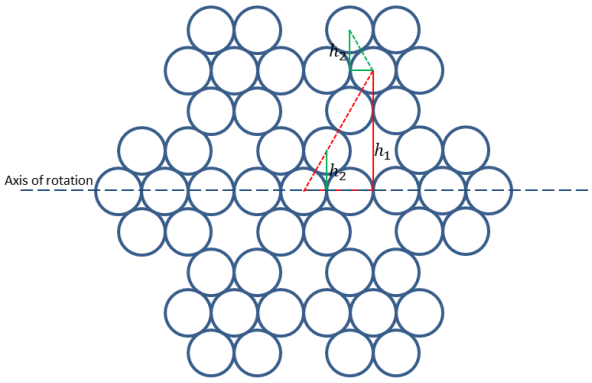

Figure C.2: IWRC with axis of rotation and parameters needed for calculating EI_{stick}

$$EI_{stick,corestrand} = \sum EA_{wire}h_2^2 \cos\alpha^3 \tag{C.6a}$$

$$EI_{stick,outerlayerstrands} = \sum EA_{wire}h_1^2 \cos\beta^3 + E * A_{wire}(h_1 + h_2)\cos\beta^3 \tag{C.6b}$$

The total value of EI_{stick} is acquired by summing the above equations for all wires in a IWRC which are not located on the axis of rotation. In equation C.6b the lay angle α of the wires in the strand has not been taken into account as one half of the wires approximately cancel out the other half, so all wires can be assumed in the direction of the strand.

The maximum value of the bending stiffness is equal to

$$EI_{max} = EI_{min} + EI_{stick}. \tag{C.7}$$

C.3. Bending stiffness during slip

For the bending stiffness during slip the IWRC is assumed to be a simple strand according to figure C.3 while assuming that the winding angle and radius of the wires in the assumed strand are equal to that of the strands in the IWRC as is shown in figure C.3. The area of a red wire is equal to the area of the wires in a strand combined. Now that the problem is reduced, the method described in chapter 3 can be used to calculate EI_{slip} and so the bending stiffness during slip.

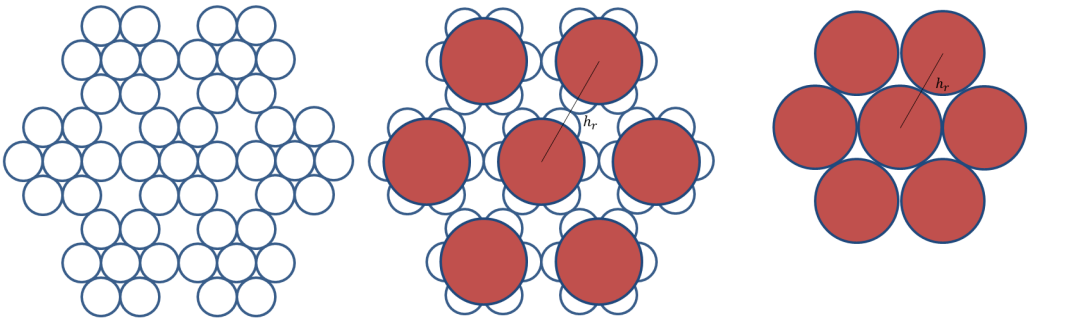

(a) Original IWRC

(b) Strands replaced with circles

(c) Simple strand assumption while preserving winding radius and angle

Figure C.3: Assuming IWRC as a simple strand

Note that the method to determine the bending stiffness during slip is a rough estimate of the actual results. It should only be used as an indication.

D

Costello

For the calculations using methods from Costello [7] a few variables have to be defined before showing the calculations. This makes the calculations in this appendix easier to follow. The variables and parameters used can be found in table D.1. The orientation of some of these forces and moments can be found in figure D.2.

Table D.1: Variables and parameters while using methods from [7]

Parameter	Unit	Description
ζ_1	[–]	Axial strain in the centre wire
ζ_2	[–]	Axial strain in an outer wire
ρ_2	[rad]	Initial pitch of an outer wire
ϵ	[–]	Axial strain of the strand
α_2	[rad]	Lay angle
ν	[–]	Poisson's ratio
r_1	[m]	Wire radius centre wire
r_2	[m]	Wire radius outer wire
hr	[m]	Helix radius
κ	[m^{-1}]	Curvature
τ	[m^{-1}]	Torsion
G'	[Nm]	Component of the bending moment on a wire cross section
H	[Nm]	Twisting moment in a wire
N'	[N]	Force along cross section
T	[N]	Axial force
X'	[N^{-1}]	External load per unit length
F_1	[N]	Axial reaction force on centre wire
M_1	[Nm]	Torsional reaction moment on centre wire
F_2	[N]	Axial reaction force on outer wire
M_2	[Nm]	Torsional reaction moment on outer wire
m_2	[–]	Number of outer wires

D.1. Pure bending of a simple straight strand

In this section the theory from Costello [7] is applied to a simple straight strand with dimensions as in table A.1. Only pure bending is analysed.

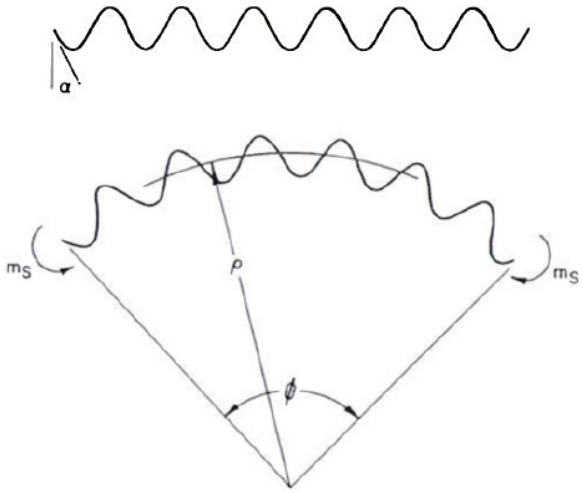

Figure D.1: Helical spring bent by a coupled moment M_s (Costello [7])

The initial curvature and twist of the helical spring in unloaded condition are

$$\kappa = 0 \tag{D.1a}$$

$$\kappa' = \frac{\cos(\alpha)^2}{r} \tag{D.1b}$$

$$\tau = \frac{\sin(\alpha)\cos(\alpha)}{r} \tag{D.1c}$$

where r is the initial radius of the helix. Only a bending moment is applied on the spring

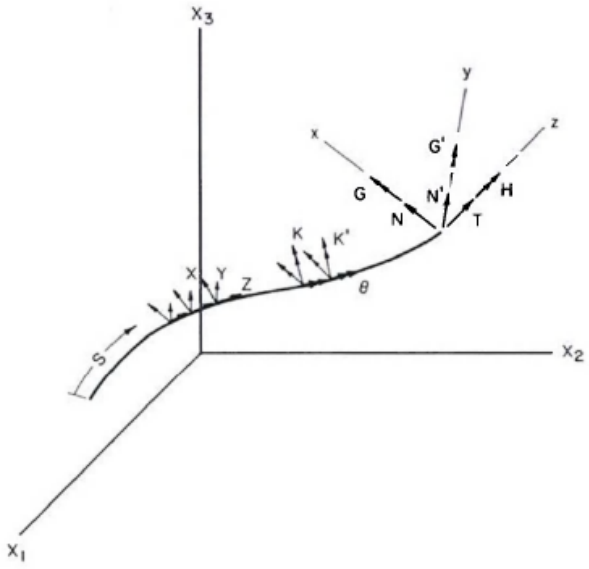

Figure D.2: Thin wire loads (Costello [7])

D.2. Axial torsional coupling

If the strain in the strand is known the strains in the individual wires can be determined if it is assumed that the strand will not twist. With this assumption the following can be stated,

$$\epsilon = \zeta_2 + \frac{\Delta\alpha_2}{\tan(\alpha_2)} \tag{D.2a}$$

$$0 = \frac{\zeta_2}{\tan\alpha_2} - \Delta\alpha_2 + \nu\frac{r_1\zeta_1 + r_2\zeta_2}{r_2\tan\alpha_2} \tag{D.2b}$$

after which the curvature and the change in twist per unit length can be linearized which results in the following.

$$r_2\Delta\kappa_2 = -\frac{2\sin(\alpha_2)\cos(\alpha_2)}{hr/r_2}\Delta\alpha_2 + \nu\frac{r_1\zeta_1 + r_2\zeta_2}{r_2}\frac{\cos^2(\alpha_2)}{hr/r_2} \tag{D.3a}$$

$$r_2\Delta\tau_2 = \frac{(1-2\sin^2(\alpha_2))}{hr/r_2}\Delta\alpha_2 + \nu\frac{r_1\zeta_1 + r_2\zeta_2}{r_2}\frac{\sin(\alpha_2)\cos(\alpha_2)}{hr/r_2} \tag{D.3b}$$

Assuming small displacements and using the equations of equilibrium as they are described in the book by Costello [7] the following can be stated for an outer wire. Forces and moments are as they are in figure D.2 and in table D.1.

$$\frac{G_2'}{Er_2^3} = \frac{\pi}{4}r_2\Delta\kappa_2' \tag{D.4a}$$

$$\frac{H_2}{Er_2^3} = \frac{\pi}{4(1+\nu)}r_2\Delta\tau_2 \tag{D.4b}$$

$$\frac{N_2'}{Er_2^2} = \frac{H_2}{Er_2^3}\frac{\cos^2\alpha_2}{hr/r_2} - \frac{G_2'}{Er_2^3}\frac{\sin(\alpha_2)\cos(\alpha_2)}{hr/r_2} \tag{D.4c}$$

$$\frac{T_2}{Er_2^2} = \pi\zeta_2 \tag{D.4d}$$

$$\frac{X_2}{Er_2} = \frac{N_2'}{Er_2^2}\frac{\sin(\alpha_2)\cos(\alpha_2)}{hr/r_2} - \frac{T_2}{Er_2^2}\frac{\cos^2(\alpha_2)}{hr/r_2} \tag{D.4e}$$

Now that the forces and moments are known, all that is left is projecting them in the axial direction of the outer wires.

$$\frac{F_2}{Er_2^2} = m_2\left[\frac{T_2}{Er_2^2}\sin(\alpha_2) + \frac{N_2'}{Er_2^2}\cos(\alpha_2)\right] \tag{D.5a}$$

$$\frac{M_2}{Er_2^3} = m_2\left[\frac{H_2}{Er_2^3}\sin(\alpha_2) + \frac{G_2'}{Er_2^3}\cos(\alpha_2) + \frac{T_2}{Er_2^2}\frac{hr}{r_2}\cos(\alpha_2) + \frac{N_2'}{Er_2^2}\frac{hr}{r_2}\sin(\alpha_2)\right] \tag{D.5b}$$

For the centre wires, no correction is needed.

$$\frac{F_1}{Er_1^2} = \pi\zeta_1 \tag{D.6a}$$

$$\frac{M_1}{Er_1^3} = \frac{\pi}{4(1+\nu)}r_1\tau \tag{D.6b}$$

Total axial force and twisting moment on the strand can be found by summing up the accuired forces and moments for the outer and centre wires.

$$F = F_1 + F_2 \tag{D.7a}$$

$$M = M_1 + F_2 \tag{D.7b}$$

E

Marc Mentat

E.1. Element type

Element type 7 is chosen from the Marc library [29] for the analysis performed in this thesis. Element type 7 is an eight node isoperimetrical, arbitrary hexahedral. The element has a cubic form as can be seen in figure E.1. The element type uses trilinear interpolation functions where the multivariate interpolation is used on a regular grid in 3D. This interpolation technique is shown in appendix F. It approximates the value of a point in the tetrahedra given values at the vertices of the cube. Because of this, the strains tend to be constant throughout the element which results in a poor shear behaviour. Therefore, more of these elements need to be used to describe shear and bending behaviour well.

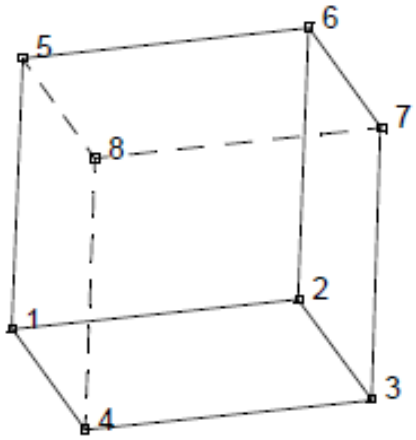

Figure E.1: Arbitrary cube simulating element 7 Marc [29]

According to the Marc library [29] this element is preferred over higher-order elements when used in a contact analysis. The stiffness of this element is calculated using the eight-point Gaussian integration. A 2-point Gaussian integration is shown in figure E.2 comparing it to a trapezoid integration technique. Higher point Gaussian quadratures used higher order polynomials to integrate the function and provide a more accurate interpolation.

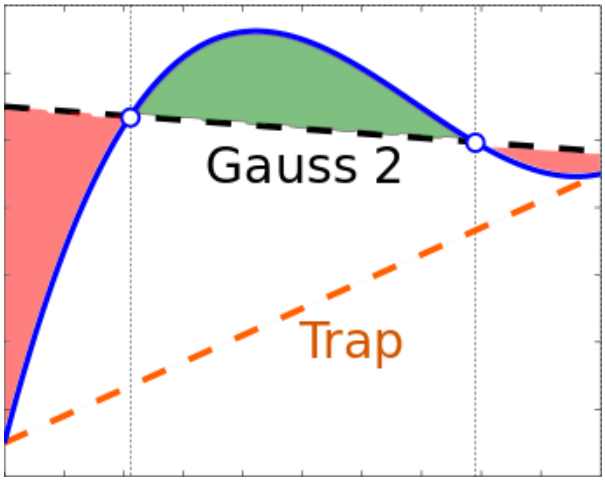

Figure E.2: 2-point Gaussian compared to trapezoidal quadrature

E.2. Load step

In figure E.3, results for the bending stiffness where different load steps have been used are presented. From the figure can be concluded that a load step of $LS = 0.02$s is to high to come up with reliable results. The graphs corresponding with load steps of $LS = 0.01$s and $LS = 0.005$s show more reliable results where the latter is the best of the two.

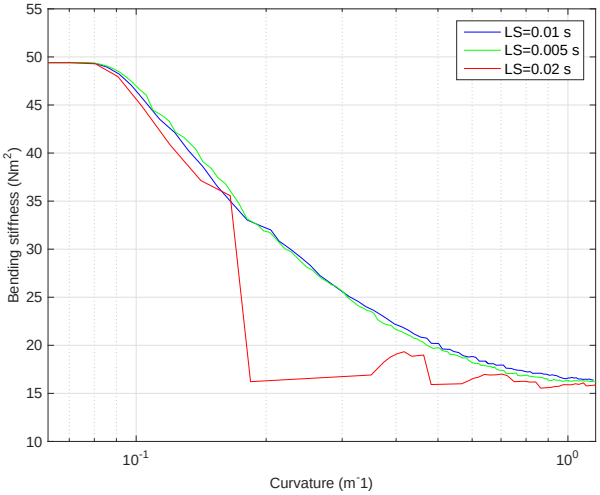

Figure E.3: Relationship between bending stiffness and curvature for different load steps

E.3. Contact

E.3.1. Friction

Segment to segment contact is selected as contact mechanism with frictional behaviour assumed to be governed by Coulomb's friction law which can be expressed as,

$$\theta = ||\lambda_t|| - \mu\lambda_n \leq 0 \tag{E.1}$$

where μ is the friction coefficient, λ_n represents the contact normal stress and λ_t represents the tangential stress vector; $\theta \leq 0$ corresponds to stick and $\theta = 0$ corresponds to slip.

However, numerical modelling of this discontinuity proves difficult. The coulomb model shown in E.4 is therefore interpreted by the bilinear model which can be found in figure E.5.

Marc assumes that the stick and slip conditions correspond to reversible ($\dot{u_t^e}$) and permanent ($\dot{u_t^p}$) relative displacement, respectively.

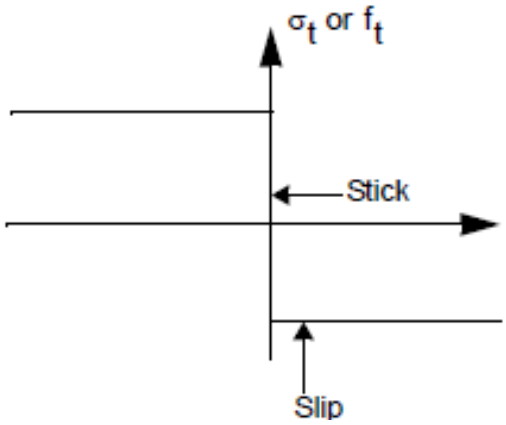

Figure E.4: Coulomb's friction law illustrated with σ_t equal to the tangential stress and f_t equal to the tangential force vector

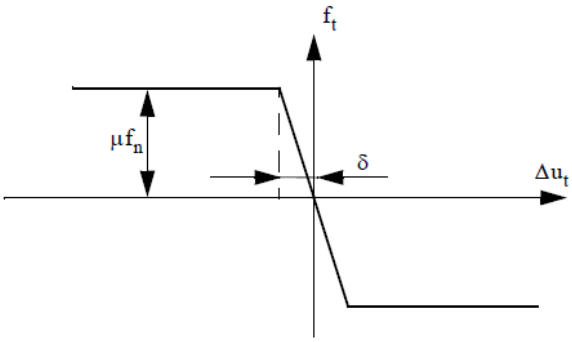

Figure E.5: Bilinear interpretation of Coulomb's friction law illustrated with δ equal to the slip threshold value and Δu_t equal to the relative tangential displacement

$$\dot{u}_t = \dot{u}_t^e + \dot{u}_t^p \tag{E.2}$$

By expressing the Coulomb law for friction by a slip surface ϕ, the stick domain is given by $\phi < 0$, while $\phi > 0$ is physically impossible.

$$\phi = ||f_t|| - \mu f_n \tag{E.3}$$

The rate of change of the friction force $\dot{f}_t$ is equal to a frictional stiffness term D times the elastic relative motions $\dot{u}_t^e$,

$$\dot{f}_t = D\dot{u}_t^e \tag{E.4}$$

in which D is defined by $\frac{\mu f_n}{\delta}$. δ is equal to the slip threshold value.

E.3.2. Contact check

To verify if certain contact bodies are in contact, Marc uses a contact detection procedure divided into two passes, the first pass consists of the *distance* check followed by a *direction* check. During the first check, the distance between a point on a contact body and its closest point projection on an other contact body is calculated and compared with a reference value. This reference value can be set by the user and is dependent on the contact tolerance ϵ and the bias factor B, where $0 \leq B < 1$. The default settings are used, where the program enters 5% of the smallest element side for the contact tolerance. The default bias factor is zero which is left untouched in the analysis in this thesis. If the position of a point on a body is x_a and that of its point projection on an other body is x_s, than the first pass will be completed if:

$$||x_a - x_s|| \leq (1 - B)\epsilon \tag{E.5}$$

When the distance check has been passed, the direction check is performed. This check compares the angles between the normal vectors of the two points on the two contact bodies. If the angle between the normal vectors is larger than a certain threshold value α the check is passed. This comes down to $\angle(n_a, n_s \geq \alpha)$ where the default value for α is used ($\alpha = 120\,\mathrm{deg}$). The total contact check is illustrated in figure E.6.

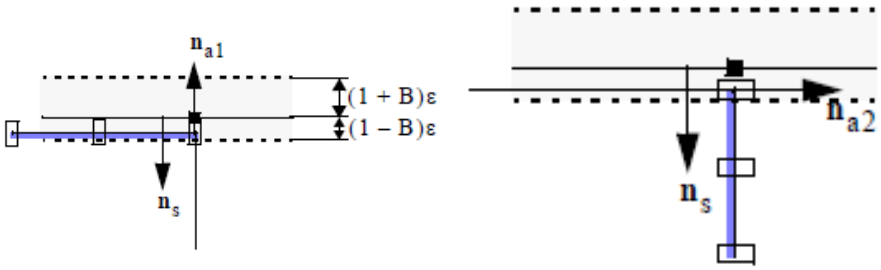

(a) Distance and direction check passed

(b) Distance check passed while direction check failed

Figure E.6: Contact detection method

In the second pass of the contact detection phase, each point is checked for contact using the same procedure as described above. At the end of these checks, the sets of points being in contact are represented by a contact area. Such as can be seen in figure E.7. These contact areas are used for the normal and friction stresses during the analysis.

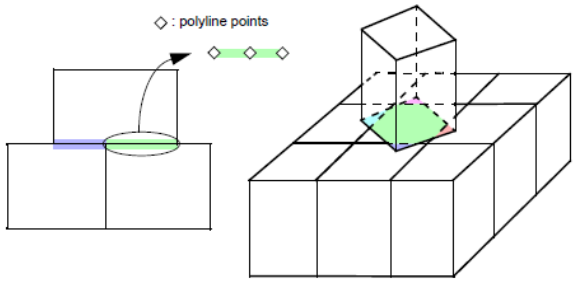

Figure E.7: Contact area segments [28]

In Marc, contact bodies can be defined. It can be selected which contact body is in contact which a certain other body, or if the body is in self contact. By selecting certain contact relations between bodies the method described in this section is ignored or activated.

E.4. Subroutines

Subroutines can be called within the Marc solver, allowing the user to substitute a custom subroutine in Marc. Subroutines are written in Fortran and are made compatible with Marc using Microsoft Visual Studio. The subroutine UBEAM [30] is used in the simulation in chapter 6. This user subroutine can be used to define non-linear elastic cross sectional properties as a function of generalized elastic strains for certain beam elements [30]. All values displayed in equation E.6 can be manipulated during the analysis.

$$\begin{Bmatrix} F \\ M_x \\ M_y \\ T \end{Bmatrix} = \begin{bmatrix} D_{11} & 0 & 0 & 0 \\ 0 & D_{22} & 0 & 0 \\ 0 & 0 & D_{33} & 0 \\ 0 & 0 & 0 & D_{44} \end{bmatrix} \begin{Bmatrix} \epsilon \\ K_x \\ K_y \\ T \end{Bmatrix} \tag{E.6}$$

F, M_x, M_y and T stand for the axial, bending and twist forces. No shear is taken into account for this beam element so the stiffness matrix will become four by four and consisting of D_{11}, D_{22}, D_{33} and D_{44} respectively being the axial, bending and torsional stiffness's. The axial strain, curvatures and twist are described by ϵ, K_x, K_y and T.

At the start of each time step the subroutine will call for the calculated forces and strains. These values will be interpreted by the subroutine code. In the subroutine the stiffness matrix shown in equation E.6 has to be determined. By changing the stiffness's the forces and moments have to be changed as well.

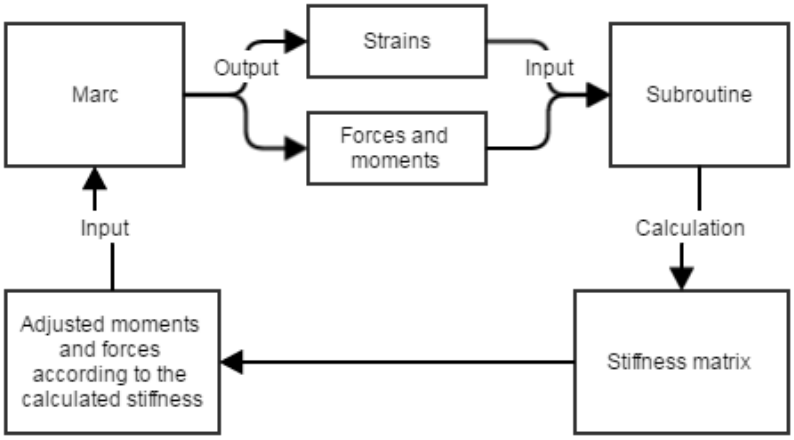

Figure E.8: Flowchart subroutine

Figure E.8 shows a flowchart describing the process involving the subroutine used in this model.

F

Interpolation

In this thesis, three forms of interpolation have been used, bilinear, trilinear and cubic interpolation. This appendix will be used to explain the different forms of interpolation. It is assumed that the reader understands the method of linear interpolation.

F.1. bilinear interpolation

Bilinear interpolation is an extension of linear interpolation. It can be used for the interpolation of functions containing two variables. By interpolating along one direction and then performing the interpolation for the remaining direction a value for the function can be derived. This process can be visualized as is shown in figure F.1.

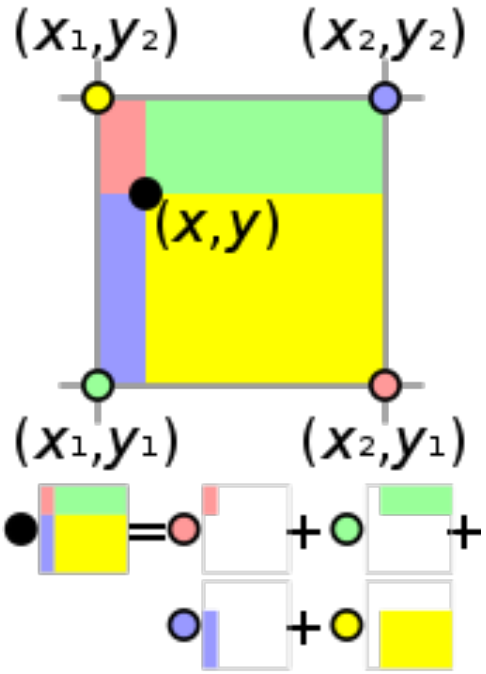

Figure F.1: Geometric visualisation of the bilinear interpolation process

Suppose there is an unknown function $f(x,y)$ dependent on the variables x and y. The function values are known for certain combinations of x and y. The unknown value for f at the point (x_s, y_s) has to be derived. For the interpolation technique to work it has to be assumed that the four nearest values for f namely; $f(x_1,y_1)$, $f(x_1,y_2)$, $f(x_2,y_1)$ and $f(x_2,y_2)$ are known. First, interpolation along

the x direction is performed.

$$f(x_s, y_1) \approx \frac{x_2 - x_s}{x_2 - x_1} f(x_1, y_1) + \frac{x_s - x_1}{x_2 - x_1} f(x_2, y_1) \tag{F.1a}$$

$$f(x_s, y_2) \approx \frac{x_2 - x_s}{x_2 - x_1} f(x_1, y_2) + \frac{x_s - x_1}{x_2 - x_1} f(x_2, y_2) \tag{F.1b}$$

After interpolation along the x axis, interpolation along the y axis is performed. Note here that the order of interpolation does not influence the found result.

$$f(x_s, y_s) = \frac{y_2 - y_s}{y_2 - y_1} f(x_s, y_1) + \frac{y_s - y_1}{y_2 - y_1} f(x_s, y_2) \tag{F.2a}$$

F.2. Trilinear interpolation

Trilinear interpolation is an extension of the pre discussed bilinear interpolation technique and operates with spaces of dimension $D = 3$, a visualisation can be seen in figure F.2. The method is approximately the same as is discussed in section F.1 only an extra interpolation axis is present.

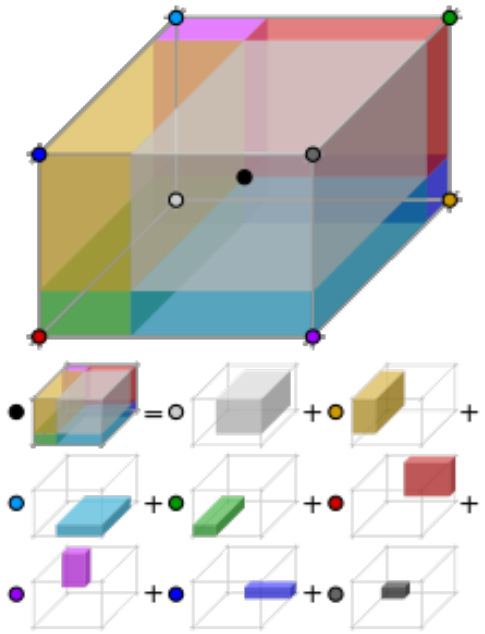

Figure F.2: Geometric visualisation of the trilinear interpolation process

State, the unknown function value $f(x_s, y_s, z_s)$ has to be found. Again, the assumption that the neighbouring points are known has to be made. The first step is defining the differences between the points describing the unknown function value and the smaller coordinate are found.

$$x_d = \frac{x_s - x_0}{x_1 - x_0} \tag{F.3a}$$

$$y_d = \frac{y_s - y_0}{y_1 - y_0} \tag{F.3b}$$

$$z_d = \frac{z_s - z_0}{z_1 - z_0} \tag{F.3c}$$

The 0 and 1 indices represent the smaller and larger coordinate value respectively. Secondly, the interpolations along the x will be performed. It has to be noted that as in the bilinear method, order of interpolation does not influence the found results. The corners of the cubic representation seen in

figure F.2 are called C_{000},C_{001},C_{010},C_{100},C_{110},C_{011},C_{101} and C_{111} where again the 0 and 1 represent the smaller and larger coordinate.

$$C_{s00} = f(x_0, y_0, z_0)(1 - x_d) + f(x_1, y_0, z_0)x_d \quad \text{(F.4a)}$$
$$C_{s01} = f(x_0, y_0, z_1)(1 - x_d) + f(x_1, y_0, z_1)x_d \quad \text{(F.4b)}$$
$$C_{s10} = f(x_0, y_1, z_0)(1 - x_d) + f(x_1, y_1, z_0)x_d \quad \text{(F.4c)}$$
$$C_{s11} = f(x_0, y_1, z_1)(1 - x_d) + f(x_1, y_1, z_0)x_d \quad \text{(F.4d)}$$

Thirdly, the interpolation along one of the other axis has to be performed. In this example, the y axis has been chosen.

$$C_{ss0} = C_{s00}(1 - y_d) + C_{s10}y_d \quad \text{(F.5a)}$$
$$C_{ss1} = C_{s01}(1 - y_d) + C_{s11}y_d \quad \text{(F.5b)}$$

The last operation, is the interpolation along the remaining unused axis. Now the value of the function at the given coordinates is found.

$$f(x_s, y_s, z_s) = C_{ss0}(1 - z_d) + C_{ss1}z_d \quad \text{(F.6)}$$

G

Hysteresis

In chapter 5, results for the bending behaviour of a simple steel wire rope strand are given. Curvatures are increased from 0m^{-1} to approximately a value of 1m^{-1} depending on the analysis. In reality, cables will bend in all directions, from lower to higher curvatures and visa versa. Because of the non-linear bending behaviour of wire ropes and the tension variation during an A&R operation, hysteresis is important to take into account.

Hysteresis is a phenomenon of a physical system, describing the dependence of the state of that system on its history in time. If a system is exited by an external influence, that system will not only react to the magnitude of that influence but also on the history of the system itself. It is important to state that hysteresis is not taken into account during the practical implementation in chapter 6.

Describing the hysteresis loop of a steel wire rope in bending starts with explaining a simple friction interface model illustrated in figure G.1a. Two bodies with frictional contact where one is considered the body and the other one the ground. The body is exited by the harmonic displacement $u = A\cos\omega t$ of a point connected to a spring with a stiffness k_d. If the exiting force reaches the counteracting frictional force $f = \mu n$ then the body will start to slide over the ground. The stick slip response that is the result of this harmonic excitation can be seen in the hysteresis loop of figure G.1b where $\theta = \omega t$.

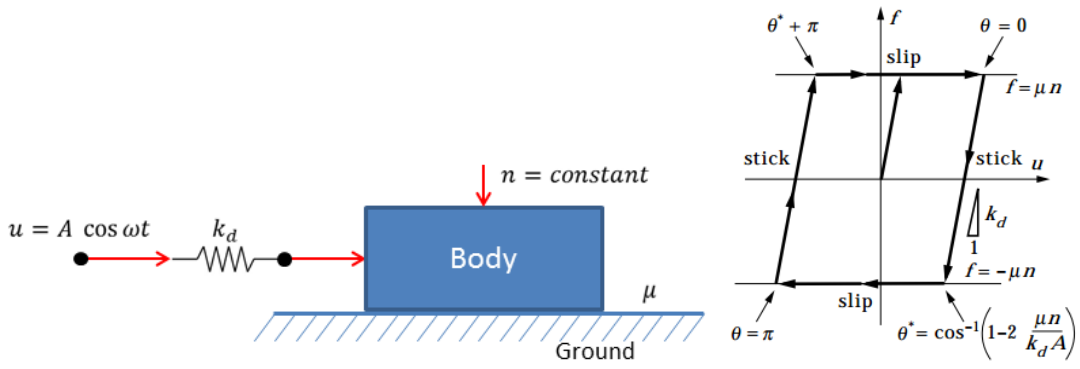

(a) Friction model (b) Hysteresis loop [53]

Figure G.1: Hysteresis loop of the model in figure G.1a experiencing a constant normal load

In this case, the transition from stick to slip can be predicted easily. When the exiting forces reverses its direction from $+$ to $-$ or the other way around ($\theta = 0\,\text{deg}$ or $\theta = 180\,\text{deg}$) the transition from stick to slip or from slip to stick is made as can be seen in figure G.1b.

However, stick slip does not always occur under a constant normal force. When the normal force varies over time and has an arbitrary phase angle from the varying exiting force, determining stick to slip is more of a challenge. Transitions do not have to occur when the exiting force reverses its direction. It is also possible for the normal force to decrease to a certain level so that stick to slip is activated. An example of this model set-up is illustrated by figure G.2a. The corresponding hysteresis loop can be found in figure G.2b.

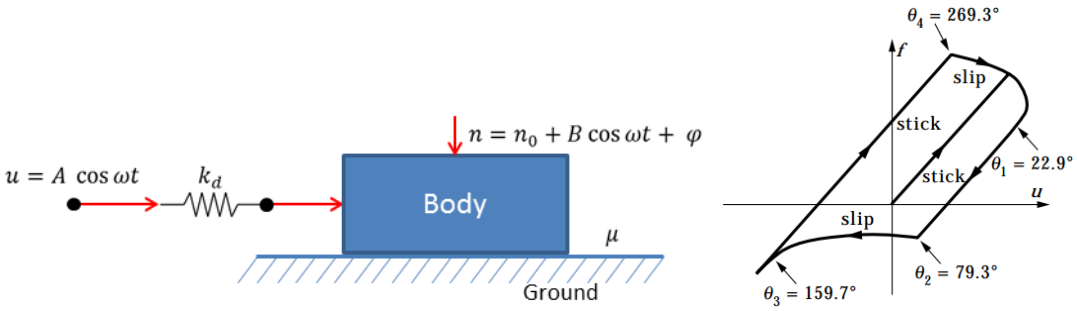

(a) Friction model (b) Hysteresis loop [53]

Figure G.2: Hysteresis loop of the model in figure G.2a experiencing a varying normal load

Again, the four alternating stick and slip regions can be seen, but the transition from stick to slip is not as easy to determine and recognize as it was in figure G.1a with a constant normal force. Thus, varying normal forces while harmonically exiting a body connected to the ground with frictional contact results in a non-symmetric complex hysteresis loop.

G.1. Inter wire friction

In steel wire ropes, hysteresis plays a role when loading the rope in tension and/or bending. Hysteresis in steel wire ropes almost entirely exist because of inter wire friction. Figure G.3 shows the external loads on a strand and illustrates the internal normal and frictional forces between wires.

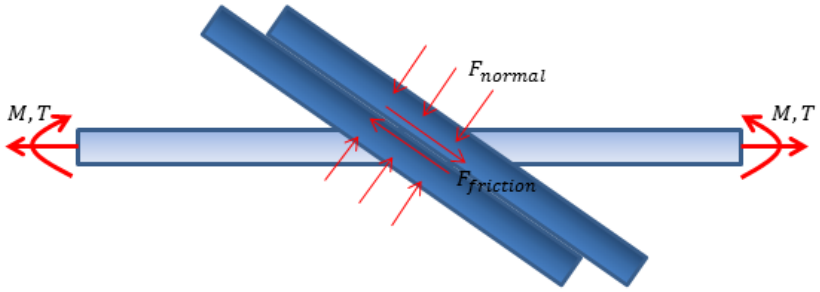

Figure G.3: Load directions of wires in a strand during slipping conditions where M and T represent the bending moment and the axial tension on the strand. F_{normal} and $F_{friction}$ are respectively the normal and the frictional forces between the wires

Energy will dissipate in a strand under tension or bending because off inter wire friction. The frictional sliding of wires relative to each other generates heat which will leave the system. In figure G.4 the hysteresis loop of a simple strand is given. A very coarse model is used for this analysis where approximately the same method is used as was explained in section 4.1.4. First a tension of $T = 20$kN is applied on the strand. Bending starts after this tension has been applied while having a friction coefficient of $\mu = 0.5$ between the wires. The bending moment that has been applied varies between $M_b = +20$Nm and $M_b = -20$Nm. The loop can be divided into multiple sections;

- Stick, where the friction between wires is enough to prevent slip
- Slip, where wires move relative to each other restricted by friction

The energy that is dissipated is equal to the area in the loop and can be represented by:

$$E_D = \oint M_b d\kappa \tag{G.1}$$

The hysteresis loop in figure G.4 can be compared to the hysteresis loop in figure G.1a with constant normal force. However, the loop corresponding with the steel wire rope bending does not display a

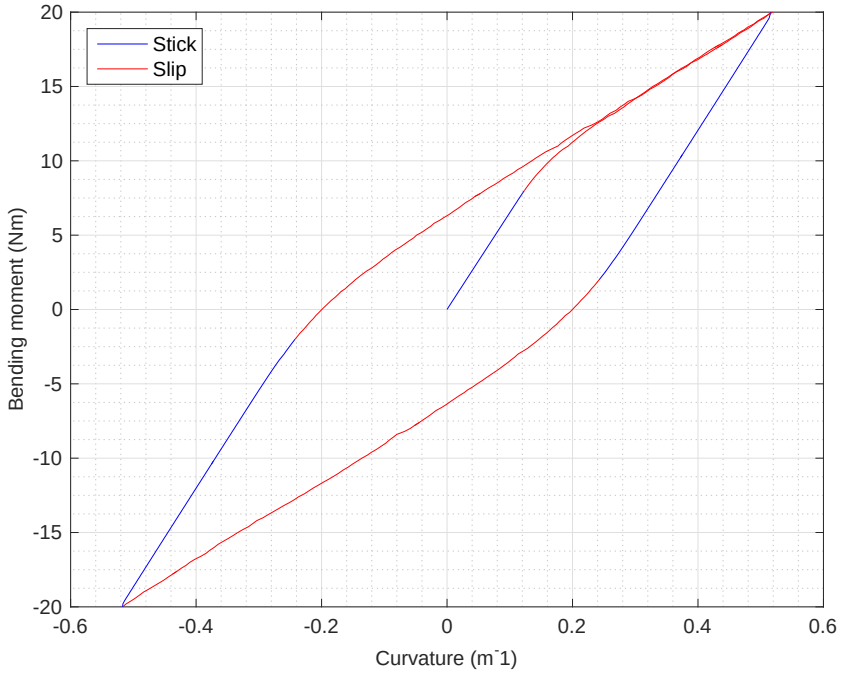

Figure G.4: Hysteresis loop for a simple strand with configurations as in appendix A calculated using the FEM model described in chapter 4

horizontal displacement when the transition point is reached. It describes a more compliant response than in the sticking state, and still continues to resist to bending when the slipping state is reached.

Tension has been assumed constant is this analysis. In reality however, this tension will not be constant as is for example the case in A&R operations. The vessel connecting the wire rope with the pipeline end will be continuously exposed to wave induced motions which will exert variational tension forces on the rope. Tension has a direct relationship with the normal forces that exist between wires due to their helical geometry. In reality the hysteresis loop for steel wire ropes in abandonment and recovery operations will most likely correspond more with the loop illustrated by figure G.2a.

H

Practical implementation: Case 2

The results from case 2 with input conditions shown in figure 6.5b are shown in figure H.1 and in H.2. The results are similar to that of case 1. The lay angle variation along the cable length shown in figure H.1c shows that the lay angles at the beginning of the cable reach the lowest researched lay angle of $9°$. For more reliable results, lower lay angles have to be researched so that the whole range of possible lay angles can be taken into account.

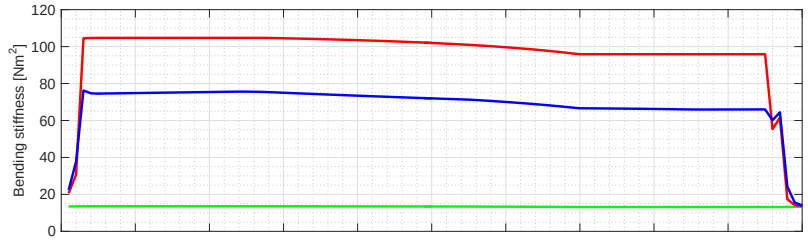

(a) Bending stiffness

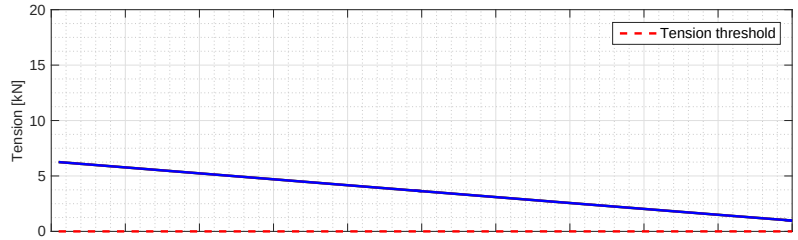

(b) Tension

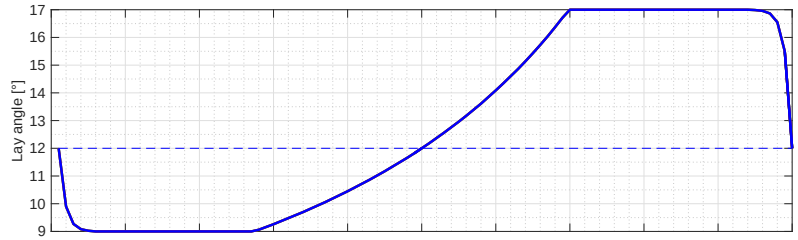

(c) Lay angle

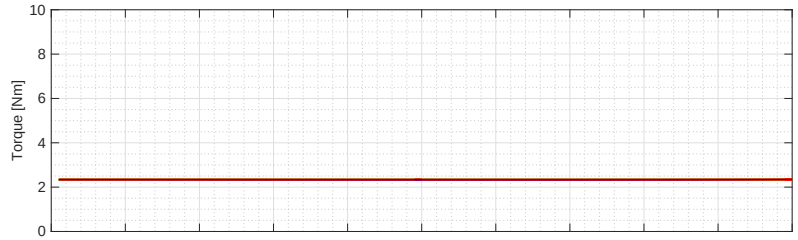

(d) Lay angle

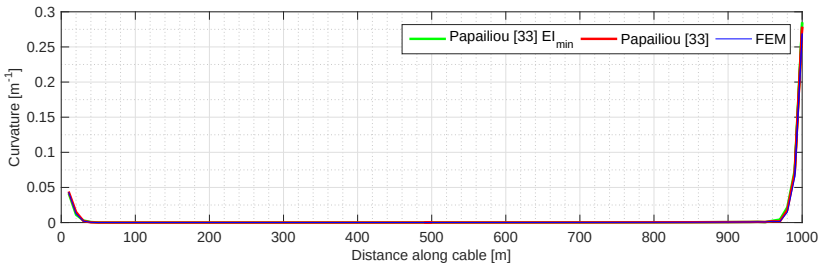

(e) Curvature

Figure H.1: Various parameters monitored along the length of the cable using the input from case 1 shown in figure 6.5b at increment number 190

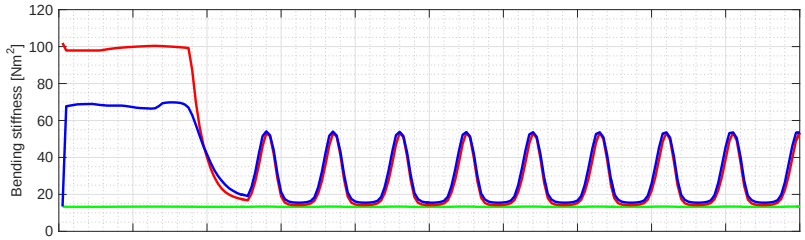

(a) Bending stiffness

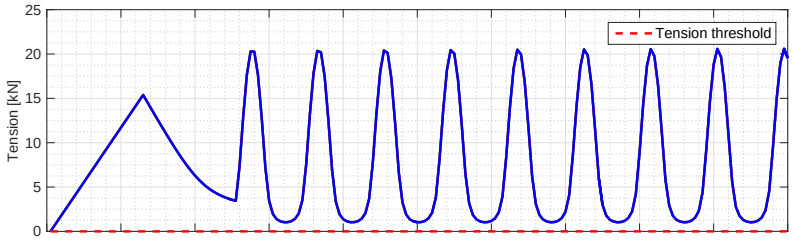

(b) Tension

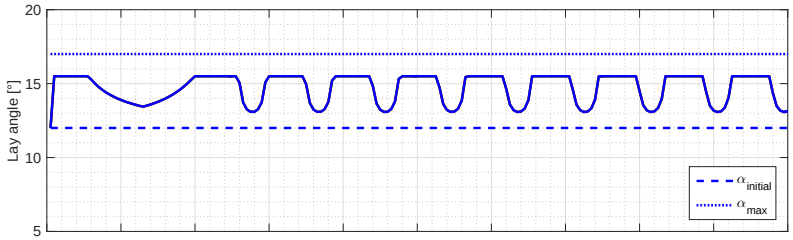

(c) Lay angle

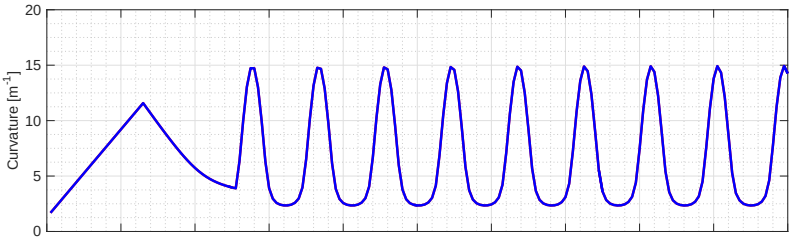

(d) Lay angle

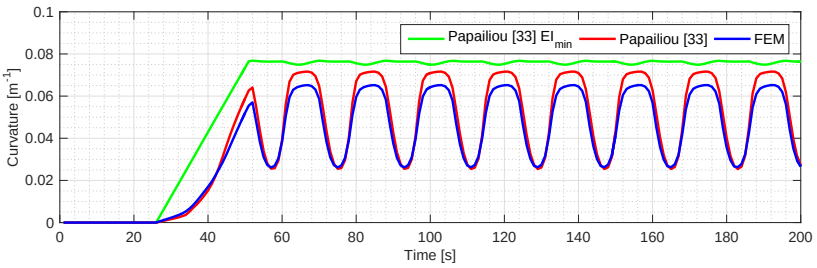

(e) Curvature

Figure H.2: Various parameters monitored for all cable increments using the input from case 1 shown in figure 6.5b for element number 99 (closest to the seabed)

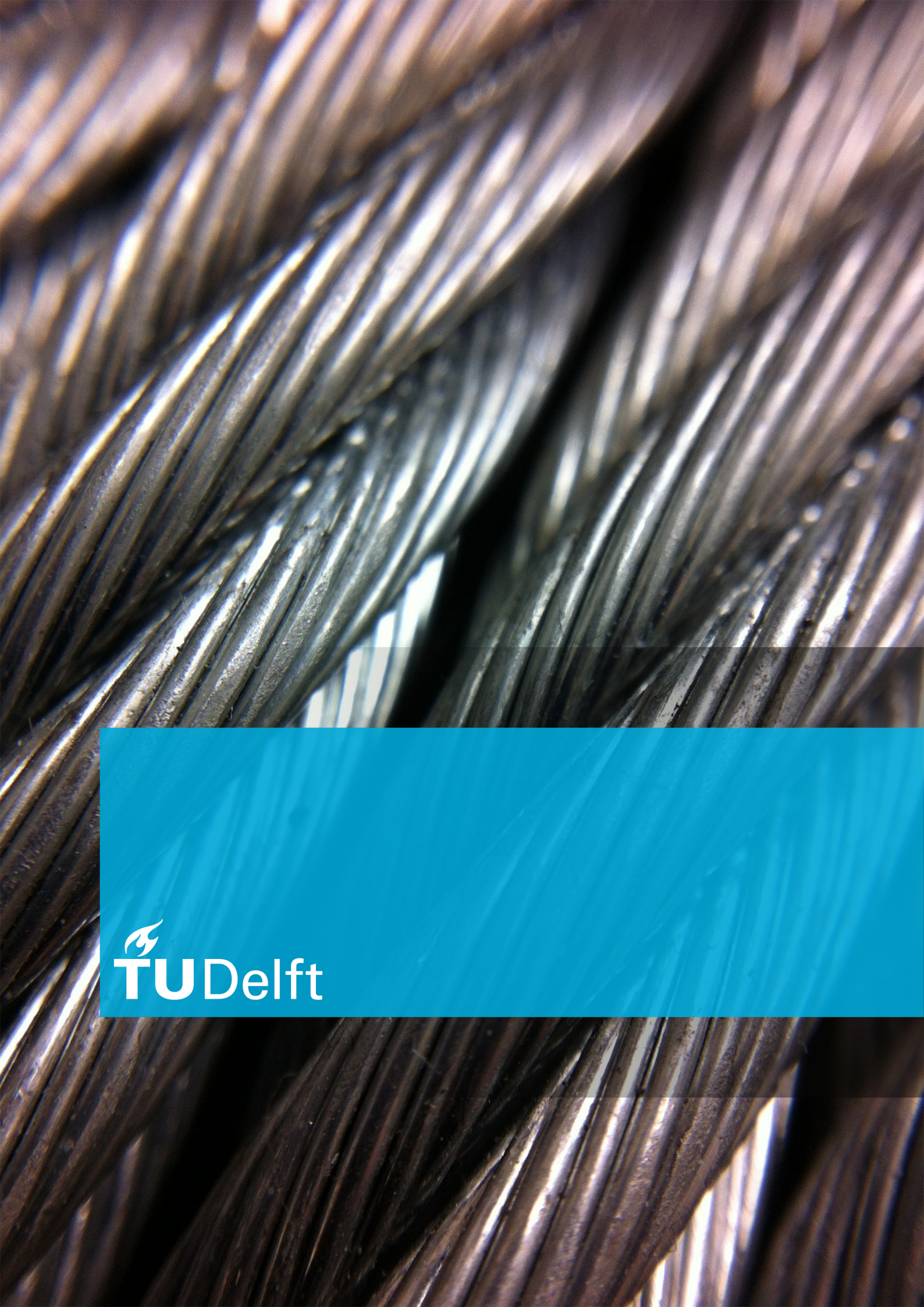
TU Delft